Dissertation

Aus dem Physiologischen Institut
Lehrstuhl: Physiologie – Zelluläre Physiologie (Biomedizinisches Zentrum München) der Ludwig-Maximilians-Universität München
Vorstand: Prof. Dr. Claudia Veigel

Calbindin-D28k and its role in apoptosis: Inhibition of Caspase-3 activity and interaction with Pro-Caspase-3 investigated by in-situ FRET microscopy.

Dissertation zum Erwerb des Doktorgrades der Medizin an der Medizinischen Fakultät der Ludwig-Maximilians-Universität zu München

vorgelegt von
Johannes Lohmeier
aus Bong Town, Liberia

2018

Mit Genehmigung der Medizinischen Fakultät der Universität München

Berichterstatter:	Prof. Dr. Michael Meyer
	Prof. Dr. Alexander Faussner
Mitberichterstatter:	Prof. Dr. Nikolaus Plesnila
	Prof. Dr. Dr. Bernd Sutor
Dekan:	Prof. Dr. med. dent. Reinhard Hickel

Tag der mündlichen Prüfung: 14.06.2018

Eidesstattliche Versicherung

Lohmeier, Johannes
Name, Vorname

Ich erkläre hiermit an Eides statt,

dass ich die vorliegende Dissertation mit dem Thema

Calbindin-D28k and its role in apoptosis:
Inhibition of Caspase-3 activity and interaction with Pro-Caspase-3 investigated by in-situ FRET microscopy.

selbständig verfasst, mich außer der angegebenen keiner weiteren Hilfsmittel bedient und alle Erkenntnisse, die aus dem Schrifttum ganz oder annähernd übernommen sind, als solche kenntlich gemacht und nach ihrer Herkunft unter Bezeichnung der Fundstelle einzeln nachgewiesen habe.

Ich erkläre des Weiteren, dass die hier vorgelegte Dissertation nicht in gleicher oder in ähnlicher Form bei einer anderen Stelle zur Erlangung eines akademischen Grades eingereicht wurde.

München, den 23.12.2016

Table of contents

Acknowledgements

I want to express my gratitude and appreciation towards my supervisor, Prof. Dr. Michael Meyer, for his support, guidance and advice during the last 4 years of research! My sincere gratitude goes to my coworkers, Sabine Mach, Marion Parch and Markus Weidelt, for their great technical assistance and advice! I am grateful for the opportunity to put my own ideas into practice and deepen my knowledge in science, molecular biology and experimental methods.

Moreover, I would like to thank the German Academic Scholarship Foundation (Studienstiftung des deutschen Volkes) for their ideational and financial support, Rüdiger Ilg, Priv.-Doz. Dr. med. (Technical University Munich) for his general advice and recommendations, Robert E. Campbell, Ph.D. (Department of Chemistry, University of Alberta) for providing the biosensor, Laurent Gelman, Ph.D. (Friedrich Miescher Institute, University of Basel) for his advice regarding PixFRET, Joachim Goedhart, Dr. Ir. (Swammerdam Institute for Life Sciences, University of Amsterdam) for the data on the mTurquoise2 spectrum, and Jan Erik Heil, Dr. rer. nat. (ZEISS, Munich) for his introductory training in confocal microscopy. I also want to thank Alex Scheiter, fellow doctoral student, for providing me his mTurquoise2-labeled Calbindin-D28k construct.

At last, special thanks to Julia and my mother, Christiana, for their support, love and backup!

"Faber est suae quisque fortunae."

(Every man is the artisan of his own fortune)

Appius Claudius Caecus

(340 BC - 273 BC)

Abstract:

In recent years, there was growing evidence that Calbindin-D28k, a common calcium binding protein, highly conserved among mammals, might be cytoprotective by inhibiting active Caspase-3, an important effector of apoptosis and, thereby, a crucial factor in cell physiology, oncogenesis and neurodegenerative diseases. Few in-vitro studies suggested that there might also be an interaction with the pro-domain of its zymogen, Pro-Caspase-3. To date, evidence on the various intermolecular interactions of Calbindin-D28k is essentially based on in-vitro studies. However, occasionally in-vitro studies yield results that might not correspond with conditions in living cells. To our knowledge, it is the first time that the proposed intermolecular Calbindin-D28k-Pro-Caspase-3 interaction and, moreover, the inhibition of Caspase-3 activity in a more complex, natural milieu of a cell is investigated using in-situ FRET microscopy (Acceptor-Photobleaching and Sensitized Emission). There is conclusive evidence for a calcium-independent interaction between Calbindin-D28k and an Inositol monophosphatase (IMPase) peptide sequence. Contrary to previous in-vitro studies based on peptide sequences, these results do not indicate an interaction with Pro-Caspase-3 regardless of intracellular calcium levels. This finding suggests that the inhibition of Caspase-3 activity is attributable to the intermolecular interaction with active Caspase-3. Moreover, the current findings indicate inhibition of Caspase-3 activity in a concentration-dependent manner. Further understanding of these cytoprotective pathways and mechanisms might prove beneficial to develop new cytoprotective or radio-/chemosensitizing agents and therapeutic strategies to modulate programmed cell death in neurodegenerative diseases, such as Morbus Alzheimer, Chorea Huntington or Amyotrophic lateral sclerosis, and various tumor diseases.

Keywords:

calbindin, calcium binding protein, caspase, apoptosis, modulation, interaction, inhibition, cytoprotection, FRET, förster resonance energy transfer, photobleaching, sensitized emission, photoconversion, biosensor, caspase activity, neuron, hippocampus, inositol monophosphatase

Deutschsprachige Kurzfassung:

Calbindin-D28k ist ein hoch konserviertes Kalzium-bindendes Protein, dem ein protektiver Effekt zugesprochen wird. In-vitro Studien haben gezeigt, dass Calbindin-D28k in der Lage ist, die aktive Caspase-3 zu hemmen, ein wichtiger Effektor des programmierten Zelltodes, die eine Schlüsselrolle in Zellphysiologie, Tumorentstehung und neurodegenerativen Erkrankungen einnimmt. Wenige in-vitro Studien haben ebenso zeigen können, dass eine Interaktion mit dem Zymogen, der Pro-Caspase-3, möglich ist. Bis heute stützt sich nahezu die gesamte Beweislage zu den verschiedenen intermolekularen Interaktionen von Calbindin-D28k im Wesentlichen auf in-vitro Studien. Jedoch können in-vitro Studien vereinzelt Ergebnisse hervorbringen, die sich nicht auf das komplexe Milieu von lebenden Zellen übertragen lassen. Daher untersucht die vorliegende Forschungsarbeit, die Calbindin-D28k-Pro-Caspase-3 Interaktion und die Inhibition der Caspase-3 Aktivität im komplexeren Milieu einer Zelle mittels in-situ FRET-Mikroskopie (Acceptor-Photobleaching und Sensitized Emission). Die Daten weisen auf eine Kalzium-unabhängige Interaktion zwischen Calbindin-D28k und einem Peptid der Inositol monophosphatase (IMPase) hin. Allerdings können die Ergebnisse, unabhängig von der intrazellulären Kalzium-Konzentration, keine Interaktion mit der Pro-Caspase-3 bestätigen. Diese Ergebnisse stehen im Gegensatz zu in-vitro Studien, die eine Interaktion mit den jeweiligen Peptidsequenzen zeigen konnten. Dies legt nahe, dass die Inhibition der Caspase-3 Aktivität auf die intermolekulare Interaktion mit der aktiven Caspase-3 zurückzuführen ist. Die Ergebnisse sprechen außerdem für eine konzentrationsabhängige Hemmung der Caspase-3 Aktivität. Ein tieferes Verständnis der protektiven Signalwege und Funktionsweisen kann bei der Entwicklung von neuen protektiven oder radio-/chemosensibilisierenden Pharmaka und therapeutischen Behandlungsstrategien richtungsweisend sein, die den programmierten Zelltod in neurodegenerativen Erkrankungen, wie Morbus Alzheimer, Chorea Huntington oder Amyotrophe Lateralsklerose, aber auch diversen Tumorerkrankungen modulieren könnten.

Abbreviations

A	Acceptor
AB	Antibody
AD	Alzheimer's disease
ADR	Acceptor-to-Donor
BS	Biosensor
CASP3	Pro-Caspase-3
CBD28k	Calbindin-D28k
CBP	Calcium binding protein
CD	Chromatin condensation
CFP	Cyan fluorescent protein
cFRET	Corrected FRET (Photobleaching)
CH	Chorea Huntington
CICD	Caspase-independent cell death
CNS	Central nervous system
CS	Coverslip
D	Donor
DMSO	Dimethyl sulfoxide
DNA	Deoxyribonucleic acid
E	Efficiency
EDTA	Ethylenediaminetetraacetic acid
EXP	Experiment
FP	Fluorescent protein
FRET	Förster/Fluorescence resonance energy transfer
GFP	Green fluorescent protein
I	Intensity
IAP	Inhibitors of apoptosis
IMPase	Inositol monophosphatase
INM	Ionomycin
LB	Lysogeny broth
M	Molar
MCS	Multiple cloning site
MW	Molecular weight
nFRET	Normalized FRET (Sensitized Emission)
PB	Photobleaching
PBS	Phosphate buffered saline
PCD	Programmed Cell Death
PCR	Polymerase Chain Reaction
PD	Parkinson's disease
PFA	Paraformaldehyde
PLL	Sigma-Aldrich Poly-L-Lysine
ranBPM	ranBP9 / BPM-L / BPM90
RE	Restriction enzyme
RFP	Red fluorescent protein
RIPA	Radioimmunoprecipitation assay buffer
ROI	Region of interest
RS	Restriction site

S	Samples
SBT	Spectral bleed-through
SDS-Page	Sodium dodecyl sulfate polyacrylamide gel electrophoresis
SE	Sensitized Emission
SOC	Super Optimal broth with Catabolite Repression
STS	Staurosporine
Suppl.	Supplement
Temp.	Temperature
w/	with
w/o	without
YFP	Yellow fluorescent protein

Table of figures

Table of tables

1. Introduction

1.1. Calbindin-D28k (CBD28k)

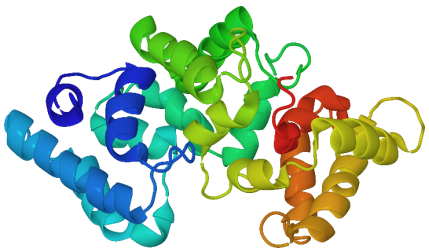

Figure 1. Structure of Calbindin-D28k. CBD28k (~ 30 kDa) displayed using Jmol and colored according to groups. [PDB 2F33, (Kojetin et al. 2006)]

Calbindin-D28k (CBD28k), first discovered in 1966 in chick intestinal mucosa (Wasserman & Taylor 1966), belongs to the family branch sharing an EF-hand motif, among more than 200 calcium-binding proteins (CBPs). Its sequence, genetically encoded by CALB1, is highly conserved among mammals and predominantly expressed in neurons. CBD28k constitutes up to 1.5 % of the total soluble brain protein (Berggård et al. 2002a), particularly abundant in cerebellar Purkinje cells (Barski et al. 2003), hippocampal granule cells (Iritani et al. 2001) and neocortical interneurons, but was also reported in bone, kidney, pancreas and other tissues (Christakos et al. 1989). Besides Calcitriol, neurotrophins (NT-3, BDNFa), IGF-1 and fibroblast growth factor were reported to stimulate expression of CBD28k (Collazo et al. 1992, Murayama et al. 2015, Nieto-Bona & Busiguina 1995, Wasserman & Fullmer 1989).

Featuring 6 EF-hands of which 4 are considered functional (see figure 1), CBD28k forms a single globular domain (Kojetin et al. 2006), facilitating calcium binding with low cooperativity, medium affinity and medium to fast kinetics (Schmidt 2012). In resting state, its binding sites are primarily occupied by magnesium (Berggård et al. 2002a), whereas with increasing intracellular calcium concentration, it unbinds magnesium to bind calcium, limiting intracellular increases in calcium levels (Schmidt 2012). It is considered a calcium sensor, buffer and transporter (see figure 2), as it regulates calcium-dependent downstream signaling, controls spatiotemporal calcium dynamics and homeostasis by transporting free calcium within intracellular compartments (Berggård et al. 2002a).

Furthermore, there are findings suggesting a role in a wide range of physiological processes, such as Long-Term-Potentiation (LTP) (Molinari et al. 1996) and cerebellar motor coordination (Airaksinen et al. 1997a).

Centrifugation and electron microscopic studies have shown that CBD28k is predominantly located in the cytosolic fraction. However, there are inconsistent reports of an association with fractions such as the nuclear fraction, mitochondria, endoplasmic reticulum, synaptic membranes, synaptic vehicles and the cerebellar microsomal fraction. Interestingly, decreased membrane fraction association at low calcium levels, indicated an interaction with membrane associated target molecules at increased calcium levels (Winsky & Kuźnicki 1995).

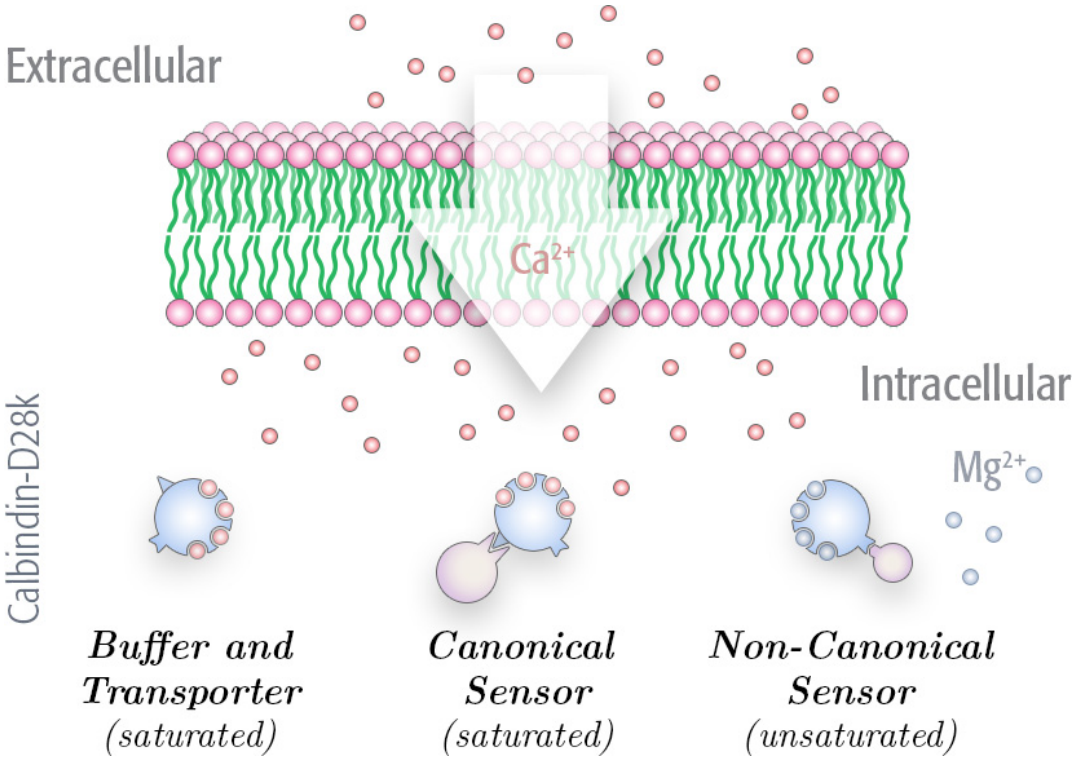

Figure 2. Calbindin-D28k and its function as a buffer, transporter and sensor.
CBD28k is demonstrated exhibiting its common buffer and transporter function (left section) during calcium influx. Upon binding calcium, CBD28k undergoes conformational change. This leads to exposed hydrophobic regions, that facilitate interaction with other proteins. This behavior (middle section) is typical for canonical sensors. At resting state, CBD28k is predominantly saturated with magnesium. It was shown that regardless of its saturation, CBD28k exposes a hydrophobic region, which facilitates calcium-independent interaction (right section).

1.1.1. EF-hand motif

The EF-hand motif is a highly conserved helix-loop-helix structural domain that is common in many CBPs. The perpendicularly oriented alpha helices resemble an outstretched thumb (F-helix) and index finger (E-helix), connecting a loop, which forms a binding site for calcium (see figure 3). Calcium ions are bound by both negatively charged amino acid residues, namely aspartate and glutamate, and protein backbone atoms (Johnson et al. 2014).

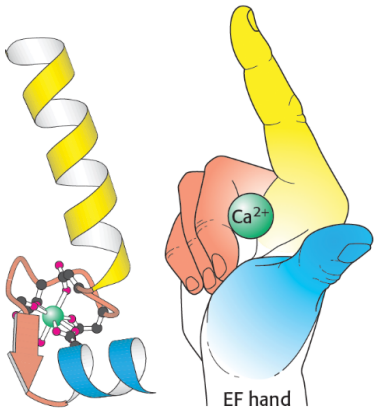

Figure 3. EF-hand motif.
Calcium is chelated in a loop (red, phalanx 3 - 5) connecting the F-helix (blue, thumb) and the E-helix (yellow, index finger), which are oriented perpendicular to each other. (adapted from (Berg et al. 2012) (pp445)).

After its discovery in Parvalbumin (Kretsinger & Nockolds 1973), many CBPs were found with varying numbers of EF-hands such as Troponin-C and Calmodulin, each with 4 EF-hand motifs, or Calretinin and CBD28k, each with 6 EF-hand motifs. Dependent on the number of EF-hand motifs and the differentiation in canonical/regulatory and structural/pseudo EF-hands, many EF-hand motif family branches are distinguished (Heizmann 1992). Regulatory EF-hands typically induce conformational changes, whereas structural EF-hands are restricted to calcium buffering and transport.

1.1.2. Cytoprotection

Substantial calcium level fluctuation is known to be a trigger of apoptosis. Therefore, calcium buffering can protect cells from Calpain-mediated activation of Caspase-3 (Pochet et al. 2000, Sharma & Rohrer 2004). Correspondingly, several studies reported cytoprotective effects upon CBD28k expression (Burke & Baimbridge 1993, Iacopino et al. 1992, Mattson et al. 1991). However, there was growing evidence that an alternate calcium-independent cytoprotective pathway exists, which involves the inhibition of Caspase-3 (Bellido et al. 2000, Choi et al. 2008, Christakos & Liu 2004, Liu et al. 2003). To date, CBD28k is the only endogenous, non-oncogenic Caspase-3 inhibitor besides the inhibitors of apoptosis (IAP) (Christakos & Liu 2004).

1.1.3. Intermolecular interaction

Upon binding calcium, CBD28k undergoes conformational change that leads to exposed hydrophobic regions, which facilitate protein-protein interaction. However, it was shown that in its apo-state (unloaded state), a hydrophobic region, corresponding to EF-hand 2, is permanently exposed, suggesting that CBD28k might additionally interact in a calcium-independent manner (Schmidt 2012).

To date, a wide array of proteins was reported to interact with CBD28k. Among the various interaction partners are Ca^{2+}-Mg^{2+}-ATPase (Morgan et al. 1986), 3'-5'-cyclic nucleotide phosphodiesterase (Reisner et al. 1992), Ran-binding-protein-M (RanBPM) (Lutz et al. 2003), TRPV5 channel (Lambers et al. 2006), Alkaline phosphatase (Norman & Leathers 1982), polypeptide Mellitin (La Bella et al. 1996), Myo-inositol monophosphatase-1 (IMPase-1) (Schmidt et al. 2005) and Pro-/Caspase-3 (Bellido et al. 2000, Kojetin et al. 2006). However, to date, the evidence on interaction partners is still essentially based on cell-free systems.

Inositol monophosphatase (IMPase)

As reported in various studies, there is evidence for an interaction site in Mus musculus lithium-sensitive Myo-inositol monophosphatase A1 (IMPase1), which shows activity enhancement upon binding CBD28k (Almog et al. 2011, Berggård et al. 2002b, Schmidt et al. 2005). Dephosphorylating inositol monophosphate (IP) to myo-inositol and inorganic phosphate, IMPase1 is of importance to the phosphatidylinositol (PI) signaling pathway (Hallcher & Sherman 1980) and might be involved in the mood stabilizing effect of lithium according to the inositol depletion hypothesis (Almog et al. 2011, Klein & Melton 1996).

Caspase-3

Caspase-3 belongs to a family of cysteine-aspartic acid proteases, which can induce apoptosis and, therefore, play an important role in programmed cell death (PCD). Synthesized as a zymogen, Pro-Caspase-3 undergoes a proteolytic conversion to its active form once the common apoptotic pathway is triggered. Later, its activation leads to the cleavage of essential cellular proteins, which ultimately results in cell death.

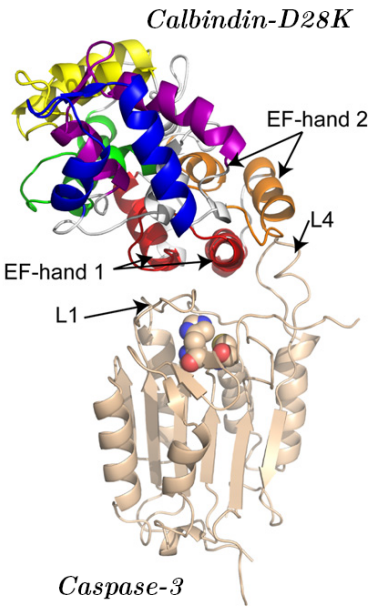

Figure 4. Caspase-3 and CBD28k complex. Catalytic residues are demonstrated as spheres within Caspase-3. EF-hands are colored red (EF-hand 1), orange (EF-hand 2), yellow (EF-hand 3), green (EF-hand 4), blue (EF-hand 5), purple (EF-hand 6). (adapted and modified from (Bobay et al. 2012)).

In recent years, various studies provided evidence for a CBD28k-mediated inhibition of Caspase-3 (Bellido et al. 2000, Bobay et al. 2012, Choi et al. 2008, Christakos & Liu 2004, Kojetin et al. 2006, Liu et al. 2003). It was shown that contrary to other common CBPs, such as Calmodulin and Calbindin-9K, only CBD28k was capable of inhibiting Caspase-3 activity (see figure 4). Furthermore, from active caspases 1 - 10, only active Caspase-3 was affected by CBD28k in a concentration-dependent manner (Liu et al. 2003). Using glutathione-S-transferase (GST) pull down assays, it was demonstrated that CBD28k can directly bind mature, active Caspase-3 (Christakos & Liu 2004). Another study revealed that the mechanism underlying the inhibition is substrate access restriction to the catalytic site and change of loop regions within Caspase-3. While previous reports proposed that the interaction occurs in a calcium-independent manner (Bellido et al. 2000, Liu et al. 2003), this study also provided evidence that the binding might not occur in apo-state (Bobay et al. 2012).

However, there were few reports suggesting that the interaction might also occur with its precursor, Pro-Caspase-3 (Bellido et al. 2000). Based on NMR studies and homology searches, an interaction site within the pro-domain was suggested, featuring a sequence (SKSIKNLEP) similar to RanBPM (LASIKNR) and IMPase (ISSIKEKYPSHS) target peptide sequences. Consequently, it was proposed that inhibition might occur by

interception of pro-domain cleavage, which is essential for Caspase-3 maturation (Kojetin et al. 2006). Another study provided similar evidence (Kordys et al. 2007).

1.2. Apoptosis

Apoptosis (*apóptōsis;* from Ancient Greek; "a falling off") is an essential and, therefore, highly conserved mechanism mediating programmed cell death (PCD) in multicellular organisms. Its key role in balancing growth and death upon physiologic and pathological stimuli is important in regular cell physiology, embryogenesis and various other developmental changes, particularly the maturation of the nervous and immune system, oncogenesis, aging, tissue repair, inflammation and infection. Dysfunction and imbalance of apoptosis, resulting either in massive over-proliferation or induction of excessive cell death, usually lead to various severe diseases, such as Alzheimer's disease (AD), Parkinson's disease (PD), several autoimmune diseases, ischemia, acquired immunodeficiency syndrome (AIDS) or cancer (Elmore 2007).

The necrosis-apoptosis continuum describes a theory that is based on the assumption that dependent on the circumstances, cell death might occur in a carefully regulated fashion, such as in apoptosis, or in an uncoordinated manner, such as in necrosis. Particularly the availability of caspases and energy in form of adenosine triphosphate (ATP), but also the developmental stage, tissue type, cytotoxic stimuli and its dose determine which pathway eventually dominates. Both types of cell death are associated with distinct morphological and biochemical changes. Necrosis is induced by external factors, such as lack of energy or cell membrane damage and affects groups of contiguous cells. It is typically characterized by cell lysis, inflammation, metabolic and homeostatic collapse, random DNA fragmentation and cell swelling. In contrary, apoptosis affects individual cells due to extrinsic or intrinsic physiological stimuli and leads to an energy-dependent, regulated, non-inflammatory response with chromatin condensation (CD), cell fragmentation and, subsequently, phagocytosis (Elmore 2007).

In recent years, there was growing evidence that there are other pathways available mediating PCD, all featuring their own phenotypes and biochemical mechanisms compared with classical apoptosis (Elmore 2007). Aponecrosis is a form of PCD that shows morphological changes of both necrosis and apoptosis (Formigli et al. 2000). Caspase-independent cell death (CICD) was found in distinct neuronal cells that leads to characteristic apoptotic changes although the caspase-dependent pathways were previously inhibited (Volbracht et al. 2001).

Both intrinsic/mitochondrial-mediated and extrinsic/death receptor-mediated signaling (see figure 5) can lead to the activation of the caspase-dependent cascade. Caspases can be categorized in 2 groups, the initiators (Caspase-8, -9, and -10) that activate the respective effectors (Caspase-3, -6, and -7), ultimately leading to cleavage of several intracellular proteins (Li & Yuan 2008).

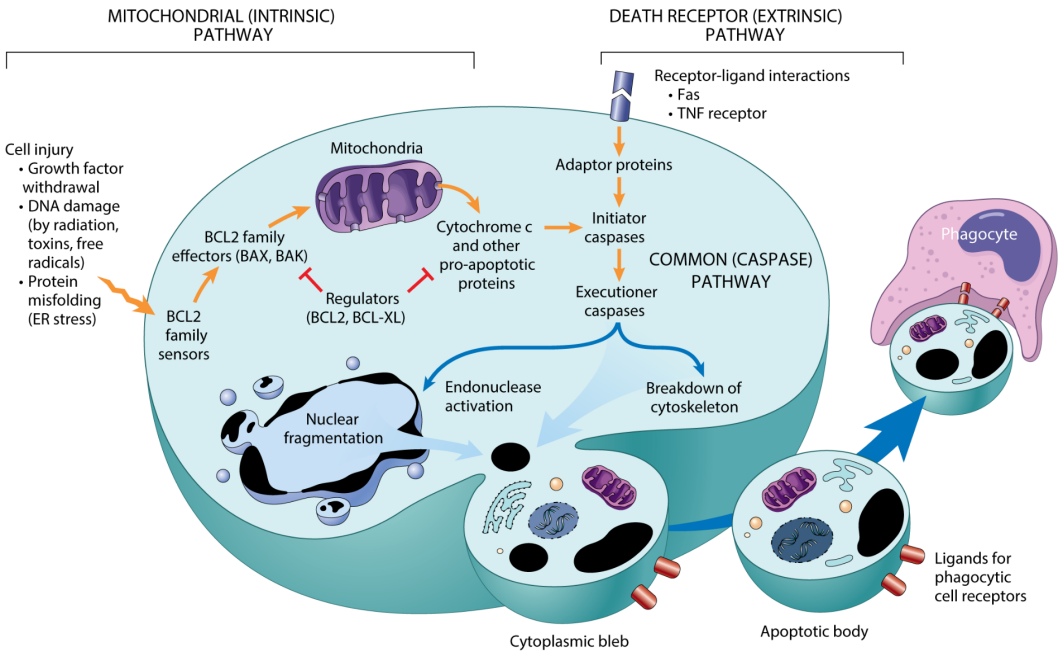

Figure 5. Apoptosis: Extrinsic and intrinsic pathway.
(adapted and modified from (Kumar et al. 2014) (pp74)).

Extrinsic pathway

The extrinsic pathway is characterized by cell surface ligand binding. Ligands, such as tumor necrosis factor alpha (TNF-alpha) or FAS, binding to death receptors, induce the oligomerization of receptors and the recruitment of death domain-containing adaptor proteins, such as Pro-Caspase-8 and -10. The accumulation and clustering of Pro-Caspases near these receptors leads to a death-inducing signaling complex (DISC). Within this multi-protein complex, Pro-Caspase-8 and -10 undergo autoactivation by cleavage, resulting in downstream caspase activation (Li & Yuan 2008).

Intrinsic pathway

The intrinsic pathway is triggered by internal stress signals, such as DNA damage, leading to destabilization of the mitochondrial membrane. Changes within its integrity and permeability, result in an imbalance between pro- and anti-apoptotic Bcl-2-family proteins, which can consequently trigger apoptosis. The cytoplasmic release of pro-apoptotic proteins, such as Cytochrome c, leads to the formation of a protein complex, the apoptosome (Cytochrome c and APAF-1), which recruits Pro-Caspase-9 and initiates its activation. Alternatively, in the case of DNA damage, Caspase-2 activation might occur within the PIDDosome in a p53-dependent manner (Li & Yuan 2008).

Common pathway

The active initiator caspases then subsequently lead to activation of effector Pro-Caspases-3, -6 and -7. The active effector caspases then target various essential cellular proteins, which ultimately leads to the disassembly of the cell.

1.3. Förster resonance energy transfer (FRET)

1.3.1. Theoretical background of FRET

Förster's theory, published in the 1940s, contributed to a great extent to the advancements made in the field of microscopy imaging.

Förster resonance energy transfer (FRET) describes a non-radiative transfer of excitation energy (see figure 6) from an excited donor to an acceptor molecule leading to a decrease of the donor quantum yield and donor excitation lifetime. As a result, the acceptor molecule shows sensitized acceptor emission, if fluorescent. However, this form of energy transfer occurs only if distinct conditions are met (Day & Davidson 2012):

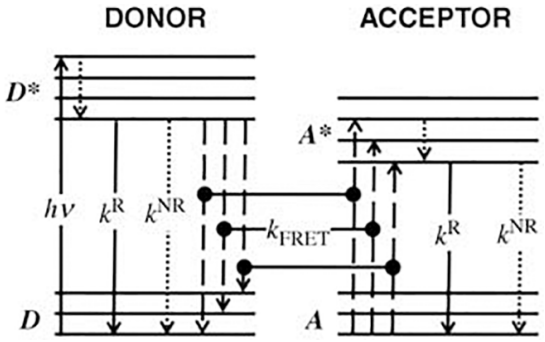

Figure 6. Simplified Jablonski diagram.
The absorption of energy leads to a switch from electronic ground state (D) to an excited state (D*). After relaxation (dotted arrow) to an excited ground state, further relaxation to the electronic ground state occurs through fluorescence/radiation (k^R) or non-radiative decay (k^{NR}) or non-radiative FRET (k^{FRET}). Only if resonance conditions are met, energy is transferred to the acceptor protein, leading to an excited state (A*) of the acceptor protein. To return to its ground state (A), energy is once again emitted by radiation (k^R) or in a non-radiative manner (k^{NR}). (adapted from (Medintz & Hildebrandt 2013) (pp109)).

- Close proximity (10 - 100 Ångström): At close range of up to 10 nm energy can be transmitted.
- Spectral overlap: This non-radiative energy transfer requires the overlap between the wavelength spectrums of both fluorophores, the donor emission spectrum and the acceptor absorption spectrum.
- Transition dipole orientations: The emission and absorption transition dipoles need to be in a favorable orientation ((k^2 = 0 - 4) towards each other, namely side-by-side (k^2 = 1) or head-to-tail (k^2 = 4). Usually k^2 is assumed to be 2/3 (Day & Davidson 2012, Sun et al. 2010).
- Quantum yield of the donor: The ratio of photons emitted to the photons absorbed should be reasonably high.

Förster regarded donors as linked electrical oscillators with an electrical field with 4 zones: starting with the inner zone, then the Dexter or contact zone, followed by the near-field zone within a range of 1 - 10 nm from the donor, where the Förster theory applies, and, at last, the intermediate zone (10 - 1000 nm from the donor) and far field or electromagnetic radiation zone. The basic theory of resonance declares that a vibrating/oscillating system can cause another system to vibrate/oscillate when specific resonance frequencies are met. In the case of FRET: the donor, excited by an electromagnetic field caused by photons/light, oscillates and creates an electromagnetic field, which in turn drives the acceptor to oscillate. This oscillating electromagnetic dipole-interaction (Coulomb interaction) in the near-field zone is the foundation of the energy transfer (Medintz & Hildebrandt 2013) (pp31-37).

Förster's formula states that FRET-efficiency (E) is strongly dependent on the inverse of the 6th power of the distance (r_{DA}) and the Förster radius (R_0) (see figure 7). Consequently, energy transfer occurs only if both fluorescent proteins (FPs) are in nanometer scale proximity to each other. Determination of the overlap integral (J) can be used to calculate the Förster distance (R_0) of the respective donor and acceptor pair, typically displaying values from 2 - 8 nm (Padilla-Parra & Tramier 2012). Knowing both the FRET-efficiency (E) and Förster distance (R_0), the distance between donor and acceptor (r_{DA}) can be determined.

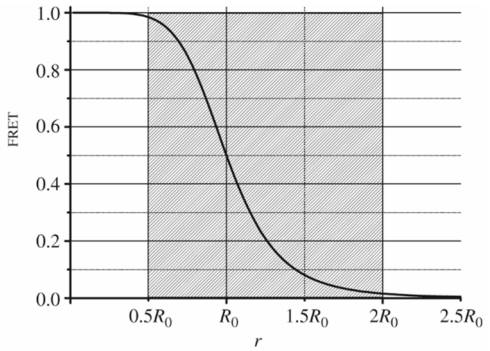

Figure 7. FRET-efficiency in dependence of the fluorophore distance.
R_0 is the Förster distance at which 50 % of the energy of the excited donor is transferred to the acceptor. This dependence explains the sensitivity of the FRET-efficiency (E) to the distance (rDA) in the 0.5 - 2.0 R_0 range. It is advisable to choose a FRET pair with a R_0 value within the range mentioned above. (adapted from (Medintz & Hildebrandt 2013) (pp110)).

Conclusions of Förster's theory in mathematical terms:

(1) $$E = \frac{k_t}{(k_t + \frac{1}{\tau_D})} = \left(\frac{R_0}{(R_0 + r_{DA})}\right)^6$$

(2) $$k_t = (\frac{1}{\tau_D})\left(\frac{R_0}{r_{DA}}\right)^6$$

(3) $$R_0^{\,6} = \frac{9\,(ln\ 10)\kappa^2\Phi_D J}{128\pi^5 n^4 N_A}$$

(4) $$J = \int F_D(\lambda)\cdot\varepsilon_A(\lambda)\cdot\lambda^4 d\lambda$$

(5) $$r_{DA} = R_0^{\,6}\sqrt{\frac{(1 - E)}{E}}$$

(adapted from (Medintz & Hildebrandt 2013) (pp26)).

E	Transfer efficiency
k_t	Rate of FRET energy transfer
τ_D	Lifetime of donor excited state in the absence of acceptor
r_{DA}	Donor and acceptor distance
R_0	Förster distance at which 50 % (E = 50 %) of the energy of the excited donor is transferred to the acceptor.
ln10	2.302585093
κ^2	Orientation factor (in intermolecular applications approximately 2/3)
Φ_D	Quantum yield of the donor fluorescence in the absence of acceptor
J	Overlap integral
π	3.14159
n	Refractive index of the medium
N_A	6.0221415 x 10^{23} per mole (Avogadro's number)

1.3.2. FRET microscopy

In the last few decades, a wide array of methods and dedicated equipment for different FRET applications were developed. Essentially, 2 major groups of methods are distinguished: implementations based on donor quenching and acceptor sensitization, such as Acceptor-Photobleaching, Sensitized Emission, Fluorescence Lifetime Imaging Microscopy/FLIM, and emission anisotropy-based procedures (Jares-Erijman & Jovin 2003). Ever since, FRET proved to be exceptionally useful for a range of applications such as the monitoring of protein-protein interaction, conformational changes and biochemical activity (see figure 8). Contrary to other commonly applied approaches for the assay of intermolecular association, FRET applications enable the user to increase the spatial resolution of confocal microscopy and, moreover, acquire reliable data within the natural, cellular environment. As its occurrence is limited to close spatial proximity of 10 - 100 angstrom, FRET commonly implies molecular association and direct interaction (Bastiaens & Pepperkok 2000, Grecco & Verveer 2011, Sekar & Periasamy 2003).

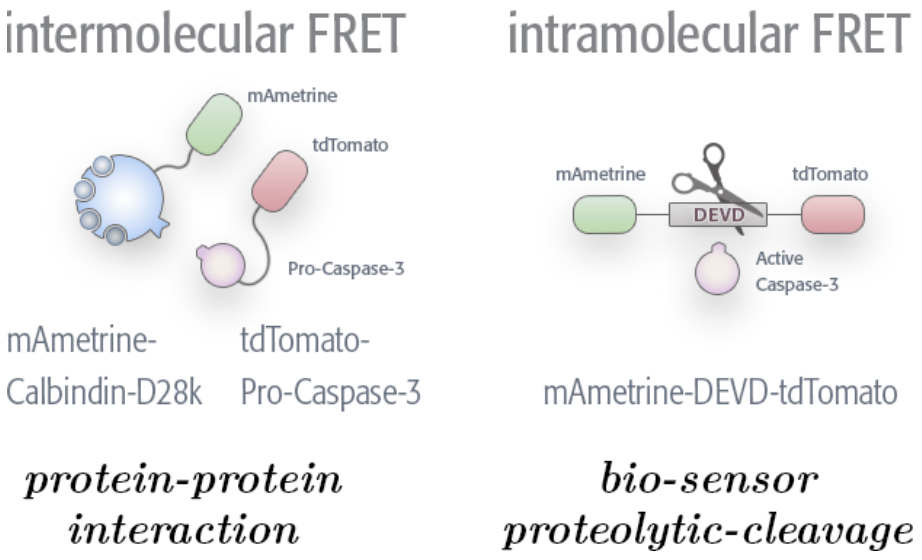

Figure 8. Applications of FRET: Monitoring of protein-protein interaction and biochemical activity.
Protein-protein interaction between 2 fusion constructs, mAmetrine (FP) linked to Calbindin-D28k and tdTomato (FP) linked to Pro-Caspase-3, can be assayed using FRET. Intramolecular FRET is demonstrated for a Caspase-3 bio-sensor. Cleavage of the characteristic DEVD motif leads to decreased FRET-efficiency during apoptosis.

1.3.2.1. Acceptor-Photobleaching (PB)

Among the methods at choice, Acceptor-Photobleaching (PB) is a reliable, accurate and straightforward solution for measuring protein co-localization. If FRET occurs, the original signal should be decreased due to energy transfer to the acceptor. Then, the acceptor molecules are irreversibly bleached by strong irradiation to approximately 1/10 of their initial intensity. In the absence of energy transfer, the donor population shows increased signal, which is commonly described as dequenching. If necessary, a corrective approach for crosstalk and other artefacts should be applied. The FRET-efficiency is quantified with the following formula:

$$E = \frac{transfer\ of\ energy}{donor\ excitation} = \frac{I_{POST} - I_{PRE}}{I_{POST}}$$

(adapted from (Bastiaens et al. 1995, Gadella & Jovin 1995))

I_{POST}	Donor intensity after the bleaching event
I_{PRE}	Donor intensity before the bleaching event

Advantages of Photobleaching:

- simple method
- implementation with most confocal microscope systems
- accurate measurement, as the determination of quenched and unquenched donor signal is performed on the same specimen
- not generally affected by spectral bleed-through (SBT)

Limitations of Photobleaching:

- can be used only once per cell due to its destructive nature
- limited to immobile or fixated cells
- non-dynamic measurement
- slow bleaching event might be accompanied by protein movement
- possible photoconversion

1.3.2.2. Sensitized Emission (SE)

Sensitized Emission (SE) is one of the easiest and frequently used methods to detect FRET. Due to its simplicity and non-destructive nature, it is commonly preferred. However, Sensitized Emission is considered to be less robust and, therefore, is primarily applied in qualitative research. Sensitized Emission describes the increase in acceptor emission upon donor excitation, provided that FRET occurs. FRET-efficiency is then calculated based on the change of intensity.

Commonly, 3 samples (Acceptor-only control, Donor-only control and FRET sample) and 3 filter sets (Acceptor filter set, Donor filter set and FRET filter set) are required. Based on the control samples, correction factors need to be determined, which account for crosstalk, concentration differences and artefacts. Among the different corrective approaches available, normalized FRET (nFRET) was calculated, as it corrects for emission crosstalk, cross excitation and, additionally, all values are normalized for the concentration of donor and acceptor (Xia & Liu 2001).

$$nFRET = \frac{I_{DA} - (R_A \times I_{AA}) - (R_D \times I_{DD})}{\sqrt{I_{AA} \times I_{DD}}}$$ (adapted from (Gordon et al. 1998, Xia & Liu 2001))

I_{DA}	Donor excitation and acceptor detection
I_{AA}	Acceptor excitation and acceptor detection
I_{DD}	Donor excitation and donor detection
R_A	Acceptor correction factor: $\frac{I_{DA}}{I_{AA}}$ (acquired from Acceptor-only samples)
R_D	Donor correction factor: $\frac{I_{DA}}{I_{DD}}$ (acquired from Donor-only samples)

Advantages of Sensitized Emission

- simple method
- non-destructive
- dynamic measurement
- not generally affected by spectral bleed-through

Limitations of Sensitized Emission:

- extensive control experiments
- correction of crosstalk and cross excitation
- quantitatively inaccurate measurement

1.3.3. Fluorescent proteins (FPs)

The discovery of Green Fluorescent Protein (GFP), one of the most popular fluorophores in life sciences research, had great impact on microscopy after its isolation from jellyfish *Aequorea Victoria* in 1922 (Prasher et al. 1992). Early FRET studies were predominantly performed with GFP and its variants (Romoser et al. 1997). However, today, a vast variety of fluorescent proteins (FPs) is available with distinct characteristics and applications. Like GFP, all FPs known to date feature a chromophore within a helical segment in the center of a characteristic β-barrel (11 β-sheets) fold (see figure 9).

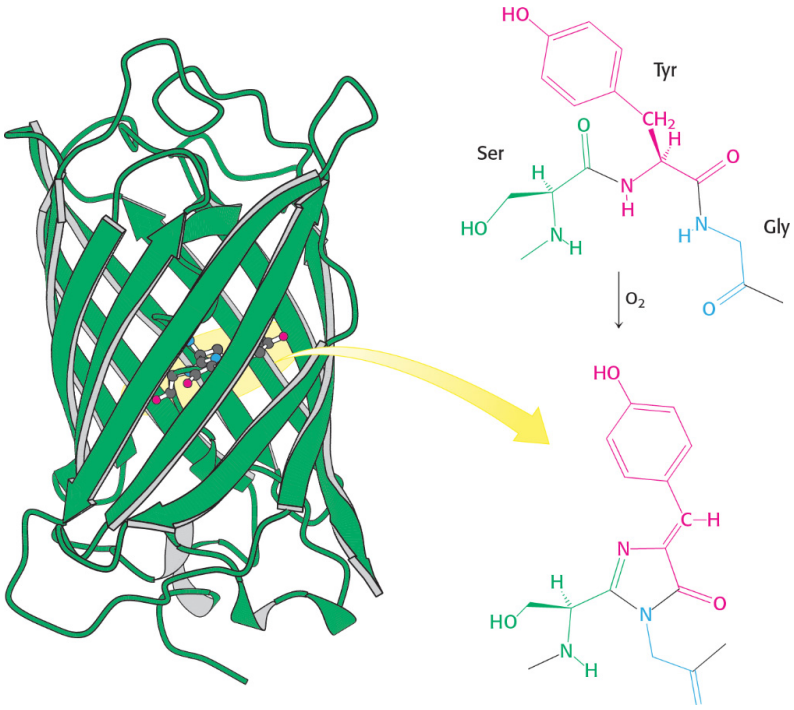

Figure 9. Structure of GFP and its chemical changes during fluorescence.
Chemical modification of the Ser-Tyr-Gly sequence leads to green fluorescence in GFP (27 kDa) after excitation with ultraviolet or blue light. (adapted from (Berg et al. 2012) (pp92)).

mAmetrine and tdTomato FP pair

With regard to stability in an apoptotic environment, negligible excitation bleed-through (unwanted direct acceptor excitation at the donor wavelength) and minimal cross talk (detection of donor emission in the acceptor channel), the FP pair was chosen to be mAmetrine and tdTomato (see figure 10 and table 1). Both FPs are considered fairly pH-

insensitive, which makes them suitable for experiments in apoptotic environments (Medintz & Hildebrandt 2013, Miyawaki 2011). The FP pair was isolated from a FRET Caspase-3 biosensor from the group of Hui-Wang Ai and Robert E. Campbell (Ai et al. 2008).

Table 1. Properties of fluorescent proteins.

Fluorophore	λ Peak-Em (nm)	λ Peak-Abs (nm)	ε (10^3 M^{-1} cm^{-1})	ϕ
mAmetrine	526	406	45	0.58
tdTomato	581	554	138	0.69
mTurquoise2	474	434	30	0.93

Note:
ε: extinction coefficient (absorbance of electromagnetic radiation based on the Beer-Lambert law).
φ: quantum yield (probability of photon emission in excited state).
(data adapted from (Ai et al. 2008, Goedhart et al. 2012)).

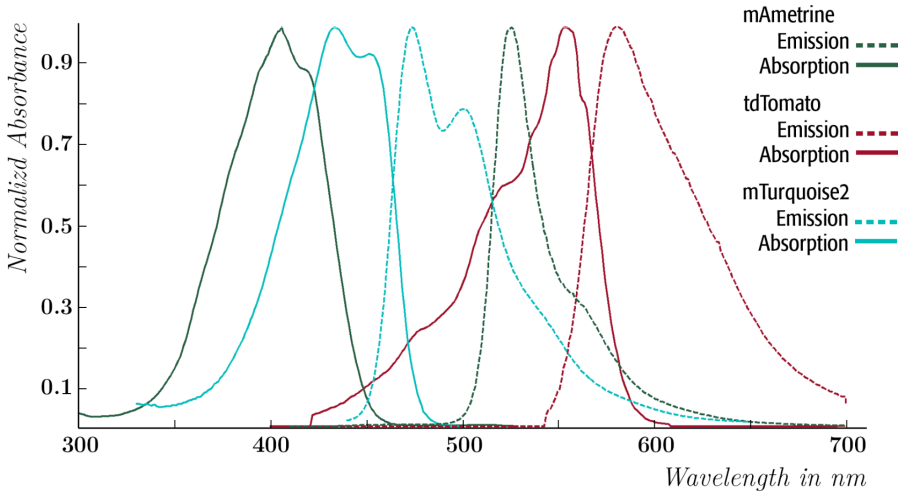

Figure 10. Fluorophore spectra of mAmetrine, tdTomato and mTurquoise2.
Datasets from (Ai et al. 2008, Goedhart et al. 2012).

mAmetrine is an *Aequorea* GFP variant with a large stoke's shift (difference between the peak emission and excitation wavelengths) and modest photostability. It features violet excitation (406 nm) and yellow emission (526 nm) wavelengths (Ai et al. 2008). If paired with a red or orange fluorescent protein, the risk of unwanted cross-excitation becomes negligible.

tdTomato, a variant of DsRed, is a highly photostable (intramolecular) tandem dimer (excitation at 554 nm; emission at 581 nm), exhibiting monomeric behavior, and is considered one of the brightest red-shifted FPs. It was particularly designed to show

good maturation and minimal aggregation and allows both N- and C-terminal fusions but may render the target protein dysfunctional due to its large size (Shaner et al. 2004).

1.3.4. FRET Caspase-3 biosensor

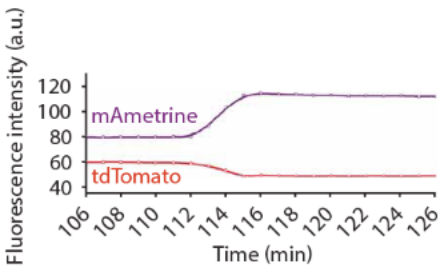

Figure 11. Caspase-3 biosensor.
After the cleavage of the intramolecular construct, the absence of FRET results in increased intensity in the mAmetrine channel and decreased intensity in the tdTomato channel. (adapted and modified from (Ai et al. 2008)).

Most FRET biosensors are built from linking fluorophores to opposite ends of a target peptide. mAmetrine-DEVD-tdTomato is an intramolecular FRET construct devised to monitor Caspase-3 activity (Ai et al. 2008). Once cleavage of the DEVD (Asp-Glu-Val-Asp) target peptide sequence occurs, a decrease in FRET can be observed (see figure 11).

1.4. Research objectives

1.4.1. Pilot experiment: In-situ assay of Caspase-3 activity upon expression of Calbindin-D28k

As of yet, evidence on the inhibition of Caspase-3 activity induced by CBD28k is still limited to in-vitro experiments. Restricted to a far less complex environment, in-vitro studies were occasionally shown to yield results that might not correspond with conditions in living cells. Thus, in-vivo/in-situ research is often necessary to confirm that these results are not limited to artificial circumstances. With the objective of providing a proof-of-concept experiment for investigating the proposed inhibition of Caspase-3 activity upon expression of CBD28k, quantitative Acceptor-Photobleaching experiments based on the intramolecular Caspase-3 biosensor with optional STS-treatment were carried out (see table 2). Caspase-dependent aggregation of chromatin (CD) as dense spherical masses, peripheral to the nucleus, was used as a morphological marker for apoptosis (Jäättelä & Tschopp 2003). For further investigation, the original experiment was adjusted and replicated with FP-labeled CBD28k, facilitating screening for co-transfection and quantification of plasmid expression.

Table 2. Experimental setup: Caspase-3 activity upon expression of Calbindin-D28k.

Experiments	Samples
Unlabeled CBD28k	mAmetrine-DEVD-tdTomato
	mAmetrine-DEVD-tdTomato + STS 10 µM, 11 hours w/ CD
	mAmetrine-DEVD-tdTomato + STS 10 µM, 11 hours w/o CD
	mAmetrine-DEVD-tdTomato + unlinked CBD28k
	mAmetrine-DEVD-tdTomato + unlinked CBD28k + STS 10 µM, 11 hours w/ CD
	mAmetrine-DEVD-tdTomato + unlinked CBD28k + STS 10 µM, 11 hours w/o CD
FP-labeled CBD28k	mAmetrine-DEVD-tdTomato
	mAmetrine-DEVD-tdTomato + mturq2-CBD28k
	mAmetrine-DEVD-tdTomato + mturq2-CBD28k + STS 15 µM, 4 hours w/o CD
	mAmetrine-DEVD-tdTomato + mturq2-CBD28k + STS 15 µM, 4 hours w/ CD

1.4.2. Investigation of intermolecular interaction between Calbindin-D28k and Pro-Caspase-3 by Acceptor-Photobleaching and Sensitized Emission

Based on evidence suggesting a possible interaction between CBD28k and Pro-Caspase-3 (Kojetin et al. 2006, Kordys et al. 2007), an intermolecular FRET experiment was carried out to investigate this association. Using the structural information available, donor (D) and acceptor (A) constructs were designed, linking target proteins with genetically-encoded FPs. In order to investigate if the occurrence of apoptosis and the conformational change of CBD28k upon calcium binding might have an effect on these interactions, cells were additionally treated with Ionomycin (INM) in order to raise intracellular calcium levels (see table 3).

Due to evidence on the interaction between CBD28k and IMPase (Almog et al. 2011), an intermolecular FRET experiment with an IMPase peptide sequence was additionally prepared.

Table 3. Experimental setup: Intermolecular interaction between Calbindin-D28k (CBD28k) and Pro-Caspase-3 (CASP3) by Acceptor-Photobleaching and Sensitized Emission.

Experiments	Samples
Controls	Untransfected cells mAmetrine-CBD28k (D) tdTomato-CASP3 (A) mAmetrine-DEVD-TdTomato (positive control) Unconjugated FPs (negative control) mAmetrine-CBD28k and tdTomato (negative control) mAmetrine and tdTomato-CASP3 (negative control)
FRET	mAmetrine-CBD28k (D) and tdTomato-CASP3 (A) ± INM 2 µM, 24 hours mAmetrine-CBD28k (D) and tdTomato-pIMPase (A) ± INM 2 µM, 24 hours

2. Materials and methods

Following section is a documentation of materials/software, which are referenced hereafter.

(A) Plasmids:

- pmAmetrine-DEVD-tdTomato (Addgene plasmid #18879) and mAmetrine-C1 (Addgene plasmid #54660) (Ai et al. 2008) was a gift from Robert Campbell & Michael Davidson.
- tdTomato-N1 was a gift from Michael Davidson & Roger Tsien (Addgene plasmid #54642).
- Calbindin-D28k cDNA originally obtained from Harry Orr (Plasmid pCD2915) (Nordquist et al. 1988).
- Caspase-3 was obtained from Source Bioscience LifeSciences, Cambridge, UK (RIKEN FANTOM clone ID I730035O10 (M13F)).
- pCMV5 (with deleted PstI, Sal I restriction sites) was obtained from Hans Thoenen's Lab (Joseph et al. 1990).
- HN10e hippocampal cell line (Lee et al. 1990), from Yves-Alain Barde's lab.
- mturq2-CBD28k construct was provided by Alex Scheiter (fellow graduate student): CBD28k-TSGTGSGAT-mTurquoise2 (58 kDa) in pcDNA3.1 vector (Mammalian expression vector w/ CMV promoter and Ampicillin resistance gene)

(B) Software:

- SerialCloner (v2.61). BioEdit (v7.2.5). Jmol (v14.6.3_2016.09.18). SnapGene Viewer (v2.8.3). NEB TM calculator (≤v1.9.4). Science Gateway Protein Molecular Weight Calculator [http://www.sciencegateway.org/tools/proteinmw.htm]. NCBI BLAST [http://blast.ncbi.nlm.nih.gov]. ImageJ (v1.49). PixFRET (v1.50). MS Office 2016. IBM SPSS Statistics 21. GraphPad Prism 7. a|e - UV-Vis-IR Spectral Software (v2.2). Adobe Photoshop and Illustrator CC 2014. ScientiFig (v2.99). Template-based protein structure modeling was created using RaptorX web server (Källberg et al. 2012, Ma et al. 2013-b). PSSpred (Protein Secondary

Structure PREDiction) (Yan et al. 2013). PSIPRED secondary structure prediction method (Buchan et al. 2013, Jones 1999).

(C) Buffers and Solutions

Buffers, solutions and chemicals were prepared according to Sambrook & Russel 2001, if not otherwise stated. Chemicals were analytical grade, from *Sigma*, if not otherwise stated.

(Joseph Sambrook and David W. Russell, Molecular Cloning - A Laboratory Manual Cold Spring Harbor Laboratory Press, Cold Spring Harbor, New York, 2001, Appendix 1)

- Radioimmunoprecipitation assay buffer (RIPA) lysis buffer: 150 mM NaCl, 1 % NP-40, 0.5 % Na-Deoxycholat, 0.1 % SDS, 50 mM Tris pH 8.0.
- MOWIOL embedding medium: 25 ml water, 6 ml 1 M Tris pH 8.5, 6 g MOWIOL (Fluka, 81381), 18.9 g glycerol.
- 10x Orange G loading buffer (NEB).

(D) Chemicals

Chemicals were of analytical grade, from Sigma, if not otherwise stated.

- Staurosporine (S4400, Sigma).
- Ionomycin (I9657, Sigma).
- DMSO (D8418, Sigma).
- PBS for cell culture: DPBS (Dulbecco's PBS, Gibco, 14200-059, devoid of calcium and magnesium).
- LB Medium and LB Agar (Roth).
- Culture medium: 450 ml Dulbecco's MEM, 50 ml heat-inactivated FBS (10 % fetal calf serum), 5 ml PS (1 %) (Penicillin, Streptomycin); sterile filtration; cold storage.
    - Penicillin-Streptomycin (P11-010, 10000 U/ml Penicillin G,10000 µg/ml Streptomycin, PAA/GE Healthcare).
    - DMEM (Dulbecco's Modified Eagle's Medium, GlutaMax, 4,5 g/l Glucose, 61965-026, Gibco).
    - FBS (Fetal Bovine Serum) (S0115, tested for mycoplasma, viruses, Biochrom AG).

- Cryo freezing medium (culture medium, DMSO (10 %); sterile filtration; cold storage at -20 °C).
- Trypsin-EDTA (0.25 % Trypsin, 1 mM EDTA, 25200-072, Gibco).
- MACSfectin reagent (Miltenyi Biotec).
- Water for cell culture and molecular biology (except gel electrophoresis). Aqua Braun (distilled, endotoxin-free, sterile, B. Braun). Millipore water.
- Skimmed milk powder (Heirler Cenovis GmbH).
- Nucleobond PC500 (Plasmid-Midi/Maxi-Prep, Machery-Nagel).
- Protein Quantification Kit, BC Assay (Interchim).

(E) Antibodies (AB) for Western Blots

- Secondary AB
    - ECL anti-rabbit IgG Horseradish Peroxidase coupled (GE Healthcare).
- Primary ABs
    - RFP: 600-401-379, polyclonal (rabbit) (Biomol).
    - αGFP: AB3080, polyclonal (rabbit) (Millipore).
    - Calbindin-D28k: Cb38a, polyclonal (rabbit) (SWANT).
    - Caspase-3: 8G10, monoclonal (rabbit) (Cell Signaling).

(F) Other Materials

- General
    - Eppendorf Safe-Lock tubes (Eppendorf).
    - Pipette tips (sterile, RNAase-free, DNAse-free, DNA-free, pyrogen-free, Starlab).
- Cell culture and microscopy
    - Microscope Coverslips (12 mm diameter, #CB00120RA1, Menzel/Thermo Fisher). Microscope slides (#02-1203, Menzel/Thermo Fisher).
    - Cell culture dishes and Centrifuge tubes (Greiner Cellstar).
    - Nalgene Rapid-Flow Sterile Disposable Filter Units (500 ml, aPES membrane, #569-0020, Thermo Fisher).
- Molecular biology and protein biochemistry
    - Amersham Hybond blotting membrane (0.2 µm, PVDF, Sigma).
    - Rotilab blotting paper (1.5 mm, #CL75.1, Roth).
    - Spectra Multicolor Broad Range Protein Ladder (Thermo Fisher).

- PCR tubes (ABgene).
- Various restriction endonucleases and CutSmart Buffer (NEB).
- 2-log DNA ladder (NEB).
- Phusion High-Fidelity DNA Polymerase (NEB).
- T4 DNA Ligase-Kit (NEB).
- 5-alpha competent Escherichia coli (NEB).
- Nucleospin Extract II-Kit (Macherey Nagel).
- SERVA Agarose (Serva GmbH).

(G) Laboratory devices

- General
  - Pipettes (2, 20, 200, 1000 µl, Gilson).
  - LABOPORT Diaphragm Vacuum Pumps (NB6 KN.18, Neuberger).
  - Various water baths. Rotilabo Block Heater H250 (Roth).
  - LSM710 confocal microscope (ZEN software, ZEISS).
- Cell Culture
  - Sterile workbenches (Berner B-MaxPro-160).
  - Thermoshake Incubator Shaker (C. Gerhardt Analytical Systems).
  - Microscope DMI (Leica).
  - Incubator New Brunswick Galaxy 170S (Eppendorf).
  - Eppendorf 5804 Series Centrifuge (Eppendorf).
  - Neubauer counting chamber.
- Molecular biology, protein biochemistry
  - Epoch Microplate Spectrophotometer (Take 3 plate, Gene 5 software, BioTec).
  - Minigel System Mini-PROTEAN 3 (Comb 1.5 mm, Bio-Rad).
  - Blotting device, semi-dry (self-constructed, Max-Planck-Institute of Neurobiology, Martinsried).
  - Powersupply: Desatronic 500/500 und Pharmacia LKB GPS 200/400.
  - Centrifuge: Biofuge Pico (Heraeus) und Eppendorf 5415 R (Eppendorf).
  - Mastercycler gradient (Eppendorf).
  - ChemiDoc Imaging System (Image Lab Software, Bio-Rad).
  - Gel Doc (Quantity One 4.4.0 software, Bio-Rad).

2.1. Molecular biology

2.1.1. pCMV5 vector plasmid

Vector plasmids are commonly used vehicles to insert foreign DNA fragments into cells. Among the basic characteristics of vector plasmids are an origin of replication, a multiple cloning site (MCS), a polyadenylation site and a selective genetic marker, providing resistance to an antibiotic agent.

pCMV plasmids are mammalian expression vectors created by the Department of Molecular Genetics, University of Texas Southwestern Medical Center (Andersson et al. 1989). The pCMV5 plasmid (4.7 kb) was acquired from Hans Thoenen's Lab. Restriction enzyme digestion and DNA sequencing were performed for verification. This pCMV5 vector features a pBR22 and bacteriophage f1 origin of replication (ori), an Ampicillin resistance gene, a SV40 origin, a human growth hormone fragment (hGH) that includes polyadenylation and transcription termination signals, a CMV promoter and a multiple cloning site that contains unique restriction sites for EcoR1, Bgl2, Kpn1, Miu1, Cla1, Hind3, Xba1, BamH1, XmaI and Sma1 (see table 4). For further details, see *Suppl.: pCMV5 vector plasmid*.

Table 4. Restriction enzymes incompatible with target proteins.

RE	mAmetrine*	CBD28k	CASP3	tdTomato	pIMPase*
EcoRI (920)		**X**	**X**		
Bgl2 (926)		**X**			
Kpn1(932)	**X**				
MluI (938)	**X**				
ClaI(944)					
Hind3 (950)					
XbaI (974)					
BamH1 (980)					
XmaI (984)					
SmaI (984)					

Note:
[*with linker sequence] [X=cutting the specified sequence]

2.1.2. Primer design and Polymerase Chain Reaction (PCR)

Polymerase Chain Reaction (PCR) is a standard laboratory procedure used for exponential amplification of specific DNA sequences. Utilizing thermostable DNA polymerases, specific DNA is exponentially amplified by reiterated cycles of denaturation (~ 95 °C), annealing (~ 50 - 72 °C) and elongation (~ 72 °C).

All PCR reactions were performed with a thermostable polymerase (Phusion High-Fidelity DNA Polymerase, NEB), based on an enhanced Pyrococcus-like fusion enzyme. Forward and reverse primer pairs were designed in BioEdit for N-terminal fusion proteins. Virtual PCRs were simulated in SerialCloner. Designed primers were ordered from *biomers.net GmbH* and processed according to the supplied protocol. PCRs were performed with respective settings calculated by NEB TM calculator.

2.1.2.1. mAmetrine primers

Complete forward primer (EcoR1):
5'-GAC-TAT-gaattc-GCC-ACC-ATG-GTG-AGC-AAG-3'

Complete reverse primer (Hind3):
5'-TAG-ATC-aagctt-TCC-ACT-GCC-ACT-GCC-GGT-3'

NEB TM calculator [Phusion High-Fidelity DNA Polymerase (HF Buffer], 500 nM)

- PCR Annealing Temp.: Complete Primer 72 °C / Gene-specific 66 °C
- Forward primer: Complete Primer 76 °C / Gene-specific 66 °C
- Reverse primer: Complete Primer 79 °C / Gene-specific 71 °C

A detailed documentation of the primer design can be found in *Suppl.: mAmetrine forward and reverse primer*.

2.1.2.2. Calbindin-D28k primers

Complete forward primer (Hind3):
5'-TAA-GTA-aagctt-ACT-ACG-ATG-GCA-GAA-TCC-3'

Complete reverse primer (BamH1):
5'-TAA-GTA-ggatcc-CTA-GTT-GTC-TCC-AGC-AGA-3'

NEB TM calculator [Phusion High-Fidelity DNA Polymerase (HF Buffer], 500 nM)

- PCR Annealing Temp.: Complete Primer 70 °C / Gene-specific 54 °C
- Forward primer: Complete Primer 67 °C / Gene-specific 58 ° C
- Reverse primer: Complete Primer 70 °C / Gene-specific 54 ° C

A detailed documentation of the primer design can be found in *Suppl.: CBD28k forward and reverse primer*.

2.1.2.3. tdTomato primers

Complete forward primer (EcoR1):
5'-TAT-GTA-gaattc-GAT-GGT-ATG-GTG-AGC-AAG-3'

Complete reverse primer (Kpn1):
5'-CAC-CTA-ggtacc-CTT-GTA-CAG-CTC-GTC-CAT-3'

NEB TM calculator [Phusion High-Fidelity DNA Polymerase (HF Buffer], 500 nM)

- Annealing Temp.: Complete Primer 72 °C / Gene-specific 53 °C
- Forward primer: Complete Primer 70 °C / Gene-specific 56° C
- Reverse primer: Complete Primer 73 °C / Gene-specific 53 °C

A detailed documentation of the primer design can be found in *Suppl.: tdTomato forward and reverse primer*.

2.1.2.4. Caspase-3 primers

Complete forward primer (Kpn1):
5'- GGT-CGT-ggtacc-ACC-ATG-GAG-AAC-AAC-AAA-3'

Complete reverse primer (Cla1):
5'-GCG-GGC-atcgat-CTA-GTG-ATA-AAA-GTA-CAG-3'

NEB TM calculator [Phusion High-Fidelity DNA Polymerase (HF Buffer], 500 nM)

- Annealing Temp.: Complete Primer 72 °C / Gene-specific 40 °C
- Forward primer: Complete Primer 77 °C / Gene-specific 56 °C
- Reverse primer: Complete Primer 72 °C / Gene-specific 40 °C

A detailed documentation of the primer design can be found in *Suppl.: CASP3 forward and reverse primer*.

2.1.2.5. Partial IMPase primers

Oligonucleotide primer pair:
5'-gta-tta-ggt-acc-gga-agt-gga-agc-ggc-agc-ggc-agc-ggc-agc-acc-ggc-ctg-gtg-acc-gtg-acc-gac-cag-aag-gtg-gag-aag-atg-ctg-3'

5'-gcg-cta-atc-gat-tta-tca-ctc-ctc-gcc-gat-gaa-gct-gtg-gca-ggg-gta-ctt-ctc-ctt-gat-gct-gct-cat-cag-cat-ctt-ctc-cac-ctt-ctg-gtc-3'

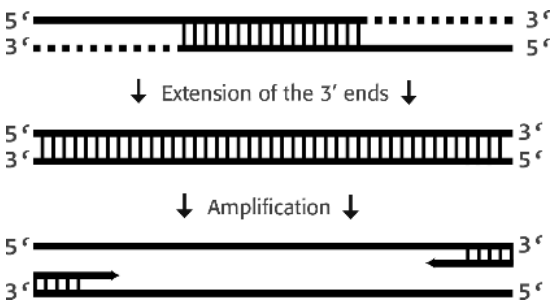

Figure 12. pIMPase PCR.
PCR was performed without template. 5 cycles extending the 3' ends, where followed by amplification of the PCR product with 2 amplification primers.

- Primers were hybridized to yield partially overlapping double strand
- 5 cycles to extend the 3' ends
- Annealing Temp.: 68 °C

Amplification forward primer (Kpn1):
5'-GTA-TTA-ggt-acc-GGA-AGT-GGA-3'

Amplification reverse primer (Cla1):
5'-GCG-CTA-atc-gat-TTA-TCA-CTC-3'

- 30 cycles
- Annealing Temp.: 61 °C

PCR was performed as illustrated in figure 12. A detailed documentation of the primer design can be found in *Suppl.: IMPase design and construction*.

2.1.3. Restriction enzyme (RE) digestion

Restriction endonucleases, commonly used as molecular cutting tools, are proteins that are capable of detecting and cutting specific DNA sequences. After detection of a specific restriction site, REs cut DNA leaving either sticky or blunt ends.

Vector plasmids and the PCR products were processed with respective matching REs, so that resulting fragments could be inserted into linearized vector plasmids. After mixing DNA samples with REs and the respective buffers, samples were usually (shortly) centrifuged and incubated at 37 °C for approximately 1 hour in a block heater.

2.1.4. Gel electrophoresis (GE)

Gel electrophoresis (GE) is a standard laboratory procedure for separating DNA molecules by size. Making use of its negative charge, DNA moves towards the anode through pores of the agarose gel in an electrical field. Speed is strongly dependent on size and conformation of the respective fragments. When labelled with ethidium bromide, an intercalating agent used for DNA detection, DNA becomes visible under UV light.

Analytical and preparative gels were prepared with SERVA-Agarose (Agarose (1 %) gels). Agarose powder was mixed with Tris-acetate-EDTA (TAE) buffer and then heated in a microwave. Afterwards, ethidium bromide was added. The mixture was then

poured into the GE-chamber (with a suitable comb) and could gel for about 20 - 30 minutes. DNA samples were mixed with a loading buffer (w/ tracking dye), to increase density and visibility of the sample. At last, a 2-log DNA ladder and DNA samples were loaded. GEs were usually performed at 75 V/68 mA for 45 minutes.

GE was primarily used for verification of PCR products by size of the amplificate, isolation of fragments or for the purpose of verification of plasmids in analytic digests. Gels were then visualized and documented.

2.1.5. Ligation of DNA

Ligations were used to insert DNA fragments into linearized vector (pCMV5) backbones.

Eluates obtained from purification (see chapter 2.1.6), were ligated using a T4 DNA Ligase kit (NEB). The average DNA concentrations were determined using a spectrophotometer. A control sample without DNA insert was prepared as well as a ligation sample with 1:3 and 1:6 molar ratio of DNA insert and vector. Incubation was carried out at room temperature for 10 minutes (for sticky ends). Heat inactivation was done at 65 °C (where applicable) for 10 minutes, followed by chill on ice and subsequent transformation (see chapter 2.2.1).

2.1.6. Purification of DNA

Purifications were performed after isolating bands from agarose gels. Dyed fragments were cut out from the gel under UV light control and were then purified by binding DNA to a silica membrane prior to elution (Nucleospin Extract II-Kit, Macherey-Nagel).

2.1.7. DNA sequencing

DNA sequencing was performed by *Eurofins Genomics GmbH* using the dideoxy-chain termination method (Sanger et al. 1977). For verification, the reports were then compared with the respective anticipated sequence.

2.1.8. SDS-Page and Western Blot

Western blot is an analytical method for specific protein detection (Towbin et al. 1979). Using protein-specific antibodies, proteins within a cellular lysate are stained on a

membrane. Western Blots were primarily used for fusions construct verification and assay of protein expression.

Cells were lysed with RIPA buffer (0.5 ml/6 cm dish). Cell culture plates on ice were carefully shaken on a swivel plate for 30 minutes. Loaded into a tube, the mixture was centrifuged for 10 minutes at 10000 g and 4 °C. Afterwards, the pellet was stored and the protein concentration of the supernatant was determined using a spectrophotometer. Proteins were then separated by sodium dodecyl sulfate (SDS) polyacrylamide gel electrophoresis (PAGE) as described in Sambrook & Russel (2001). Protein samples (20 µg in 20 µl) were mixed with 5 µl 1 M dithiothreitol (DTT) and 8 µl SDS-Page loading buffer. The mixture was shortly centrifuged, heated to 95 °C for 5 minutes for denaturation and then cooled at room temperature. A protein ladder with pre-stained chromophore-labeled proteins, was used for the determination of molecular weight. Prior to electrophoresis, SDS was pre-heated to 37 °C to prevent precipitation. Electrophoresis was then performed at 100 V for approximately 30 minutes, then at 200 V for another 45 minutes.

Proteins were transferred to a membrane using transfer cassettes assembled from 2x blotting paper, PVDF membrane, SDS-PAGE gel and 2x blotting paper. Beforehand, components of the transfer cassette were primed for usage: incubation of the gel in transfer buffer for 15 minutes (on a swivel plate); immersion of the blotting paper in transfer buffer and the membrane in methanol for 10 seconds, then water for 5 minutes and at last in transfer buffer. Transfer cassettes were inserted into the loaded semi-dry blotter and blotting was performed for 1 hour at 260 mA. Afterwards, the membrane was washed in (deionized) water for 5 minutes, which was followed by reversible Ponceau S staining to assess the transfer efficiency. Then, the membrane was washed in blotting buffer and subsequently immersed in the block buffer (Dried milk powder (5 %), Tween (0.2 %) 20 in phosphate buffered saline (PBS)) for 1 hour to prevent non-specific binding. The first antibody (in 5 ml blotting buffer; at the dilution specified below) was applied and incubated overnight at 4 °C on the swivel plate. After application of the first antibody, the membrane was thoroughly washed in washing buffer and the secondary antibody, conjugated with peroxidase (details below), was added at the appropriate dilution and incubated in washing buffer for 1 hour at room temperature. After incubation with detection reagent, the membrane was washed in washing buffer and, subsequently, imaged and documented.

- Western Blot of mAmetrine-CBD28k with CBD28k-antibody:
  Antibody: Cb38 (1:10000). 2. Antibody: α rabbit peroxidase (1:10000)
- Western Blot of mAmetrine-CBD28k with GFP-antibody:
  Antibody: αGFP (1:2000). 2. Antibody: α rabbit peroxidase (1:10000)
- Western Blot of tdTomato-CASP3 with Caspase-3-antibody:
  Antibody: Caspase-3 (1:1000). 2. Antibody: anti rabbit peroxidase (1:10000)
- Western Blot of tdTomato-CASP3 with RFP-antibody:
  Antibody: RFP (1:2000). 2. Antibody: α rabbit peroxidase (1:10000)

Note:

- each lane with ~ 20 µg in 22 µl
- Calbindin-D28k: D505.11 (mouse cerebellar lysate), 10 µg

2.2. Cellular biology

2.2.1. Transformation

Transformation describes the transfer of exogenous genetic material into bacterial cells. Vectors were transformed into 5-alpha competent Escherichia coli according to the manufacturer's High Efficiency Transformation Protocol.

5-alpha competent Escherichia coli (NEB), stored at -80 °C in dry ice, were thawed on ice for 10 minutes. 5 µl with 100 ng of plasmid DNA were added, gently mixed and then put on ice for 30 minutes. A heat shock (90 seconds at 42 °C) was applied, which was followed by 5 minutes on ice. 950 µl (room temperature) SOC were added to the tube, which was then incubated in a bacterial incubator shaker for 45 minutes at 37 °C for optimal cell recovery and antibiotic resistance expression. Afterwards, 100 µl of each sample (1:3 and 1:6 molar ratios, digested and intact vector, ligation control sample) was evenly spread onto a pre-warmed (37 °C) Ampicillin selection plate. Finally, the selection plates were incubated at 37 °C for 12 - 24 hours.

2.2.2. Isolation and expansion of clones

Clones were carefully picked from the incubated selection plates and suspended in a mixture of 5 ml LB-medium and 100 µg/ml Ampicillin. Then, the cell mixture was incubated overnight at 37 °C in a bacterial incubator shaker.

2.2.3. Plasmid preparation

DNA-Mini- and DNA-Maxi-Preps are commonly used methods to extract and purify plasmid DNA. Maxi-Preps were carried out using anion-exchange chromatography, according to the manufacturer's specifications (Nucleobond PC500, Machery-Nagel).

DNA-Mini-Prep: 1.5 ml of bacterial culture was added into a tube. The tube was centrifuged for 10 minutes at 12000 g. While supernatant was carefully removed, the pellet was resuspended with a resuspension buffer. Then, an alkaline lysis buffer was added to the sample to induce cell lysis. This was followed by a neutralization buffer. Afterwards, the sample was centrifuged at 12000 g to clarify the lysate. For precipitation, 300 µl of the supernatant were added to 300 µl isopropyl alcohol. Each

sample was then mixed, incubated for 5 minutes at room temperature and centrifuged at 12000 g for 10 minutes. Following, supernatants were carefully removed, pellets were washed with ethanol (70 %) and centrifuged for 1 minute at 12000 g. Again, supernatant fluid was removed and pellets were dried at 37 °C, and in a final step resuspended in 5 µl RNAase-free water. Afterwards, a restriction enzyme digestion was carried out for verification.

2.2.4. Preparation of eukaryotic cell lines

All experiments were carried out with the murine hippocampal HN10e cell line.

Revitalization/Thawing of HN10e cells

A falcon tube (6 ml) and a culture dish (8 ml) were filled with pre-warmed (37 °C) culture medium. Cryopreserved cells were warmed up to 37 °C in a water bath and transferred into the falcon tube for dilution of the potentially cell damaging cryo freezing medium. Then, the tube was centrifuged at 300 g for 5 minutes. After removal of supernatant fluid, pelleted cells were resuspended with 2 ml of culture medium, transferred onto the culture dish and finally incubated at 37 °C and 10 % CO_2 in air for the period required.

Cell passage

After aspiration of culture medium, a washing step with either 2 - 5 ml of PBS + 1 mM EDTA solution or Trypsin (0.25 %) solution was carried out. This was followed by aspiration of residual fluids and addition of 1 ml Trypsin (0.25 %) to detach cells. Plates were then incubated at 37 °C and 10 % CO_2 in air for up to 10 minutes if required. For dilution and inhibition of trypsin, the cell mixture was added into a falcon tube with 2 - 5 ml culture medium. Subsequently, falcon tubes were centrifuged at 300 g for 5 minutes. Supernatant fluid was carefully removed and cells were resuspended with 2 - 4 ml of culture medium. Cells were then allocated on culture dishes in culture medium and finally incubated at 37 °C and 10 % CO_2 in air as required.

Preparation of cells for experiments

After cell passage, cells were counted in a counting chamber and plated at the desired subconfluent densities.

Preparation of cells for Western Blot

After cell passage, cells were plated on 6 cm cell culture dishes in culture medium of the subconfluent densities detailed in the protocol of the transfection kit (see chapter 2.2.5.) and prepared for Western Blot according to protocol.

Preparation of cells for indirect immunofluorescence

After cell passage, allocation of approximately 20000 cells/100 µl onto each CS (3 CS per each 3 cm dish). Incubation at 37 °C and 10 % CO_2 in air for approximately 2 hours. Culture dishes were finally filled with 1.5 ml culture medium. If needed, cells were treated with cytotoxic agents (see chapter 2.2.6.).

2.2.5. Transient transfection

Transfection describes the transfer of exogenous genetic material into eukaryotic cells. Transient transfections were performed to insert vector plasmids into the murine hippocampal HN10e cell line. All transfections were carried out according to protocol using a transfection kit (MACSfectin reagent, Miltenyi Biotec) based on cationic lipopolyamines.

Standard transfections were performed with 6 or 12 µg of total DNA per 6 or 10 cm dish, respectively, on 60 - 80% subconfluent cells (equal amount of each DNA in case of double transfections). Transfection efficiencies were between 50 - 70%.

After separately diluting DNA and reagent in DMEM (without additions), both samples were briefly mixed and incubated at room temperature for 20 minutes to allow complex formation. After drop-wise addition of transfection complexes, cells were incubated under standard conditions for 1 – 3 days.

2.2.6. Application of cytotoxic agents

Dimethyl sulfoxide (DMSO)

Dimethyl sulfoxide is a commonly used aprotic solvent for polar and nonpolar molecules.

However, it is known that DMSO causes cytotoxic plasma membrane pore formation at low concentration of 10 %. Interestingly, even at very low concentrations of 2 – 4 %, DMSO seems to be able to induce Caspase-3 independent cell death in neuronal cell lines (Galvao et al. 2014).

Ionomycin (INM)

Ionomycin is a Ca^{2+}-ionophore, which is produced by the bacterium Streptomyces conglobatus. It is widely used as a research tool to induce Caspase-3-mediated cell death, raise intracellular calcium levels and stimulate an inflammatory response by expressing cytokines (Liu & Hermann 1978).

Treatment with INM was performed with 2 µM for 24 hours (see 1.4.2.).

Staurosporine (STS)

Staurosporine, which was isolated from the bacterium Streptomyces staurosporeus, is an ATP-competitive kinase inhibitor, which is capable of inducing caspase activation a few hours after its application (Nakano 2009).

Treatment with STS was performed with either 10 µM for 11 hours or 15 µM for 4 hours (see 1.4.1.).

2.2.7. Preparation of slides for confocal microscopy

Preparation of coverslips (CS)

After cleansing with ethanol (100 %), 3 CS were placed on each 30 mm cell culture dish. All dish plates were washed with distilled water to remove residual ethanol. Following aspiration, CS were left to dry at room temperature. 100 µl of Poly-L-Lysine (average molecular weight 70 kDa; 0.01 %) (PLL) was added to each CS. Dishes were then incubated at 37 °C and 10 % CO_2 in air for at least 1 hour. After aspiration of residual PLL, 3 more washing steps with distilled water were carried out and CS were subsequently dried.

Preparation of slides

Cells were transfected (see chapter 2.2.5.) and transferred to CSs (see chapter 2.2.4.). After aspiration of culture medium, a washing step with 1 ml PBS was performed. Cells were fixated with 1 ml PFA (4 %) at room temperature for 15 minutes. This was followed by 3 more washing steps with PBS (last washing step excludes the aspiration of PBS). CS were mounted in 6 µl Mowiol (warmed in a water bath at 37 °C) on standard microscopy slides. After removal of residual fluid, 3 CSs were transferred onto each slide with the CS's surface facing the slide's surface. Pressure was softly applied to reassure direct contact between CSs and slide. Slides were then stored in a light-free environment at room temperature for 12 - 72 hours. During imaging, CS were usually kept at room temperature for approximately 6 - 10 hours.

2.3. Confocal-Imaging

All cells were assayed with the ZEISS LSM710 confocal microscope. Before confocal imaging, samples were analyzed for general vitality and brightness under epifluorescence (both GFP and DsRed Preset with 60x magnification).

It is known that unfavorable stoichiometry beyond 10:1 or 1:10 can limit the validity of intermolecular FRET-measurements (Berney & Danuser 2003, Chen et al. 2006). Based on samples transfected with the intramolecular FRET biosensor and, therefore, with 1:1 ratio, an Acceptor-to-Donor ratio (mean ADR = 1.78; n = 10;) was calculated from the respective absolute intensities. Consequently, an ADR-range of 0.16 - 3.4 (mean ± 4.5-fold standard deviation) was determined and defined as sample selection criteria to avoid substantial unfavorable stoichiometry. Samples beyond this range were discarded.

In intermolecular FRET experiments, each sample was sequentially analyzed by Sensitized Emission, then Photobleaching, for the purpose of inter-methodological comparison of FRET-efficiency. Therefore, it was necessary to keep imaging-induced bleaching to a minimum. The bleaching step was performed early on after 1/5 scans and the total number of images acquired for SE was limited to 2 scans. Screening under epifluorescence was carried out with low lamp power to reduce potential photo-bleaching. Moreover, laser transmission power and scan speed settings were optimized.

Gain settings were kept low to reduce noise and allow overhead in the dynamic range. The final imaging-configuration was determined after extensive pilot experiments. Within each experiment, all samples were assayed with the same settings.

2.3.1. Imaging-Configuration

Acceptor-Photobleaching

- Image size: x: 256, y: 256 / time: 5 / channels: 2 / 16-bit / Dimension: x: 33.61 µm, Y: 33.61 µm / Zoom: 4.0 / pixel dwell time: 5.09 µs / average: 1
- tdTomato-channel: Master Gain: 700 / 561 nm laser at 0.1 % / Pinhole 49 µm | 0.78 Airy Units | 0.8 µm section / Digital Offset: 0 / Digital Gain: 1
- mAmetrine-channel: Master Gain: 675 / 405 nm Laser at 1 % / Pinhole 49 µm | 0.99 Airy Units | 0.7 µm section / Digital Offset: 0 / Digital Gain: 1
- Bleach event after 1/5 images at 561 nm with 55 % laser transmission
- Objective: Plan-Apochromat 63x/1.40 Oil DIC M27 / Detector settings: 499 - 537
- Beam splitters: MBS: MBS 458/561 / MBS_InVis: MBS -405 / DBS1: Mirror / FW1: NoneLSM
- Scan mode plane, time series

mTurquoise2 quantification

- Image size: x: 256, y: 256 / time: 2 / channels: 1 / 16-bit / Dimension: x: 33.61 µm, Y: 33.61 µm / Zoom: 4.0 / pixel dwell time: 5.09 µs / average: 1
- mTurquoise2-channel: Master Gain: 600 / 405 nm laser at 1 % / Pinhole 45 µm | 1 Airy Units | 0.7 µm section / Digital Offset: 0 / Digital Gain: 1
- Objective: Plan-Apochromat 63x/1.40 Oil DIC M27 / Detector settings: 455 - 499
- Beam splitters: MBS: MBS 458/561 / MBS_InVis: MBS -405 / DBS1: Mirror / FW1: NoneLSM
- Scan mode plane, time series

Sensitized Emission

- Image size: x: 256, y: 256 / time: 2 / channels: 2 / 16-bit / Dimension: x: 33.61 µm, Y: 33.61 µm / Zoom: 4.0 / pixel dwell time: 5.09 µs / average: 1
- Multitrack configuration: Pinhole 49 µm | 0.99 Airy Units | 0.7 µm section
  - tdTomato-channel: Master Gain: 700 / 561 nm laser at 0.1 % / Digital Offset: 0 / Digital Gain: 1
  - mAmetrine-channel: Master Gain: 675 / 405 nm Laser at 1 % / Digital Offset: 0 / Digital Gain: 1
- Objective: Plan-Apochromat 63x/1.40 Oil DIC M27 / Detector settings: Ch1: 499 - 537, Ch2: 602 - 693
- Beam splitters: MBS: MBS 458/561 / MBS_InVis: MBS -405 / DBS1: Mirror / FW1: NoneLSM
- Scan mode plane, time series

2.3.2. Data acquisition and analysis

In theory, one would assume spectral bleed-through (SBT) ratios to remain constant. However, it was demonstrated that these values can vary substantially dependent on the absolute intensity measured on confocal microscopes with more than one photomultiplier for detection of donor and acceptor channel (Feige et al. 2005). Matching SBT ratios to measured FRET-sample intensities is an alternate approach to linear or exponential SBT models that can provide FRET calculations with higher accuracy, particularly when FP concentration varies strongly and low FRET-efficiencies are expected (Feige et al. 2005). For less false positive results, SBT correction factors for each (arbitrarily designated) intensity group (4000 - 9999, 10000 - 14999, 15000 - 19999, 20000 - 25000) were defined as sum of the average SBT correction factor and its standard deviation. For these experiments, measurements with absolute intensities $< 4 \times 10^3$ and $> 25 \times 10^3$ (on a 16-bit scale) were discarded to avoid samples with substantial overexpression, which can potentially result in non-physiological effects, and, additionally, prevent growing impact of artefacts on the calculated FRET-efficiency at lower absolute intensities. SBT correction factors were determined for the donor construct and the CASP3 acceptor construct. For validation, the SBT correction factors were also calculated for the respective unconjugated FPs, which showed similar results. Therefore, SBT correction factors from the FP-conjugated constructs were applied for all nFRET calculations. In Caspase-3 activity experiments, both ADR-range and absolute intensity thresholds (for rejection) were not established.

The obtained data was analyzed in Microsoft Excel 2010 with the respective formulas (see chapter 1.3.2.). Background subtraction (variable ROI without cellular overlap) was carried out on all images. Region of interest (ROI) for analysis and bleaching was defined as the cell soma. On selected cells, a pixel-by-pixel analysis using ImageJ and PixFRET was performed to investigate compartmental FRET (Feige et al. 2005). For analysis in PixFRET, slice 1 was selected for analysis. The images were processed with a Gaussian blur of 1.5 to reduce noise and improve rendering of the computed image. Intensity-matched SBT correction factors were defined as constants. Threshold correction factor was set to 2 and normalization by the square root of the product of donor and acceptor intensities was selected. nFRET images were stored as 32-bit TIF files. For the purpose of illustration, *Rainbow2 Look Up Table (LUT)* was additionally applied.

All statistical analysis was performed in IBM SPSS Statistics 21 or GraphPad Prism 7. Homogeneity of variance was tested using Brown-Forsythe test (reported where violation of homogeneity occurred). All comparisons performed were planned and were reported. Significance was assessed using either Student's unpaired t-test or Mann-Whitney U test for two-group comparisons or one-way ANOVA (with either Bonferroni's or Dunnett's multiple comparison test) for more than two-group comparison with nearly equal sample size or Kruskal-Wallis test (with Dunn's post hoc test) with a 95 % confidence interval (* = $p < 0.05$, ** = $p < 0.01$, *** = $p < 0.001$).

2.4. Miscellaneous

GraphPad Prism 7, Adobe® Photoshop CC, Adobe® Illustrator CC and ScientiFig were used to create scientific illustrations (Aigouy & Mirouse 2013). a|e - UV-Vis-IR Spectral Software was used for the visualization of spectral properties.

3. Results

3.1. Fusion proteins

3.1.1. FRET donor: mAmetrine-CBD28k

The amino-/N-terminal fusion protein was constructed within the MCS of a pCMV5 vector plasmid consisting both of mAmetrine (without Stop-Codon) and CBD28k (with Stop-Codon) (see figure 13). Both components were bridged by a flexible linker sequence (GTGSGSG-KLTT). The sequenced construct can be seen in *Suppl.: mAmetrine (incl. linker and without TAA stop codon) + EcoR1 + CBDK28k (incl. stop codon) inserted in pCMV5 multiple cloning site*. Protein expression was confirmed by Western Blot (see figure 14). Construct appeared functional in indirect immunofluorescence (data not shown).

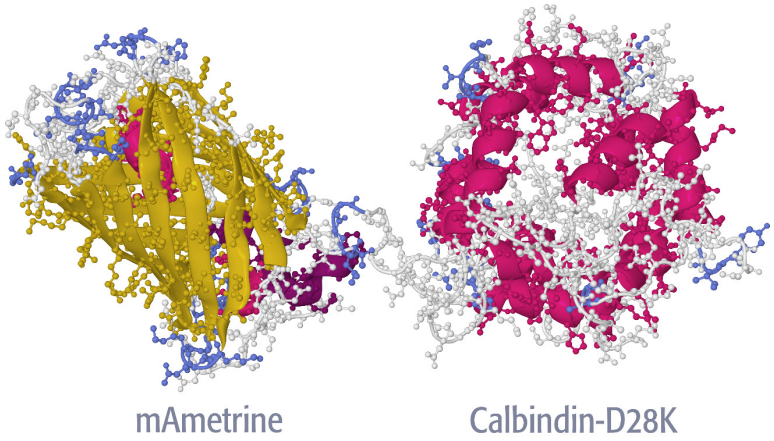

Figure 13. Structure prediction of mAmetrine-CBD28k (57 kDa).
Some residues of CBD28k are not modeled due to lack of reasonable templates. RaptorX structure prediction displayed using Jmol and colored according to secondary structure.

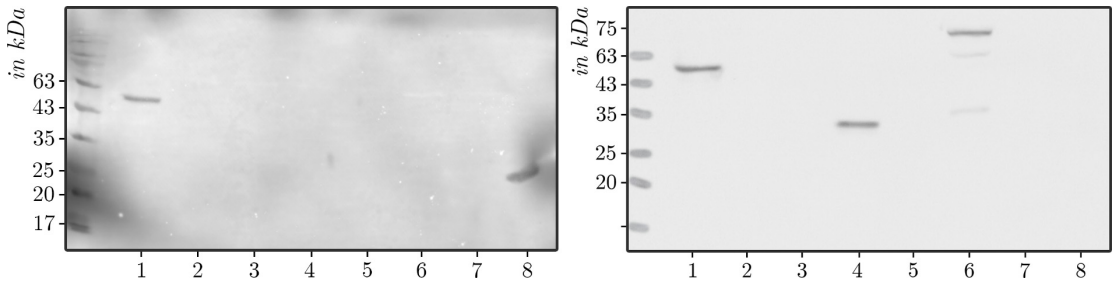

Figure 14. Western Blot of mAmetrine-CBD28k fusion construct.
Samples on the left panel were probed with a CBD28k-AB. Samples on the right panel were probed with a GFP-AB. (1) mAmetrine-CBD28k, (2) tdTomato-pIMPase, (3) tdTomato-CASP3, (4) mAmetrine, (5) tdTomato, (6) mAmetrine-DEVD-tdTomato, (7) Control, (8) CBD28k (mouse cerebellar lysate).

3.1.2. FRET acceptor: tdTomato-CASP3

An amino-/N-terminal fusion protein was constructed within the MCS of a pCMV5 vector plasmid consisting of tdTomato (without Stop-Codon) and Pro-Caspase-3 (with Stop-Codon) bridged by a linker sequence (GTT) built from small, uncharged amino acids for least interaction and high flexibility (Chen et al. 2013) (see figure 15). The sequenced construct can be found in *Suppl.: TdTomato (without TAA stop codon) + Kpn1 + GTT-Linker + CASP3 (incl. stop codon) inserted in pCMV5 multiple cloning site.* Protein expression was confirmed by Western Blot (see figure 16). Construct appeared functional in indirect immunofluorescence (data not shown).

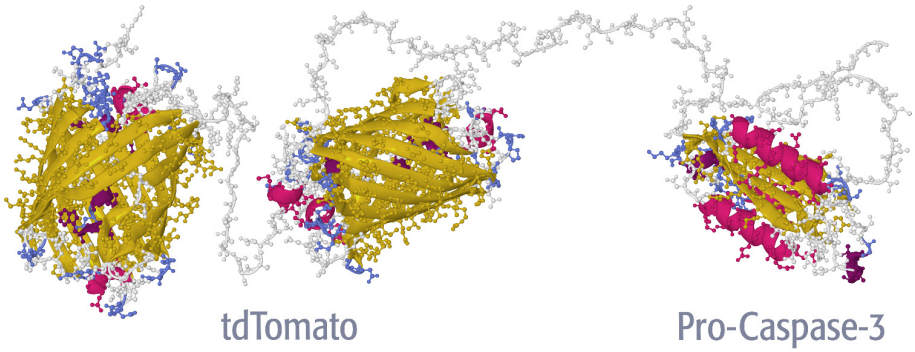

Figure 15. Structure prediction of tdTomato-CASP3 (76 kDa).
RaptorX structure prediction displayed using Jmol and colored according to secondary structure.

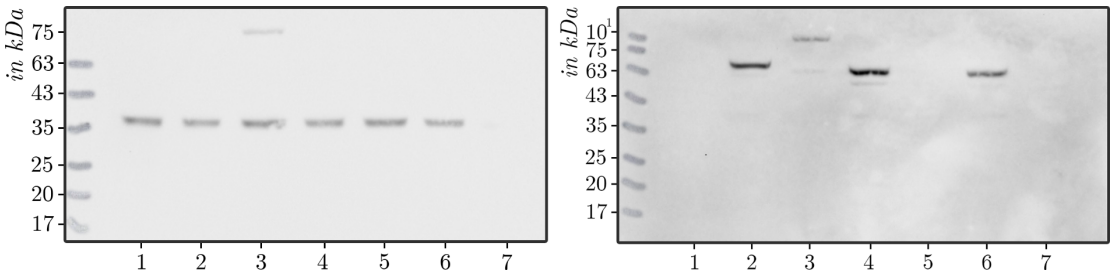

Figure 16. Western Blot of the tdTomato-CASP3 and tdTomato-pIMPase fusion constructs.
Samples on the left panel were probed with a Caspase-3-AB. Samples on the right panel were probed with a RFP-AB. (1) mAmetrine-CBD28k, (2) tdTomato-pIMPase, (3) tdTomato-CASP3, (4) mAmetrine-DEVD-tdTomato, (5) mAmetrine, (6) tdTomato, (7) CBD28k (mouse cerebellar lysate). Bands at ~ 35 kDa show endogenous Caspase-3.

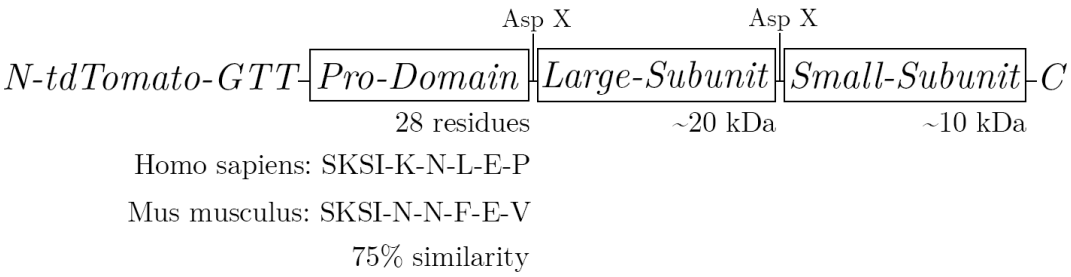

Figure 17. Caspase-3 pro-domain within tdTomato-CASP3 construct.
The suggested pro-domain interaction site of Homo sapiens and Mus musculus shows a similarity of 75 %. Similarity determined using NCBI BLAST. Asp X: Cleavage occurs after specific aspartate residues.

While large and small subunits of caspases usually share high sequence homology, the contrary applies to their pro-domains. Although initiator caspases feature long pro-domains of over 100 amino acids including specific interaction motifs, effector caspases, such as Caspase-3, characteristically have short pro-domains (~ 30 residues) (Chang & Yang 2000). As demonstrated in figure 17, a minor interspecies variation in target peptide sequence between the pro-domain of Homo sapiens and Mus musculus exists.

3.1.3. FRET acceptor: tdTomato-pIMPase

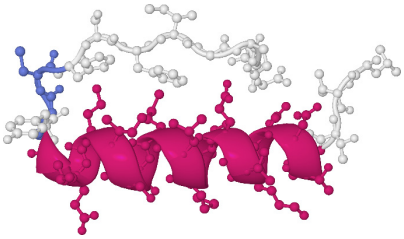

Figure 18. Structure prediction of pIMPase.
Seq.: LVTVTDQKVEKML-MSSIKEKYPCHS-FIGEE. RaptorX structure prediction displayed using Jmol and colored according to secondary structure.

Earlier studies showed that the interaction site is a helix-associated 12 amino acid sequence (residues 55 – 66; MSSIKEKYPCHS) (Almog et al. 2011). Based on predictions of IMPase's secondary structure (see *Suppl.: IMPase secondary structure*), it was concluded that the residues 42 – 71 (LVTVTDQKVEKML – MSSIKEKYPCHS - FIGEE) would make a helix formation probable (see figure 18). Moreover, matching murine IMPase1 and CBD28k were selected to prevent inter-species incompatibility as previously reported (Almog et al. 2011).

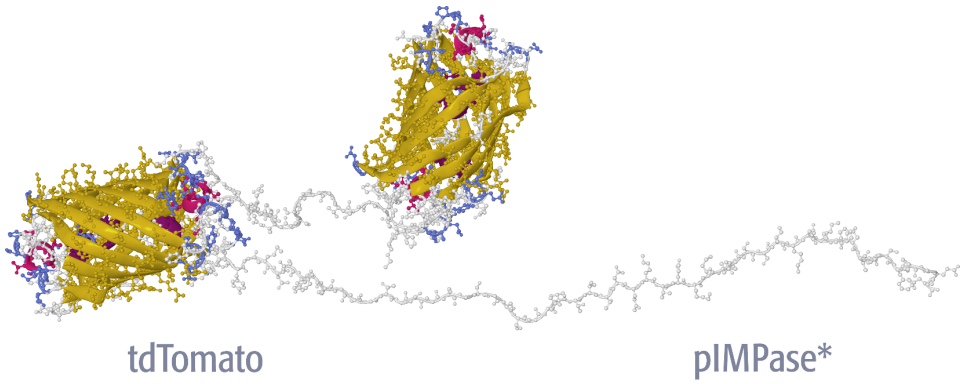

Figure 19. Structure prediction of tdTomato-pIMPase (59 kDa).
Partial IMPase is not modeled due to lack of reasonable templates. RaptorX structure prediction displayed using Jmol and colored according to secondary structure.

An amino-/N-terminal fusion protein was constructed within the MCS of a pCMV5 vector plasmid consisting both of tdTomato (without Stop-Codon) and a partial IMPase sequence (with Stop-Codon) bridged by a linker sequence (GTGTGSGSGSGSTG) (see

figure 19). The sequenced construct can be found in *Suppl.: tdTomato (without TAA stop codon) + Kpn1 + Linker + partial IMPase sequence (incl. stop codon) inserted in pCMV5 multiple cloning site*. Protein expression was confirmed by Western Blot (see figure 16). Construct appeared functional in indirect immunofluorescence (data not shown).

3.2. Pilot experiments

Unattached mAmetrine and its fusion with CBD28k were predominantly localized in the cytosol und nucleus. Unconjugated tdTomato, tdTomato-CASP3 and the mAmetrine-DEVD-tdTomato construct were mainly found in the cytosolic milieu and were excluded from the nucleus.

3.2.1. Signal increase upon photobleaching

Pilot experiments with tdTomato-CASP3-transfected cells showed that there is a signal increase in the mAmetrine-Channel upon photobleaching. While the signal increase occurred upon photobleaching (80 % laser transmission at bleaching event), it did not appear in a time series (30 images without bleaching event; each with 1 % laser transmission). The extent of signal increase appeared to correlate with the initial tdTomato intensity and the (bleaching) laser transmission power. Reducing photobleaching laser transmission (from 80 % to 55 %) resulted in decreased signal increase. A series of repetitive bleaching experiments showed that there was a gradual recovery (1.07- to 1.12-fold) of tdTomato signal after the photobleaching event. Moreover, a distinct homogenous green emitting signal, stronger than the autofluorescence of non-transfected cells, could be detected in tdTomato-CASP3 expressing cells in epifluorescence (GFP filter). Signal increase upon photobleaching in the mAmetrine channel was corrected by subtraction of the estimated increase, determined by multiplying the absolute intensity in the tdTomato-Channel with a common corrective rate, which was obtained from tdTomato-CASP3-transfected control samples (20 samples). To prevent false positives and undercorrection, the final corrective rate was determined as sum of the mean rate and its standard deviation (3.4 % + 1.1 % = 4.5 %). In Caspase-3 activity experiments, signal increase upon photobleaching was determined as in the intermolecular FRET experiments using the SE imaging profile. Due to the absence of a lower and upper limit of absolute intensity

in these experiments, a minority of samples showed intensities beyond the dynamic range (after tdTomato excitation and tdTomato detection) and, consequently, displaying saturated pixels. For more accurate determination of the signal increase upon photobleaching, these samples were re-scanned with an attenuated gain setting of 600. A group of independent measurements with both the original gain setting (of 700) and the adjusted gain setting (of 600) showed that the absolute intensity differed by the factor of 3. This gain adjustment was then compensated by multiplying the calculated corrective rate with the factor 3.

$$(1) \qquad cFRET = \frac{\left(\left(I_{POST} - \Delta I_{PC}\right) - I_{PRE}\right)}{\left(I_{POST} - \Delta I_{PC}\right)}$$

$$(2) \qquad PC = \frac{\Delta I_{POST}}{I_{FP}}$$

ΔI_{PC}	tdTomato emission after tdTomato excitation multiplied with corrective rate (PC)
PC	Corrective rate
ΔI_{POST}	Signal increase (mAmetrine channel) upon photobleaching
I_{FP}	tdTomato emission after tdTomato excitation

In addition, imaging settings and experimental setup were appropriately adjusted to account for these artefacts (see methods).

3.2.2. mTurquoise2 spectral bleed-through (SBT)

While biosensor-transfected samples demonstrated insignificant SBT into the mTurquoise2 detection channel, mturq2-CBD28k-transfected samples displayed substantial bleed-through into the mAmetrine-Channel. For this purpose, mturq2-CBB28K-transfected cells (10 samples) were analyzed to quantify SBT and mTurquoise2 emission. On the basis of SBT and mTurquoise2 emission, an average bleed-through corrective factor (pre-bleach: 0.9411; post-bleach: 0.9348) was calculated. Comparison of the measured SBT values with the calculated values showed that this corrective approach is accurate and reliable (calculated pre-bleach error: 0.1 % ± 1.6 %; calculated post-bleach error: -0.2 % ± 1.8 %).

(1) $$cFRET = \frac{\left(\left(I_{POST} - \Delta I_{BT-POST} - \Delta I_{PC}\right) - \left(I_{PRE} - \Delta I_{BT-PRE}\right)\right)}{\left(I_{POST} - \Delta I_{BT-POST} - \Delta I_{PC}\right)}$$

(2) $$C_{SBT} = \frac{SBT}{I_{FP}}$$

ΔI_{BT}	mTurquoise2 emission after mTurquoise2 excitation multiplied with the respective SBT (C_{SBT}) rate
ΔI_{PC}	tdTomato emission after tdTomato excitation (SE profile) multiplied with corrective rate (PC)
C_{SBT}	SBT corrective factor for pre- and post-bleach
SBT	SBT into the mAmetrine-Channel
I_{FP}	mTurquoise2 emission after mTurquoise2 excitation

3.2.3. In-situ assay of Caspase-3 activity upon expression of Calbindin-D28k

In order to assess whether an effect on Caspase-3 activity can be detected using the available Caspase-3 biosensor upon increased expression of CBD28k, the following FRET pilot experiments (each n = 1) were performed with unconjugated and conjugated CBD28k.

Unconjugated Calbindin-D28k

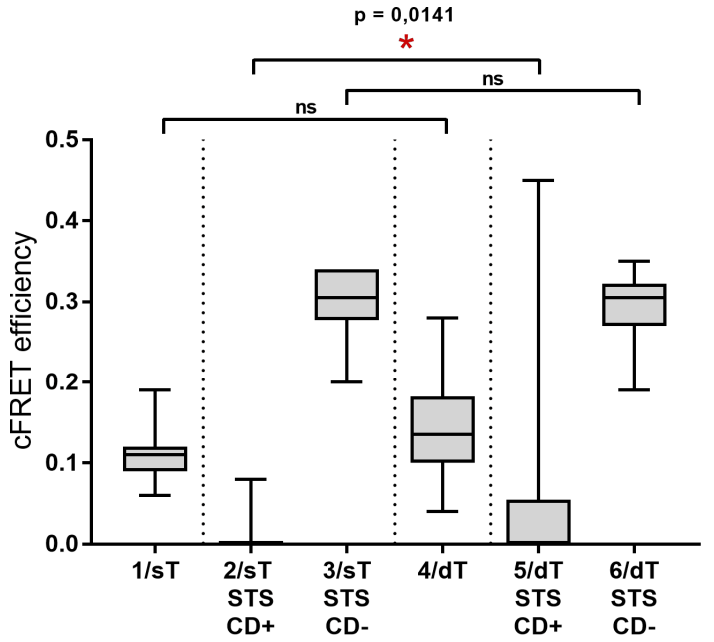

*sT/single transfection: Caspase-3 biosensor
*dT/dual transfection: Caspase-3 biosensor + unconjugated CBD28k
*STS: Staurosporine *CD: chromatin condensation

Figure 20. Biosensor co-transfected with unlinked CBD28k in treated/untreated HN10e cells.
This box plot diagram shows the effect of CBD28k co-transfection on Caspase-3 activity (n = 1; #3 ,#6 each with 10 samples; #1, #2, #4, #5 each with 20 samples) with optional STS-treatment (10 µM for 11h). (* = $p < 0.05$, ns = not significant, one-way ANOVA w/ Bonferroni post-hoc test).

A one-way analysis of variance (ANOVA) was used to compare the effect of CBD28k co-transfection on Caspase-3 activity among treatment (± STS) and apoptotic (± CD) conditions (see figure 20). There was a statistically significant difference between group means at the p<.05 level [F (5, 94) = 29,71, P<0,0001]. A post hoc test using Bonferroni's multiple comparisons procedure indicated that the STS-treated single (M = 0,004; SD = 0,01789; 20 samples) and dual (M = 0,0765; SD = 0,1533; 20 samples) transfected groups

featuring CD as a morphological marker of advanced apoptosis differed significantly at the adjusted p = 0,0141. Due to the distribution, a Mann-Whitney U test was additionally conducted, which also showed a significant difference between both groups (U = 149, z = -2.083, p = 0.037 [asymp. sig. 2-tailed]).

However, comparisons between the untreated single (M = 0,1125; SD = 0,03041; 20 samples) and dual (M = 0,139; SD = 0,06593; 20 samples) transfected groups, and, moreover, the STS-treated single (M = 0,299; SD = 0,04358; 10 samples) and dual (M = 0,293; SD = 0,04668; 10 samples) transfected groups without CD showed no significant differences. Cells were randomly selected without control of co-transfection.

While 95 % of the exclusively biosensor-transfected samples with CD showed no FRET at all, 25 % of the samples from the pool of the dual-transfected cells with CD showed high FRET-efficiencies. In addition to that, 15 % of these samples displayed FRET-efficiencies approximately 3 - 4 times greater than the untreated, exclusively biosensor-transfected samples.

FP-conjugated Calbindin-D28k

A one-way analysis of variance (ANOVA) was used to compare the effect of FP-conjugated CBD28k co-transfection on Caspase-3 activity among treatment (± STS) and apoptotic (± CD) conditions (see figure 22). There was a statistically significant difference between group means at the p<.05 level [F (3, 27) = 19,47, P<0,0001]. A post hoc test using Bonferroni's multiple comparisons procedure indicated that the untreated single (M = 0,164; SD = 0,1085; 10 samples) and dual (M = 0,44; SD = 0,1056; 5 samples) transfected groups differed significantly at the adjusted p = 0,0001.

However, both comparisons between the untreated dual (M = 0,44; SD = 0,1056; 5 measurements) transfected group either with the STS-treated dual transfected group with CD (M = 0,495; SD = 0,1167; 8 samples) or without CD (M = 0,4338; SD = 0,06927; 8 samples) showed no significant difference. Moreover, there was no significant difference between the STS-treated dual transfected group without CD (M = 0,4338; SD = 0,06927; 8 samples) and the STS-treated dual transfected group with CD (M = 0,495; SD = 0,1167; 8 samples).

Samples were randomly selected with control of co-transfection. Samples with low absolute intensities (< 10^4 on a 16-bit scale) in the mTurquoise2-Channel were excluded to represent moderate to high expression levels.

Figure 21 demonstrates Acceptor-Photobleaching performed on samples with high cFRET-efficiency even despite the occurrence of CD.

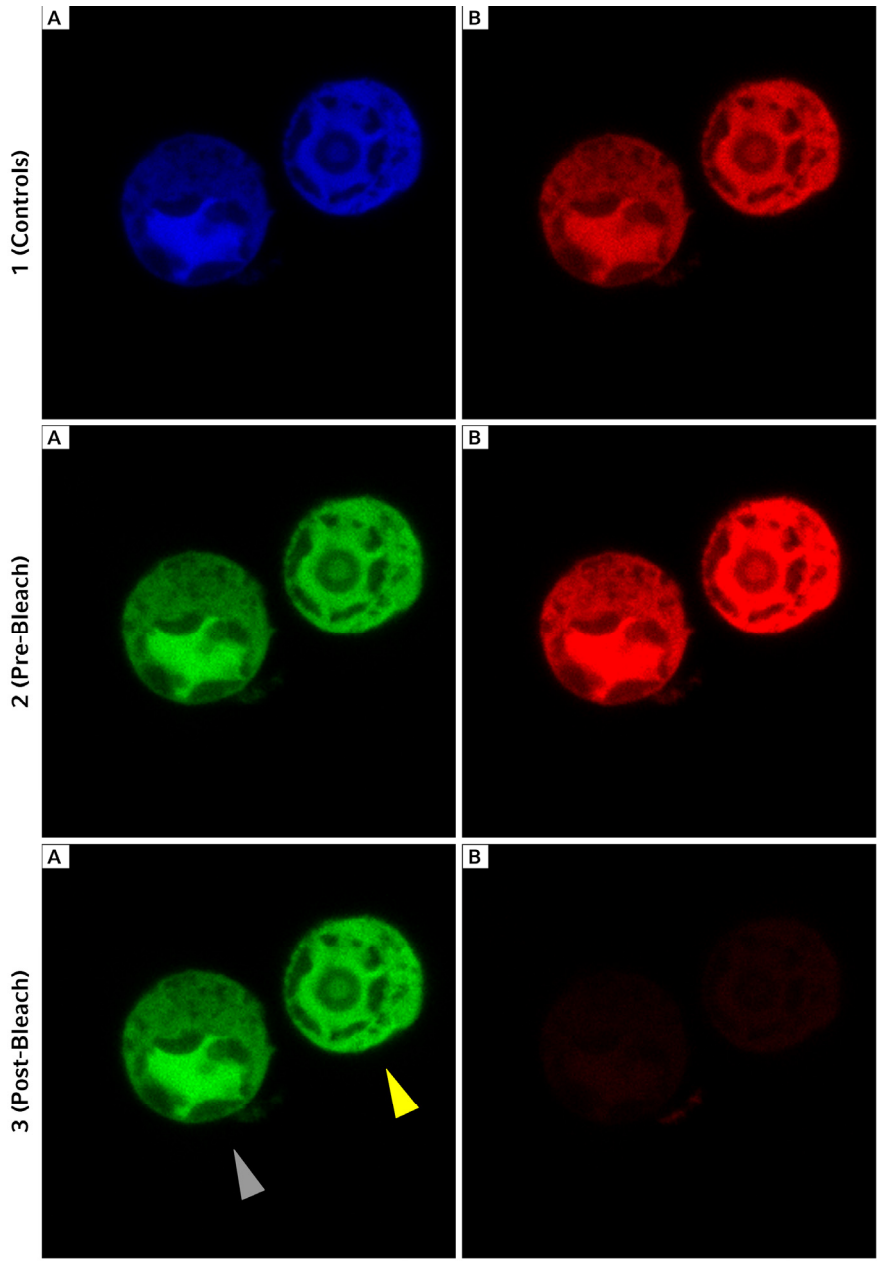

Figure 21. mAmetrine-DEVD-tdTomato and mturq2-CBD28k co-transfected samples treated with Staurosporine.

After high-dose STS (15 µM for 4h) treatment, chromatin condensation, a characteristic morphological feature of apoptosis, is apparent. (1) Before the bleaching experiment, 2 scans were acquired for the purpose of verifying co-transfection, correcting tdTomato's signal increase upon photobleaching and mTurquoise2 SBT. (A) is acquired by mTurquoise2 excitation and mTurquoise2 detection, while (B) is acquired by tdTomato excitation and tdTomato detection. (2 - 3) mAmetrine (A) and tdTomato Channel (B) are shown before (2) and after (3) the bleaching event. The cell on the left (grey arrow) demonstrated a cFRET-efficiency of 0,51, while the cell on the right (yellow arrow) shows a cFRET-efficiency of 0,65.

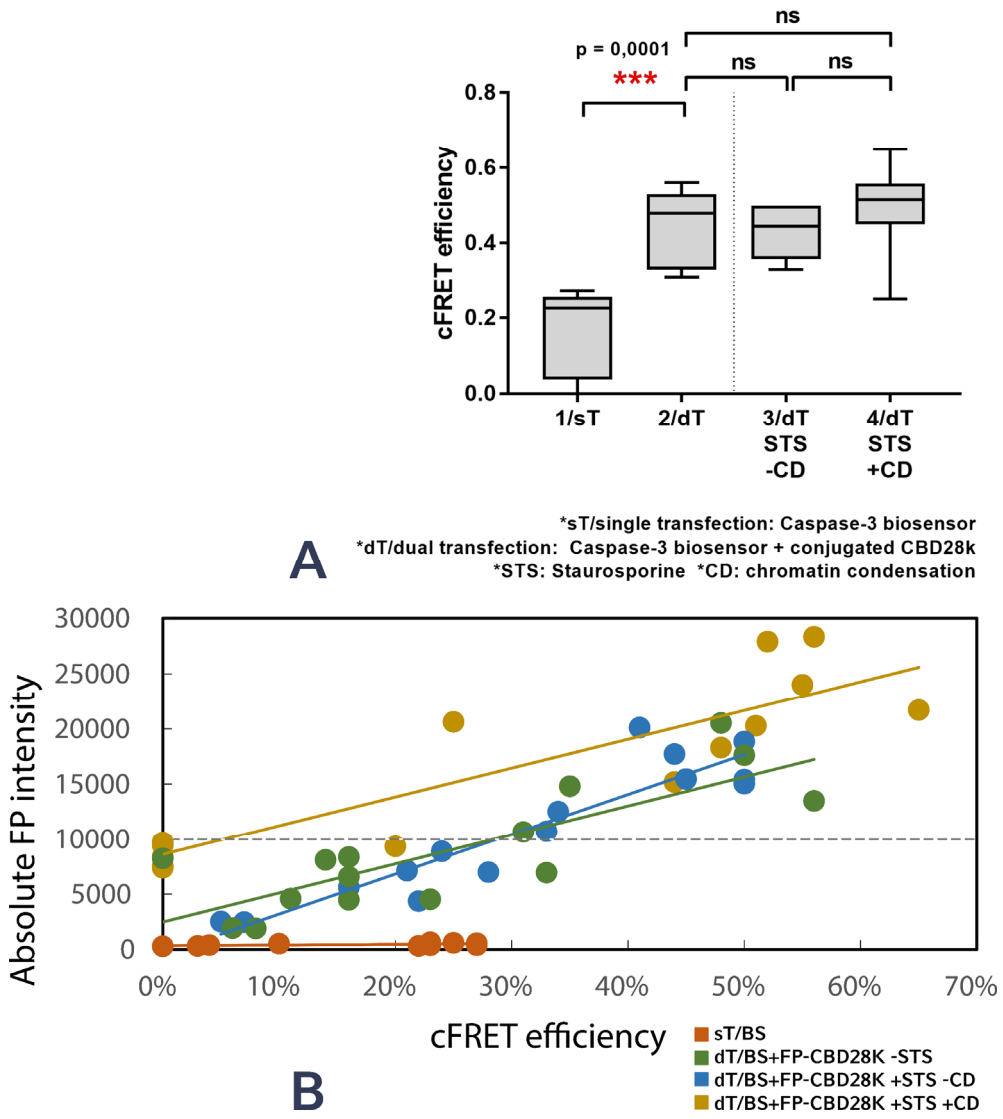

Figure 22. Biosensor co-transfected with FP-conjugated CBD28k in treated/untreated HN10e cells.
(A) The effect of FP-conjugated CBD28k co-transfection on Caspase-3 activity is demonstrated in a box plot (n = 1; #1 with 10 samples; #2 with 5 samples; #3, #4 each with 8 samples). Optional STS-treatment (15 µM for 4 h). Cells with low absolute intensities <10^4 in the mTurquoise2-channel were excluded. (*** = $p < 0.001$, ns = not significant, one-way ANOVA w/ Bonferroni post-hoc test). (B) This diagram shows that there appears to be a correlation between the measured cFRET-efficiency and the absolute FP intensity. The red line shows untreated cells exclusively transfected with the biosensor. The green line represents untreated cells transfected with both biosensor and FP-conjugated CBD28k. STS-treated dual-transfected cells without CD are demonstrated by the blue line, whereas cells with CD are shown by the yellow line. The dashed line indicates the absolute intensity threshold (< 10^4 on a 16-bit scale) that was applied for the statistical analysis in order to represent moderate to high expression levels.

3.3. Investigation of intermolecular interaction between Calbindin-D28k and Pro-Caspase-3 by Acceptor-Photobleaching and Sensitized Emission

Extensive negative and positive control experiments were performed to detect and eliminate artefacts from measurements. Each sample was sequentially analyzed, first using Sensitized Emission then Photobleaching (see chapter 2.3.). Data is shown as mean with standard deviation. An intramolecular FRET construct, mAmetrine-DEVD-tdTomato, was used as positive control. Uncorrected average FRET-efficiencies were close to the previously reported range of 0,42 – 0,45 (Ai et al. 2008). Corrected FRET (cFRET) efficiencies (M = 0,275; SD = 0,06364; n = 2; each 10 samples) were slightly lower than uncorrected FRET-efficiencies due to the correction of signal increase upon photobleaching. Normalized FRET (nFRET) efficiencies from Sensitized Emission were additionally measured as a qualitative control (M = 0,305; SD = 0,1909; n = 2; each 10 samples).

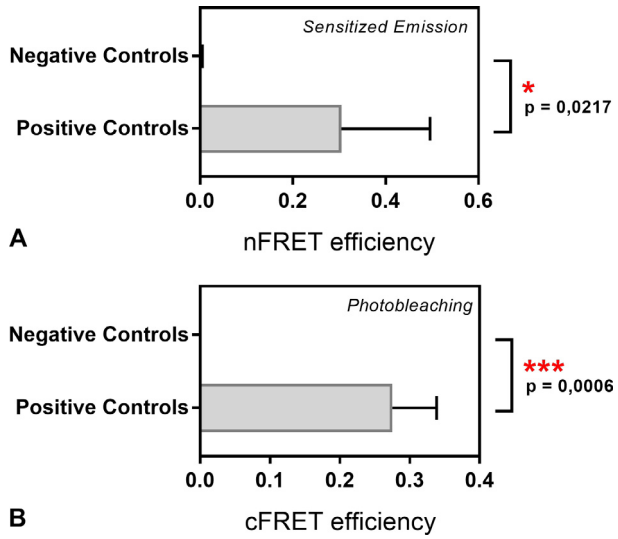

Figure 23. Negative and positive controls.
This diagram shows that there is a significant difference between negative controls experiments (n = 4; unlinked mAmetrine and tdTomato co-transfection, unlinked mAmetrine and tdTomato-CASP3 co-transfection (2 exp.), mAmetrine-CBD28k and unlinked tdTomato co-transfection) and the positive control experiment (n = 2; mAmetrine-DEVD-tdTomato). Data shows mean and SD. (* = p < 0.05, *** = p < 0.001, independent student's t test).

A total of 4 independent negative control experiments was performed (see figure 23): mAmetrine + tdTomato-CASP3 (15 samples), mAmetrine-CBD28k + tdTomato (6 samples) and the unconjugated FPs (n = 2; each 20 samples) showed similar nFRET-efficiencies close to zero. Remarkably, cFRET-efficiencies in all samples equaled zero.

For the purpose of confirming that high tdTomato concentrations would not lead to false positive results due to signal increase upon photobleaching, a small number of

cells (5 samples) with high absolute intensity in the tdTomato-Channel was additionally measured, which showed similar results. Independent negative control experiments were grouped together as control group for statistical analysis.

Independent student's t tests were conducted to compare positive and negative control groups. For Sensitized Emission, there was a statistically significant difference between positive (M = 0,305; SD = 0,135; n = 2) and negative (M = 0,0027; SD = 0,001251; n = 4) control group; t (4) = 3.656, p = 0,0217, two-tailed. For Photobleaching, there was also a significant difference between positive (M = 0,275; SD = 0,045; n = 2) and negative (M = 0; SD = 0; n=4) control group; t (4) = 9,979, p = 0,0006, two-tailed.

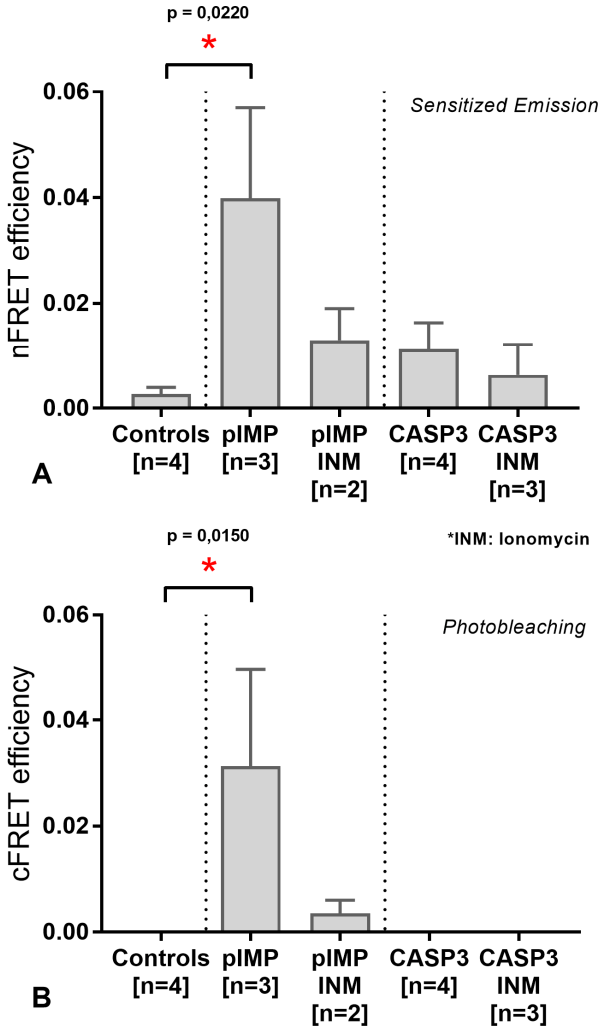

Figure 24. Intermolecular interaction experiments of mAmetrine-CBD28k with either tdTomato-pIMPase or tdTomato-CASP3 in co-transfected HN10e cells.

Comparison between control and the respective FRET experiments (n = 2 – 4, each with 10 samples) for both Sensitized Emission (A), Photobleaching (B) and optional cytotoxic treatment with Ionomycin (INM, 2 µM for 24 hours). Co-transfections of mAmetrine-CBD28k and tdTomato-pIMPase without INM-treatment present average FRET efficiencies that differ significantly from the control group. Data shows mean and S.E.M. (* = $p < 0.05$, (A) one-way ANOVA w/ Dunnett post-hoc test, (B) Kruskal-Wallis test).

Intermolecular FRET experiments (2 - 4 independent experiments, each with 10 samples) were performed using mAmetrine-CBD28k as the donor and either tdTomato-CASP3 or tdTomato-pIMPase as the acceptor in HN10e cells with optional INM treatment (2 µM, 24 hours).

A one-way analysis of variance (ANOVA) was used to compare nFRET efficiency (from Sensitized Emission) of the respective intermolecular interaction experiments (among optional treatment conditions with 2 µM INM for 24 hours) with the (negative) control group (see figure 24). There was no statistically significant difference between group means at the p<.05 level [F (4, 11) = 3,18, P= 0,0577] according to the ANOVA. A post hoc test using Dunnett's multiple comparisons procedure indicated that the co-transfection of mAmetrine-CBD28k and tdTomato-pIMPase without cytotoxic treatment (M = 0,0399; SD = 0,02962; n = 3; each 10 samples) differed significantly from the control group (M = 0,0027; SD = 0,002502; n = 4) at the adjusted p = 0,0220. However, the same co-transfection with INM-treatment (M = 0,013; SD = 0,008485; n = 2) showed no significant difference from the control group. There was also no significant difference between the control and co-transfections of mAmetrine-CBD28k with tdTomato-CASP3 without (M = 0,01125; SD = 0,01018; n = 4) and with (M = 0,006333; SD = 0,01012; n = 3) INM-treatment.

A one-way analysis of variance (ANOVA) was used to compare cFRET efficiency (from Photobleaching) of the respective intermolecular interaction experiments (among optional treatment conditions with 2 µM INM for 24 hours) with the (negative) control group (see figure 24). As Brown-Forsythe test for violation of homogeneity of variance was statistically significant at the p<.05 level [F (4, 11) = 3,418, P=0,0476], further analysis was conducted using Kruskal-Wallis test. Kruskal-Wallis test showed a statistically significant difference between groups at the p<.05 level [H = 14,57, p = 0,0002]. Dunn's post hoc test indicated that the co-transfection of mAmetrine-CBD28k and tdTomato-pIMPase without cytotoxic treatment (M = 0,03133; SD = 0,03197; n = 3; each 10 samples) differed significantly from the control group (M = 0; SD = 0; n = 4) at the adjusted p = 0,0150 (with a mean rank difference of -8,667). However, the same co-transfection with INM-treatment (M = 0,0035; SD = 0,003536; n = 2) showed no significant difference from the control group. There was also no significant difference between the control and co-transfections of mAmetrine-CBD28k with tdTomato-CASP3 without (M = 0; SD = 0; n = 4) and with (M = 0; SD = 0; n = 3) INM-treatment.

In order to investigate compartmental FRET, a pixel-by-pixel analysis was performed in ImageJ and PixFRET. For this purpose, selected scans (1 – 2 samples; selected on the basis of highest nFRET-efficiency) from each transfection were analyzed (with the exception of INM-treated samples). The result of the pixel-by-pixel analysis is summarized in figure 25.

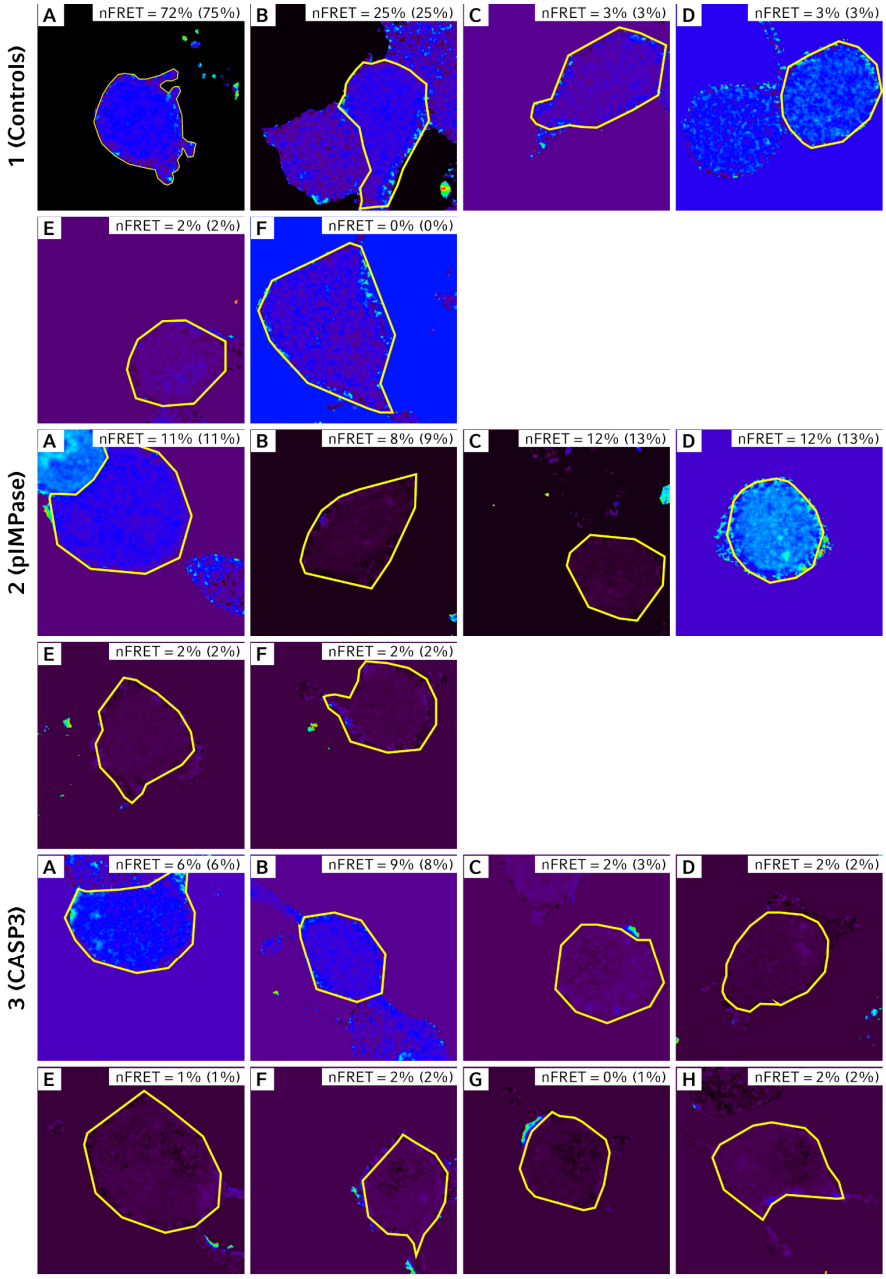

Figure 25. Pixel-by-pixel analysis of selected cells.
Mean nFRET (SE) values computationally determined by pixel-by-pixel analysis are respectively demonstrated at the top (calculated nFRET values are shown in parenthesis for comparison). Yellow lines indicate respective ROIs. (1) Positive and negative control samples: (A) and (B) demonstrate positive controls samples. (C) and (D) are unconjugated FP negative control samples. (E) shows mAmetrine + tdTomato-CASP3 and (F) mAmetrine-CASP3 + tdTomato co-transfected negative control samples. (2) mAmetrine-CBD28k + pIMPase-tdTomato (set#1: A, B; set#2: C, D; set#3: E, F). (3) mAmetrine-CBD82K + CASP3-tdTomato (set#1: A, B; set#2: C, D; set#3: E, F; set#4: G, H).

4. Discussion

To date, evidence on the various intermolecular interactions of CBD28k is still essentially based on in-vitro studies (Schmidt 2012). However, occasionally in-vitro studies were shown to yield misleading results that do not correspond with conditions in living cells. Thus, for the first time to our knowledge, this study investigates the proposed intermolecular interaction between CBD28k and Pro-/Caspase-3 and, moreover, the inhibition of Caspase-3 activity in a more complex, natural milieu of a cell using in-situ FRET microscopy. There is conclusive evidence for a calcium-independent interaction between CBD28k and the IMPase target peptide sequence. However, the results do not indicate an interaction with Pro-Caspase-3. The pilot experiments indicate inhibition of Caspase-3 activity in a concentration-dependent manner.

In-situ assay of Caspase-3 activity upon expression of Calbindin-D28k

The first pilot experiment with unconjugated CBD28k showed that there is a statistically significant difference between STS-treated (10 µM for 11 h) single- (exclusively biosensor-transfected) and dual-transfected (biosensor and CBD28k) groups featuring CD as a morphological marker of advanced apoptosis (see figure 20, chapter 3.2.3.). While single-transfected samples showed essentially no FRET after treatment with STS, approximately a quarter of the STS-treated dual-transfected samples showed increased cFRET-efficiencies and, furthermore, a share displayed substantially greater cFRET-efficiencies than what was observed in untreated single-transfected samples. This indicates that plasmid-induced expression of CBD28k can lead to inhibition of Caspase-3 activity, which can protect cells from apoptosis. Without control of co-transfection in this experiment, one can assume that the level of statistical significance might be adversely affected. As anticipated, STS-treated single-transfected and dual-transfected samples without CD showed nearly identical cFRET efficiencies. Similar mean cFRET-efficiency in STS-treated samples without CD and the substantial difference in cFRET-efficiency to samples featuring CD suggest that the occurrence of chromatin compaction serves as a suitable marker for advanced apoptosis. However, a difference in cFRET-efficiency between STS-treated samples without CD and untreated single-transfected samples is present, which might be a response of the HN10e neural cell line to cytotoxic treatment, e.g. through increased neurotrophic factor synthesis.

This pilot experiment was then adapted and modified with FP-labeled CBD28k, which enabled screening and validation of co-transfection and, moreover, investigation of concentration dependence. Interestingly, no significant difference in cFRET-efficiency was found when both untreated and high-dose STS-treated (15 µM for 4 h) dual-transfected (biosensor and mturq2-CBD28k) samples were compared regardless of the occurrence of CD (see figure 22, chapter 3.2.3.). Furthermore, in opposition to the first pilot experiment, there was no significant difference in cFRET-efficiency between CD positive and negative high-dose STS-treated dual-transfected groups. This suggests further that CBD28k overexpression can inhibit Caspase-3 activity in context of high-dose STS treatment, even despite the occurrence of CD as a distinct morphological marker of PCD. The pathway mediating PCD despite blockage of the common caspase-dependent pathway is known as Caspase-independent cell death (CICD), which shares properties with apoptosis, such as peripheral nuclear condensation, partial CD and

outer-membrane permeabilization (Tait & Green 2008). Although, in theory, residual low-level Caspase-3 activity might also induce morphological characteristics of apoptosis, while leaving the biosensor essentially unaffected.

Comparing untreated single-transfected (exclusively biosensor-transfected) samples from the pilot experiments (see figure 20 and 22, chapter 3.2.3.) and the positive control (see chapter 3.3.), a small divergence in cFRET-efficiency becomes apparent. As non-specific cleavage and hydrolysis of the DEVD motif should be negligible, the observed difference amongst experiments could be related to the FRET biosensor itself or caused by deficiency of growth and survival factors in the cell culture medium leading to starvation-induced apoptosis (Braun & Bertin 2011). However, result should remain valid for each experiment, as all samples were subject to the same conditions (except for optional cytotoxic treatment). But on this account, one might assume that in context of CBD28k overexpression starvation-induced Caspase-3 activity was inhibited, leading to significantly increased cFRET-efficiency when untreated dual-transfected samples were compared with untreated single-transfected samples, which would be consistent with observations from the previous experiment with unlabeled CBD28k.

In order to investigate a link between CBD28k concentration and inhibition of Caspase-3 activity, the absolute FP intensity, which is dependent on the protein concentration, was plotted against the measured cFRET-efficiency. The findings represented in figure 22 suggest that the inhibition occurs in a concentration-dependent manner with approximately linear dependency between CBD28k expression and inhibition of Caspase-3 activity. As anticipated, a small share of samples showed no cFRET despite high expression of CBD28k, which suggests that there are limits to the inhibitiory effect and, furthermore, that the observed effect is not of artificial nature. A similar observation of concentration dependence was previously reported from an in-vitro study (Liu et al. 2003).

These pilot experiments indicate that CBD28k can inhibit Caspase-3 in intact cellular systems in a concentration-dependent manner. While these findings would be in accordance with various reports suggesting a cytoprotective attribute and protection from cell death both in a calcium-dependent and -independent manner (Christakos et al. 2003), the results of these pilot experiments need to be interpreted with care, as appropriate reproducibility has not been shown yet. Furthermore, there are few report

stating that no cytoprotective effect was observed in CBD28k null-mutant/-deficient mice (Airaksinen et al. 1997b, Klapstein et al. 1998). Given that the inhibition of Caspase-3 activity occurs in a concentration-dependent manner, these controversial results might be linked to age-dependent CBD28k expression (Enderlin et al. 1987, Geng et al. 2015, Kishimoto et al. 1998, Varghese et al. 1988). Therefore, elevated levels of CBD28k in early, critical developmental stages might suffice to protect from cell death, whereas in adults, lower concentrations might not be able to prevent apoptosis. Consistently, it was shown that expression of CBD28k is frequently downregulated below detection by immunohistochemistry once adulthood is reached (Zhang et al. 1990). Alternatively, compensatory upregulation of Calbindin-like or closely related proteins as a consequence of absolute deficiency of CBD28k (null mutants), could potentially mask protective effects.

Investigation of intermolecular interaction between Calbindin-D28k and Caspase-3 by Acceptor-Photobleaching and Sensitized Emission

Samples co-transfected with the tdTomato-labeled IMPase target peptide and mAmetrine-labeled CBD28k demonstrated statistically significant FRET in both Sensitized Emission and Acceptor-Photobleaching (see figure 24, chapter 3.3.). This result indicates nanometer-scale co-localization, which is highly suggestive for intermolecular protein-protein interaction (Bastiaens & Pepperkok 2000, Grecco & Verveer 2011, Sekar & Periasamy 2003). Consistent with several reports, this finding provides further evidence for an interaction between CBD28k and the IMPase (ISSIKEKYPSHS) target peptide sequence (Almog et al. 2011). Optional treatment with INM (2 µM for 24 h), a commonly used ionophore for induction of apoptosis and rise of intracellular calcium levels, did not increase FRET-efficiency. While this result is consistent with reports stating that the interaction occurs in a calcium-independent manner, it is in conflict with a finding suggesting a further boosted interaction at increased calcium levels during synaptic activation (Schmidt 2012).

Samples co-expressing tdTomato-conjugated Pro-Caspase-3 and mAmetrine-conjugated CBD28k showed no significant difference to the control (see figure 24, chapter 3.3.), suggesting that there is no higher degree of co-localization, and, therefore these results are not indicative for intermolecular interaction. Remarkably, no FRET was observed in any sample using Acceptor-Photobleaching, even when Sensitized Emission displayed low, but insignificant FRET-efficiency. While Sensitized Emission is commonly viewed as less robust and, hence, is applied in qualitative research, Acceptor-Photobleaching is more precise in nature and does not necessarily require complex corrective algorithms and corrections factors. The findings of the pIMPase experiments suggested that low FRET-efficiencies were not masked by overestimation of the corrected signal increase upon photobleaching and, furthermore, that Acceptor-Photobleaching is the more sensitive method. Therefore, it is concluded that specific FRET did not occur in these samples.

While protein expression of the tdTomato-CASP3 construct was confirmed by both Western Blot and immunofluorescence, there is the remote probability that despite its linker sequence, the fusion construct might prohibit normal protein folding, which could prevent interaction (Miyawaki 2011). Although both tdTomato constructs are of similar

dimensions, abnormal size of the fusion construct could potentially affect normal protein functioning. However, induction of apoptosis with cleavage of Pro-Caspase-3 would yield a smaller, cleaved acceptor construct with solely the pro-domain attached to tdTomato (see figure 17, chapter 3.1.2.). But optional treatment with INM (2 µM for 24 h) did not result in any noteworthy change. In the case that the proportion of interacting molecules from the total of fluorescent molecules were to be exceptionally low, specific FRET could potentially be concealed by the overall fluorescent background. While interfering endogenous interaction can result in lower apparent FRET-efficiency, it is improbable that it eliminates detection of FRET entirely. As outlined, there is a minor sequence variation (see figure 17, chapter 3.1.2.) between the Pro-Caspase-3 pro-domain of Homo sapiens and Mus Musculus. Presuming, that this might cause a substantial difference in binding affinity, it is unlikely that this important mechanism, affecting an essential effector of apoptosis, is not shared among close genetic relatives, when other pro-domain interaction motifs, such as the death effector domain (DED) and caspase activation and recruitment domain (CARD), are known to be highly conserved in mammals. Although the majority of studies on this subject reported an interaction between CBD28k and the active Caspase-3, there were only few studies providing evidence that CBD28k might interact with a peptide sequence of the Pro-Caspase-3 pro-domain (Kojetin et al. 2006, Kordys et al. 2007). Contrary to these in-vitro experiments, the current study indicates that both proteins might not co-localize, suggesting that the inhibition of Caspase-3 activity is attributable to the intermolecular interaction with active Caspase-3.

There were no indications for compartmental FRET (see figure 25, chapter 3.3.). Calculated nFRET-efficiencies were consistent with computationally acquired data from pixel-by-pixel analysis. Small, artificial hotspots were occasionally associated with the cell membrane. Larger darkened hotspots correspond to the localization of the nucleus. Pilot experiments have shown that unconjugated tdTomato and its constructs were mainly localized in the cytosolic milieu and were excluded from the nucleus, likely due to the molecular weight of ≥ 54 kDa, which hinders passive diffusion through the pore (Marfori et al. 2011). As a consequence, FRET-efficiencies were slightly lower within the nucleus, but in synopsis remained negligible.

In conclusion, this experiment confirms the interaction between CBD28k and the IMPase peptide sequence. There are various reports providing conclusive in-vitro evidence on

the interaction with IMPase, RanBPM and active Caspase-3 (Bellido et al. 2000, Berggård et al. 2002b, Christakos & Liu 2004, Liu et al. 2003, Lutz et al. 2003, Schmidt et al. 2005, Shamir et al. 2005). Additionally, target peptide sequences derived from IMPase (ISSIKEKYPSHS) and RanBPM (LASIKNR) were shown to interact with CBD28k (Lutz et al. 2003). Based on homology searches, it was later discovered that the Pro-Caspase-3 pro-domain features a peptide sequence (SKSIKNLEP) with significant homology to the other peptides sequences. Further research suggested that CBD28k and Pro-Caspase-3 would interact and, additionally, similar binding traits between IMPase and Pro-Caspase-3 peptide sequences were observed (Kojetin et al. 2006). Another study reported that all 3 target peptide sequences would bind to the same binding site, which involves the canonical EF2-hand (Kordys et al. 2007). The report of similar binding traits between IMPase and Pro-Caspase-3 peptide sequences suggests that the interaction with Pro-Caspase-3 would be comparable to that of the IMPase target peptide (Kojetin et al. 2006). Therefore, it is unexpected, that no clear indications could be found for an intermolecular interaction between CBD28k and Pro-Caspase-3. While the body of evidence for an interaction with active Caspase-3 is conclusive, the interaction with its zymogen remains open to question. According to Chang and Yang (2000), it is unlikely that the pro-domains of executioner caspases facilitate intermolecular interaction. However, there is evidence that the pro-domain suppresses spontaneous activation of Pro-Caspase-3 to protect against low-level, latent initiator caspase activity (Meergans et al. 2000). Other studies suggested that removal of the pro-domain from Drosophila melanogaster effector caspases, drICE and DCP-1, enhances caspase activity (Berg et al. 2012, Song et al. 1997).

Limitations

The assay of protein interaction using FRET applications should always have a scientific rationale, such as in-vitro studies providing indications for a possible interaction, as co-localization does not necessarily involve intermolecular interaction. Thus, FRET, which only occurs in nanometer scale proximity and, hence, is highly suggestive for such a protein-protein interaction (Sekar & Periasamy 2003), needs to be carefully interpreted in synopsis with other reports.

During the pilot experiments, tdTomato or tdTomato-CASP3-transfected samples showed a signal increase in the mAmetrine-Channel upon photobleaching. Due to sample fixation and the bleaching of the cell's soma, focal drift and acceptor influx were considered implausible. However, there are various reports stating that DsRed, common origin of the red FP fruit series (Shaner et al. 2004), might display a green state, which was suggested to be either attributable to immature chromophores within the tetramer or direct photoconversion (Kremers et al. 2009, Marchant et al. 2001). DsRed is known to exhibit a long maturation process, which can lead to FRET between immature green- and mature red-emitting species (Robinson & Marchant 2005). In view of tdTomato's fast maturation rate, immature chromophores within tdTomato might have lower impact on FRET-efficiency compared with DsRed. However, the occurrence of partial photoconversion would be consistent with other studies suggesting that photoconversion among red and orange fluorescent proteins might be common (Kremers et al. 2009). Partial photoconversion was also reported to occur in cyan fluorescent protein (CFP)-yellow fluorescent protein (YFP)-FRET-experiments, where YFP is photoconvertible upon photobleaching, leading to an increase in cyan fluorescence (Kirber et al. 2007, Valentin et al. 2005). Photoconversion was not a substantial issue in most cases and, hence, was mathematically corrected (Seitz et al. 2012). Nevertheless, there is no scientific consensus regarding the photoconversion of YFP (Verrier & Söling 2006). In most cases, the photoconvertible species is reported to exhibit mono-exponential increase and photoconversion rates increase supra-linearly with rising laser power (Kremers et al. 2009). The observed gradual recovery of TdTomato signal is likely due to spontaneous recovery of immature green-emitting chromophores to red-emitting mature chromophores. In case of YFP, there was a similar report of photobleaching and spontaneous recovery after strong irradiation (Dickson et al. 1997, Miyawaki 2011). In summary, photoconversion can prove

problematic in intermolecular FRET experiments with particularly low FRET-efficiencies and high concentrations of the photoconvertible protein. Thus, photoconversion should be corrected with an appropriate corrective approach. For this purpose, a photoconversion correction factor was established to eliminate these artefacts.

The current data suggests that non-specific FRET due to high protein concentrations was no substantial limitation of this study. Common issues of experimental works implementing plasmid transfections and FRET applications were addressed in the methods section and adequate preventive arrangements were taken.

Implications and further research

It was shown that expression of CBD28k plays a role in a subset of medulloblastomas, a brain tumor with high malignancy frequently seen in younger patients. Immunohistochemical positivity for CBD28k was significantly associated with poor prognosis and, therefore, was proposed to represent a subclass of particularly aggressive tumors (Katsetos et al. 1995, Pelc et al. 2002). Other studies reported that lung cancer cells express CBD28k at significantly higher levels than non-cancerous lung tissue (Castro et al. 2000, Watanabe et al. 1994). Hence, blocking Caspase-3 inhibition to sensitize tumor cells for chemo- or radiotherapy may present a new therapeutic option for some patients. Druggablity and cyclic peptide binding analysis of CBD28k confirmed that peptide therapeutics might be used to block the interaction with Caspase-3 by changing conformational and dynamic properties (Bobay et al. 2014).

Dysfunctional execution of PCD was suggested to be associated with many neurodegenerative disorders, such as Parkinson's disease (PD) or Chorea Huntington (HD) (Elmore 2007). Altered expression of CBD28k was observed in diseases such as Alzheimer's disease (AD), Down's syndrome, ischemia and epilepsy (Heizmann & Braun 1992). Comparison of human brain tissue showed that there is a significant decrease of CALB1 gene expression in aging and neurodegenerative diseases, particularly in brain samples of substantia nigra (PD), the corpus striatum (HD), nucleus basalis of Meynert and hippocampus (AD) (Iacopino & Christakos 1990). Recently it was discovered that a dysfunction of the (PARK14-dependent) calcium homeostasis and signaling, caused by a defect of the PLA2g6 protein, is strongly related to cell death in idiopathic Parkinson's disease (Zhou et al. 2016). Various studies reported that dopaminergic neurons in a MPTP-induced PD model showed increased resistance to cell death when CBD28k was expressed (Choi et al. 2008, Crocker et al. 2003, German et al. 1992, Sheehan et al. 1997). Given these points, further investigation of the mechanisms underlying the anti-apoptotic function of CBD28k might help to develop new pharmacological treatments and distinct therapeutic strategies. Most available inhibitors of initiator caspases were shown to be either ineffective or resistance was rapidly developed (Bobay et al. 2014). Despite the advancements in the development of cytoprotective agents, there are no clinically-established caspase-3-inhibitors in therapeutic use. To date, most pre-clinical studies were performed with active-site inhibitors (Bobay et al. 2012). However, experiments with isolated peptide sequences obtained from CBD28k were unable to

inhibit Caspase-3 (Liu et al. 2003). A deeper understanding of how CBD28k inhibits Caspase-3 might prove beneficial to develop alternate solutions such as peptide therapeutics or synthetic structure mimetics. Development of new cytoprotective agents inhibiting active Caspase-3 might help to prevent apoptosis in ischemia, neurodegenerative diseases and a plethora of other diseases. While FRET experiments are commonly used to provide evidence for intermolecular interaction, negative results do not necessarily imply that there is no interaction between both target proteins. Hence, further research is necessary to rule out an interaction with Pro-Caspase-3.

In addition to the inhibition of Caspase-3 activity and buffering of calcium, there are indications for alternate pathways (Choi et al. 2008). It was shown that CBD28k expressing endometrial cancer cells, treated with hydrogen peroxide, showed decreased expression of pro-apoptotic Bax, p53 and Bcl-2 (Jung et al. 2011). Another study proposed that CBD28k might exhibit cytoprotection by modulation of ERK1/2, which can promote cell survival. (Liu et al. 2003). A similar finding showed that injection of GDNF leads to increased expression of CBD28k, which was accompanied by activation of ERK1/2 (Wang et al. 2008). Therefore, we propose that the interaction with RanBPM (Lutz et al. 2003), particularly a cytoprotective modulation of the Ras-Raf-MEK-ERK-pathway (Atabakhsh & Schild 2012, Meloche & Pouyssegur 2007) and, moreover, an effect on the binding capacity of p73alpha (Kramer et al. 2004), a protein with structural and functional similarity with the p53 tumor suppressor (Courtois et al. 2004), might be interesting subjects for future research.

5. Summary

In conclusion, CBD28k is an important cytoprotective effector, particularly during critical developmental stages of neuronal maturation. While its neuronal expression essentially occurs in a coordinated, maturation-dependent manner, it was also demonstrated that cytotoxic stimuli such as mechanical trauma or tumor necrosis factors (TNFs) can also induce expression of CBD28k in the central nervous system (Mattson et al. 1995). The present body of evidence suggests that this cytoprotective effect is mediated through direct inhibition of active Caspase-3 in a concentration dependent manner. However, there is growing evidence that other protective pathways might also exist.

Key findings:

- Conclusive evidence for a calcium-independent interaction between CBD28k and IMPase target peptide sequence, while no clear indications were found for an interaction with Pro-Caspase-3. Occurrence of FRET was not limited to subcellular compartments.
- Pilot experiments indicate that CBD28k can inhibit Caspase-3 activity in a concentration-dependent manner.

References

Ai, H.-W., Hazelwood, K. L., Davidson, M. W., & Campbell, R. E. (2008). Fluorescent protein FRET pairs for ratiometric imaging of dual biosensors. *Nature Methods*, *5*(5), 401–404. doi:10.1038/nmeth.1207

Aigouy, B., & Mirouse, V. (2013). ScientiFig: A tool to build publication-ready scientific figures. *Nature Methods*, *10*(11), 1048–1048. doi:10.1038/nmeth.2692

Airaksinen, M. S., Eilers, J., Garaschuk, O., Thoenen, H., Konnerth, A., & Meyer, M. (1997a). Ataxia and altered dendritic calcium signaling in mice carrying a targeted null mutation of the calbindin D28k gene. *Proceedings of the National Academy of Sciences of the United States of America*, *94*(4), 1488–1493. doi:10.1073/pnas.94.4.1488

Airaksinen, M. S., Thoenen, H., & Meyer, M. (1997b). Vulnerability of Midbrain Dopaminergic Neurons in Calbindin-D28k-deficient Mice: Lack of Evidence for a Neuroprotective Role of Endogenous Calbindin in MPTPtreated and Weaver Mice. *European Journal of Neuroscience*, *9*(1), 120–127. doi:10.1111/j.1460-9568.1997.tb01360.x

Almog, O., Levi, I., Eskira, Y., Eisenstein, M., Gilon, C., Hoffman, A., et al. (2011). The Calbindin-D28k binding site on inositol monophosphatase may allow inhibition independent of the lithium site of action. *Nature Precedings*.

Andersson, S., Davis, D. L., Dahlbäck, H., & Jörnvall, H. (1989). Cloning, structure, and expression of the mitochondrial cytochrome P-450 sterol 26-hydroxylase, a bile acid biosynthetic enzyme. *Journal of Biological Chemistry*, *264*(14), 8222–8229.

Atabakhsh, E., & Schild, C. (2012). RanBPM is an inhibitor of ERK signaling. *PLoS ONE*, *7*(10), e47803. doi:10.1371/journal.pone.0047803

Barski, J. J., Hartmann, J., Rose, C. R., Hoebeek, F., Mörl, K., Noll-Hussong, M., et al. (2003). Calbindin in cerebellar Purkinje cells is a critical determinant of the precision of motor coordination. *Journal of Neuroscience*, *23*(8), 3469–3477.

Bastiaens, P., & Pepperkok, R. (2000). Observing proteins in their natural habitat: the living cell. *Trends in Biochemical Sciences*, *25*(12), 631. doi:10.1016/s0968-0004(00)01714-x

Bastiaens, P., Wouters, F. S., & Jovin, T. M. (1995). Imaging the molecular state of proteins in cells by fluorescence resonance energy transfer (FRET). Sequential photobleaching of Förster donor-acceptor pairs. *2nd Hamamatsu International Symposium on Biomolecular Mechanisms and Photonics: Cell-Cell Communications*.

Bellido, T., Huening, M., Raval-Pandya, M., Manolagas, S. C., & Christakos, S. (2000). Calbindin-D28k Is Expressed in Osteoblastic Cells and Suppresses Their Apoptosis by Inhibiting Caspase-3 Activity. *Journal of Biological Chemistry*, *275*(34), 26328–26332. doi:10.1074/jbc.m003600200

Berg, J. M., Tymoczko, J. L., & Stryer, L. (2012). *Biochemistry VIIth edition (2012)* (7th ed.). New York: W. H. Freeman and Company.

Berggård, T., Miron, S., Önnerfjord, P., Thulin, E., Akerfeldt, K. S., Enghild, J. J., Akke, M., & Linse, S. (2002a). Calbindin D28k exhibits properties characteristic of a Ca2+ sensor. *Journal of Biological Chemistry*, *277*(19), 16662–16672. doi:10.1074/jbc.M200415200

Berggård, T., Szczepankiewicz, O., & Thulin, E. (2002b). Myo-inositol monophosphatase is an activated target of calbindin D28k. *Journal of Biological Chemistry*, *277*(44), 41954–41959. doi:10.1074/jbc.M203492200

Berney, C., & Danuser, G. (2003). FRET or no FRET: a quantitative comparison. *Biophysical Journal*, *84*(6), 3992–4010. doi:10.1016/s0006-3495(03)75126-1

Bobay, B. G., Butler, L. R., & Cavanagh, J. (2014). Computational Design of Cyclic Peptide Inhibitors of the Anti-Apoptotic Protein Calbindin-D28K. *Biochem Pharmacol*, *3*(142). doi:10.4172/2167-0501.1000142

Bobay, B. G., Stewart, A. L., Tucker, A. T., Thompson, R. J., Varney, K. M., & Cavanagh, J. (2012). Structural insights into the calcium-dependent interaction between calbindin-D28K and caspase-3. *FEBS Letters*, *586*(20), 3582–3589. doi:10.1016/j.febslet.2012.08.032

Braun, F., & Bertin, J. (2011). Serum-nutrient starvation induces cell death mediated by Bax and Puma that is counteracted by p21 and unmasked by Bcl-x L inhibition. *PLoS ONE*, *6*(8), e23577. doi:10.1371/journal.pone.0023577

Buchan, D. W. A., Minneci, F., Nugent, T. C. O., Bryson, K., & Jones, D. T. (2013). Scalable web services for the PSIPRED Protein Analysis Workbench. *Nucleic Acids Research*, *41*(W1), W349–W357. doi:10.1093/nar/gkt381

Burke, R. E., & Baimbridge, K. G. (1993). Relative loss of the striatal striosome compartment, defined by calbindin-D28k immunostaining, following developmental hypoxic-ischemic injury. *Neuroscience*, *56*(2), 305–315. doi:10.1016/0306-4522(93)90333-B

Castro, C. Y., Stephenson, M., Gondo, M. M., Medeiros, L. J., & Cagle, P. T. (2000). Prognostic implications of calbindin-D28k expression in lung cancer: Analysis of 452 cases. *Modern Pathology*, *13*(7), 808–813. doi:10.1038/modpathol.3880141

Chang, H. Y., & Yang, X. (2000). Proteases for cell suicide: functions and regulation of caspases. *Microbiology and Molecular Biology Reviews*, *64*(4), 821–846. doi:10.1128/mmbr.64.4.821-846.2000

Chen, H., Puhl, H. L., Koushik, S. V., Vogel, S. S., & Ikeda, S. R. (2006). Measurement of FRET Efficiency and Ratio of Donor to Acceptor Concentration in Living Cells. *Biophysical Journal*, *91*(5), L39–L41. doi:10.1529/biophysj.106.088773

Chen, X., Zaro, J. L., & Shen, W. C. (2013). Fusion protein linkers: Property, design and functionality. *Advanced Drug Delivery Reviews*, *65*(10), 1357–1369. doi:10.1016/j.addr.2012.09.039

Choi, W. S., Lee, E., Lim, J., & Oh, Y. J. (2008). Calbindin-D28K prevents drug-induced dopaminergic neuronal death by inhibiting caspase and calpain activity. *Biochemical and Biophysical Research Communications*, *371*(1), 127–131. doi:10.1016/j.bbrc.2008.04.020

Christakos, S., & Liu, Y. (2004). Biological actions and mechanism of action of calbindin in the process of apoptosis. *The Journal of Steroid Biochemistry and Molecular Biology*, *89-90*, 401–404. doi:10.1016/j.jsbmb.2004.03.007

Christakos, S., Barletta, F., & Huening, M. (2003). Vitamin D target proteins: function and regulation. *Journal of Cellular Biochemistry*, *88*(2), 238–244. doi:10.1002/jcb.10349

Christakos, S., Gabrielides, C., & Rhoten, W. B. (1989). Vitamin D-dependent calcium binding proteins: chemistry, distribution, functional considerations, and molecular biology. *Endocrine Reviews*, *10*(1), 3–26. doi:10.1210/edrv-10-1-3

Collazo, D., Takahashi, H., & McKay, R. D. G. (1992). Cellular targets and trophic functions of neurotrophin-3 in the developing rat hippocampus. *Neuron*, *9*(4), 643–656. doi:10.1016/0896-6273(92)90028-c

Courtois, S., de Fromentel, C. C., & Hainaut, P. (2004). p53 protein variants: structural and functional similarities with p63 and p73 isoforms. *Oncogene*, *23*(3), 631–638. doi:10.1038/sj.onc.1206929

Crocker, S. J., Smith, P. D., Jackson-Lewis, V, Lamba, W. R., Hayley, S. P., Grimm, E., et al. (2003). Inhibition of calpains prevents neuronal and behavioral deficits in an MPTP mouse model of Parkinson's disease. *Journal of Neuroscience*, *23*(10), 4081–4091.

Day, R. N., & Davidson, M. W. (2012). Fluorescent proteins for FRET microscopy: Monitoring protein interactions in living cells. *BioEssays*, *34*(5), 341–350. doi:10.1002/bies.201100098

Dickson, R. M., Cubitt, A. B., Tsien, R. Y., & Moerner, W. E. (1997). On/off blinking and switching behaviour of single molecules of green fluorescent protein. *Nature*, *388*(6640), 355–358.

Elmore, S. (2007). Apoptosis: A Review of Programmed Cell Death. *Toxicologic pathology*, *35*(4), 495–516. doi:10.1080/01926230701320337

Enderlin, S., Norman, A. W., & Celio, M. R. (1987). Ontogeny of the calcium binding protein calbindin D-28k in the rat nervous system. *Anatomy and Embryology*, *177*(1), 15–28. doi:10.1007/bf00325286

Feige, J. N., Sage, D., Wahli, W., Desvergne, B., & Gelman, L. (2005). PixFRET, an ImageJ plug-in for FRET calculation that can accommodate variations in spectral bleed-throughs. *Microscopy Research and Technique*, *68*(1), 51–58. doi:10.1002/jemt.20215

Formigli, L., Papucci, L., Tani, A., Schiavone, N., Tempestini, A., Orlandini, G. E., et al. (2000). Aponecrosis: Morphological and biochemical exploration of a syncretic process of cell death sharing apoptosis and necrosis. *Journal of Cellular Physiology*, *182*(1), 41–49. doi:10.1002/(SICI)1097-4652(200001)182:13.0.CO;2-7

Gadella, T. W., & Jovin, T. M. (1995). Oligomerization of epidermal growth factor receptors on A431 cells studied by time-resolved fluorescence imaging microscopy. A stereochemical model for tyrosine kinase receptor activation. *The Journal of Cell Biology*, *129*(6), 1543–1558. doi:10.1083/jcb.129.6.1543

Galvao, J., Davis, B., Tilley, M., Normando, E., & Duchen, M. R. (2014). Unexpected low-dose toxicity of the universal solvent DMSO. *The FASEB Journal*, *28*(3), 1317–1330. doi:10.1096/fj.13-235440

Geng, Y., Lin, H. T., Chen, W., Liu, Z. C., Xiang, W., & Chen, W. R. (2015). Age-related reduction in calbindin-D28K expression in the Sprague-Dawley rat lens. *Molecular Medicine Reports*, *11*(1), 422–426. doi:10.3892/mmr.2014.2672

German, D. C., Manaye, K. F., Sonsalla, P. K., & Brook, B. A. (1992). Midbrain Dopaminergic Cell Loss in Parkinson's Disease and MPTP-Induced Parkinsonism: Sparing of Calbindin-D28k - Containing Cells. *Annals of the New York Academy of Sciences*, *648*(1), 42–62. doi:10.1111/j.1749-6632.1992.tb24523.x

Goedhart, J., Stetten, von, D., Noirclerc-Savoye, M., Lelimousin, M., Joosen, L., Hink, M. A., et al. (2012). Structure-guided evolution of cyan fluorescent proteins towards a quantum yield of 93%. *Nature Communications*, *3*, 751. doi:10.1038/ncomms1738

Gordon, G. W., Berry, G., Liang, X. H., Levine, B., & Herman, B. (1998). Quantitative fluorescence resonance energy transfer measurements using fluorescence microscopy. *Biophysical Journal*, *74*(5), 2702–2713. doi:10.1016/S0006-3495(98)77976-7

Grecco, H. E., & Verveer, P. J. (2011). FRET in Cell Biology: Still Shining in the Age of Super-Resolution? *ChemPhysChem*, *12*(3), 484. doi:10.1002/cphc.201000795

Hallcher, L. M., & Sherman, W. R. (1980). The effects of lithium ion and other agents on the activity of myo-inositol-1-phosphatase from bovine brain. *Journal of Biological Chemistry*, *255*(22), 10896–10901.

Heizmann, C. W. (1992). Calcium-binding proteins: basic concepts and clinical implications. *General Physiology and Biophysics*, *11*(5), 411–425.

Heizmann, C. W., & Braun, K. (1992). Changes in Ca2+-binding proteins in human neurodegenerative disorders. *Trends in Neurosciences*, *15*(7), 259–264. doi:10.1016/0166-2236(92)90067-i

Iacopino, A. M., & Christakos, S. (1990). Specific reduction of calcium-binding protein (28-kilodalton calbindin-D) gene expression in aging and neurodegenerative diseases. *Proceedings of the National Academy of Sciences of the United States of America*, *87*(11), 4078–4082.

Iacopino, A., Christakos, S., German, D., Sonsalla, P. K., & Altar, C. A. (1992). Calbindin-D28K-containing neurons in animal models of neurodegeneration: possible protection from excitotoxicity. *Molecular Brain Research*, *13*(3), 251–261. doi:10.1016/0169-328X(92)90033-8

Iritani, S., Niizato, K., & Emson, P. C. (2001). Relationship of calbindin D28K-immunoreactive cells and neuropathological changes in the hippocampal formation of Alzheimer's disease. *Neuropathology : official journal of the Japanese Society of Neuropathology*, *21*(3), 162–167.

Jares-Erijman, E. A., & Jovin, T. M. (2003). FRET imaging. *Nature Biotechnology*, *21*(11), 1387–1395. doi:10.1038/nbt896

Johnson, C. N., Damo, S. M., & Chazin, W. J. (2014). EF-Hand Calcium-Binding Proteins. *eLS*. doi:10.1002/9780470015902.a0003056.pub3

Jones, D. T. (1999). Protein secondary structure prediction based on position-specific scoring matrices. *Journal of Molecular Biology*, *292*(2), 195–202. doi:10.1006/jmbi.1999.3091

Joseph, D. R., Sullivan, P. M., Wang, Y. M., Kozak, C., Fenstermacher, D. A., Behrendsen, M. E., & Zahnow, C. A. (1990). Characterization and expression of the complementary DNA encoding rat histidine decarboxylase. *Proceedings of the National Academy of Sciences of the United States of America*, *87*(2), 733–737.

Jung, E. M., Choi, K. C., & Jeung, E. B. (2011). Expression of calbindin-D28k is inversely correlated with proapototic gene expression in hydrogen peroxide-induced cell death in endometrial cancer cells. *International Journal of Oncology*, *38*(4), 1059–1066. doi:10.3892/ijo.2011.916

Jäättelä, M., & Tschopp, J. (2003). Caspase-independent cell death in T lymphocytes. *Nature Immunology*, *4*(5), 416–423. doi:10.1038/ni0503-416

Katsetos, C. D., Herman, M. M., Krishna, L., Vender, J. R., Vinores, S. A., Agamanolis, D. P., et al. (1995). Calbindin-D28k in subsets of medulloblastomas and in the human medulloblastoma cell line D283 Med. *Archives of Pathology and Laboratory Medicine*, *119*(8), 734–743.

Kirber, M. T., Chen, K., & Keaney, J. F. J. (2007). YFP photoconversion revisited: Confirmation of the CFP-like species. *Nature Methods*, *4*(10), 767–768. doi:10.1038/nmeth1007-767

Kishimoto, J., Tsuchiya, T., Cox, H., Emson, P. C., & Nakayama, Y. (1998). Age-related changes of calbindin-D28k, calretinin, and parvalbumin mRNAs in the hamster brain. *Neurobiology of Aging*, *19*(1), 77–82. doi:10.1016/S0197-4580(97)00166-8

Klapstein, G. J., Vietla, S., Lieberman, D. N., Gray, P. A., Airaksinen, M. S., Thoenen, H., et al. (1998). Calbindin-D28k fails to protect hippocampal neurons against ischemia in spite of its cytoplasmic calcium buffering properties: evidence from calbindin-D28k knockout mice. *Neuroscience*, *85*(2), 361–373. doi:10.1016/S0306-4522(97)00632-5

Klein, P. S., & Melton, D. A. (1996). A molecular mechanism for the effect of lithium on development. *Proceedings of the National Academy of Sciences of the United States of America*, *93*(16), 8455–8459. doi:10.1073/pnas.93.16.8455

Kojetin, D. J., Venters, R. A., Kordys, D. R., Thompson, R. J., Kumar, R., & Cavanagh, J. (2006). Structure, binding interface and hydrophobic transitions of Ca2+-loaded calbindin-D28K. *Nature Structural and Molecular Biology*, *13*(7), 641–647. doi:10.1038/nsmb1112

Kordys, D. R., Bobay, B. G., Thompson, R. J., Venters, R. A., & Cavanagh, J. (2007). Peptide binding proclivities of calcium loaded calbindin-D28k. *FEBS Letters*, *581*(24), 4778–4782. doi:10.1016/j.febslet.2007.09.004

Kramer, S., Ozaki, T., Miyazaki, K., Kato, C., Hanamoto, T., & Nakagawara, A. (2004). Protein stability and function of p73 are modulated by a physical interaction with RanBPM in mammalian cultured cells. *Oncogene*, *24*(5), 938–944. doi:10.1038/sj.onc.1208257

Kremers, G. J., Hazelwood, K. L., Murphy, C. S., Davidson, M. W., & Piston, D. W. (2009). Photoconversion in orange and red fluorescent proteins. *Nature Methods*, *6*(5), 355–358. doi:10.1038/nmeth.1319

Kretsinger, R. H., & Nockolds, C. E. (1973). Carp muscle calcium-binding protein. II. Structure determination and general description. *Journal of Biological Chemistry*, *248*(9), 3313–3326.

Kumar, V., Abbas, A. K., Fausto, N., & Aster, J. C. (2014). *Robbins and Cotran pathologic basis of disease* (9th ed.). Philadelphia: Elsevier Saunders.

Källberg, M., Wang, H., Wang, S., Peng, J., Wang, Z., Lu, H., & Xu, J. (2012). Template-based protein structure modeling using the RaptorX web server. *Nature Protocols*, *7*(8), 1511–1522. doi:10.1038/nprot.2012.085

La Bella, V., Ho, B. K., Appel, S. H., & Smith, R. G. (1996). Calbindin D28K forms a Ca(2+)-dissociable complex with mellitin in vitro. *Biochemistry and Molecular Biology International*, *38*(6), 1199–1210.

Lambers, T. T., Mahieu, F., Oancea, E., Hoofd, L., de Lange, F., Mensenkamp, A. R., et al. (2006). Calbindin-D28K dynamically controls TRPV5-mediated Ca2+ transport. *EMBO Journal*, *25*(13), 2978–2988. doi:10.1038/sj.emboj.7601186

Lee, H. J., Hammond, D. N., & Large, T. H. (1990). Neuronal properties and trophic activities of immortalized hippocampal cells from embryonic and young adult mice. *Journal of Neuroscience*, *10*(6), 1779–1787.

Li, J., & Yuan, J. (2008). Caspases in apoptosis and beyond. *Oncogene*, *27*(8), 6194–6206. doi:10.1038/onc.2008.297

Liu, C., & Hermann, T. E. (1978). Characterization of ionomycin as a calcium ionophore. *Journal of Biological Chemistry*, *253*(17), 5892–5894.

Liu, Y., Porta, A., Peng, X., Gengaro, K., Cunningham, E. B., Li, H., et al. (2003). Prevention of Glucocorticoid-Induced Apoptosis in Osteocytes and Osteoblasts by Calbindin-D28k. *Journal of Bone and Mineral Research*, *19*(3), 479–490. doi:10.1359/jbmr.0301242

Lutz, W., Frank, E. M., Craig, T. A., Thompson, R., Venters, R. A., Kojetin, D., et al. (2003). Calbindin D28K interacts with Ran-binding protein M: identification of interacting domains by NMR spectroscopy. *Biochemical and Biophysical Research Communications*, *303*(4), 1186–1192. doi:10.1016/S0006-291X(03)00499-6

Ma, J., Wang, S., Zhao, F., & Xu, J. (2013). Protein threading using context-specific alignment potential. *Bioinformatics*, *29*(13), i257–i265. doi:10.1093/bioinformatics/btt210

Marchant, J. S., Stutzmann, G. E., Leissring, M. A., LaFerla, F. M., & Parker, I. (2001). Multiphoton-evoked color change of DsRed as an optical highlighter for cellular and subcellular labeling. *Nature Biotechnology*, *19*(7), 645–649. doi:10.1038/90249

Marfori, M., Mynott, A., Bodén, M., & Kobe, B. (2011). Molecular basis for specificity of nuclear import and prediction of nuclear localization. *Biochimica et Biophysica Acta (BBA) - Molecular Cell Research*, *1813*(9), 1562–1577. doi:10.1016/j.bbamcr.2010.10.013

Mattson, M. P., Cheng, B., Baldwin, S. A., Smith-Swintosky, V. L., Keller, J., Geddes, J. W., et al. (1995). Brain injury and tumor necrosis factors induce calbindin D-28K in astrocytes: Evidence for a cytoprotective response. *Journal of Neuroscience Research*, *42*(3), 357–370. doi:10.1002/jnr.490420310

Mattson, M. P., Rychlik, B., Chu, C., & Christakost, S. (1991). Evidence for calcium-reducing and excitoprotective roles for the calcium-binding protein calbindin-1328k in cultured hippocampal neurons. *Neuron*, *6*(1), 41–51.

Medintz, I., & Hildebrandt, N. (2013). *FRET - Förster Resonance Energy Transfer*. Weinheim: Wiley-VCH Verlag GmbH & Co. KGaA. doi:10.1002/9783527656028

Meergans, T., Hildebrant, A. K., Horak, D., Haenisch, C., & Wendel, A. (2000). The short prodomain influences caspase-3 activation in HeLa cells. *Biochemical Journal*, *349*(1), 135–140. doi:10.1042/bj3490135

Meloche, S., & Pouyssegur, J. (2007). The ERK1/2 mitogen-activated protein kinase pathway as a master regulator of the G1-to S-phase transition. *Oncogene*, *26*(22), 3227–3239. doi:10.1038/sj.onc.1210414

Miyawaki, A. (2011). Development of Probes for Cellular Functions Using Fluorescent Proteins and Fluorescence Resonance Energy Transfer. *Annual Review of Biochemistry*, *80*, 357–373. doi:10.1146/annurev-biochem-072909-094736

Molinari, S., Battini, R., Ferrari, S., Pozzi, L., Killcross, A. S., Robbins, T. W., et al. (1996). Deficits in memory and hippocampal long-term potentiation in mice with reduced calbindin D28K expression. *Proceedings of the National Academy of Sciences of the United States of America*, *93*(15), 8028–8033. doi:10.1073/pnas.93.15.8028

Morgan, D. W., Welton, A. F., Heick, A. E., & Christakos, S. (1986). Specific in vitro activation of Ca,Mg-ATPase by vitamin D-dependent rat renal calcium binding protein (calbindin D28K).

Biochemical and Biophysical Research Communications, *138*(2), 547–553. doi:10.1016/S0006-291X(86)80531-9

Murayama, N., Noshita, T., Ogino, R., Masuda, T., Kadoshima, T., Oka, T., et al. (2015). SUN11602-induced hyperexpression of calbindin D-28k is pivotal for the survival of hippocampal neurons under neurotoxic conditions. *Brain Research*, *1594*, 71–81. doi:10.1016/j.brainres.2014.10.066

Nakano, H. (2009). Chemical biology of natural indolocarbazole products: 30 years since the discovery of staurosporine. *The Journal of Antibiotics*, *62*(1), 17–26. doi:10.1038/ja.2008.4

Nieto-Bona, M. P., & Busiguina, S. (1995). Insulin-like growth factor I is an afferent trophic signal that modulates calbindin-28kD in adult Purkinje cells. *Journal of Neuroscience Research*, *42*(3), 371–376. doi:10.1002/jnr.490420311

Nordquist, D. T., Kozak, C. A., & Orr, H. T. (1988). cDNA cloning and characterization of three genes uniquely expressed in cerebellum by Purkinje neurons. *Journal of Neuroscience*, *8*(12), 4780–4789.

Norman, A. W., & Leathers, V. (1982). Preparation of a photoaffinity probe for the vitamin D-dependent intestinal calcium binding protein: Evidence for a calcium dependent, specific interaction with intestinal alkaline phosphatase. *Biochemical and Biophysical Research Communications*, *108*(1), 220–226. doi:10.1016/0006-291X(82)91854-X

Padilla-Parra, S., & Tramier, M. (2012). FRET microscopy in the living cell: Different approaches, strengths and weaknesses. *BioEssays*, *34*(5), 369–376. doi:10.1002/bies.201100086

Pelc, K., Vincent, S., Ruchoux, M. M., Kiss, R., Pochet, R., Sariban, E., et al. (2002). Calbindin-d(28k): a marker of recurrence for medulloblastomas. *Cancer*, *95*(2), 410–419. doi:10.1002/cncr.10666

Peng, J., & Xu, J. (2011a). A multiple-template approach to protein threading. *Proteins: Structure, Function, and Bioinformatics*, *79*(6), 1930–1939. doi:10.1002/prot.23016

Peng, J., & Xu, J. (2011b). RaptorX: exploiting structure information for protein alignment by statistical inference. *Proteins: Structure, Function, and Bioinformatics*, *79*(S10), 161–171. doi:10.1002/prot.23175

Pochet, R., Donato, R., Haiech, J., Heizmann, C. W., & Gerke, V. (2000). *Calcium: The molecular basis of calcium action in biology and medicine*. Dordrecht: Springer Netherlands. doi:10.1007/978-94-010-0688-0

Prasher, D. C., Eckenrode, V. K., Ward, W. W., Prendergast, F. G., & Cormier, M. J. (1992). Primary structure of the Aequorea victoria green-fluorescent protein. *Gene*, *111*(2), 229–233. doi:10.1016/0378-1119(92)90691-H

Reisner, P. D., Christakos, S., & Vanaman, T. C. (1992). In vitro enzyme activation with calbindin-D28k, the vitamin D-dependent 28 kDa calcium binding protein. *FEBS Letters*, *297*(1-2), 127–131. doi:10.1016/0014-5793(92)80342-e

Robinson, L. C., & Marchant, J. S. (2005). Improved "optical highlighter" probes derived from discosoma red fluorescent protein. *Biophysical Journal*, *88*(2), 1444–1457. doi:10.1529/biophysj.104.045617

Romoser, V. A., Hinkle, P. M., & Persechini, A. (1997). Detection in living cells of Ca2+-dependent changes in the fluorescence emission of an indicator composed of two green fluorescent protein variants linked by a calmodulin-binding sequence. A new class of fluorescent indicators. *Journal of Biological Chemistry*, *272*(20), 13270–13274. doi:10.1074/jbc.272.20.13270

Sambrook, J. F., & Russel, D. W. (2001). *Molecular Cloning - A Laboratory Manual* (3rd ed.). New York: Cold Spring Harbor Laboratory Press. doi:10.1086/394015

Sanger, F., Nicklen, S., & Coulson, A. R. (1977). DNA sequencing with chain-terminating inhibitors. *Proceedings of the National Academy of Sciences*, *74*(12), 5463–5467. doi:10.1073/pnas.74.12.5463

Schmidt, H. (2012). Three functional facets of calbindin D-28k. *Frontiers in Molecular Neuroscience*, *5*(25). doi:10.3389/fnmol.2012.00025

Schmidt, H., Schwaller, B., & Eilers, J. (2005). Calbindin D28k targets myo-inositol monophosphatase in spines and dendrites of cerebellar Purkinje neurons. *Proceedings of the National Academy of Sciences of the United States of America*, *102*(16), 5850–5855. doi:10.1073/pnas.0407855102

Seitz, A., Terjung, S., Zimmermann, T., & Pepperkok, R. (2012). Quantifying the influence of yellow fluorescent protein photoconversion on acceptor photobleaching–based fluorescence resonance energy transfer measurements. *Journal of Biomedical Optics*, *17*(1), 011010–0110105. doi:10.1117/1.jbo.17.1.011010

Sekar, R. B., & Periasamy, A. (2003). Fluorescence resonance energy transfer (FRET) microscopy imaging of live cell protein localizations. *The Journal of Cell Biology*, *160*(5), 629–633. doi:10.1083/jcb.200210140

Shamir, A., Belmaker, R. H., & Agam, G. (2005). Interaction of calbindin D28k and inositol monophosphatase in human postmortem cortex: possible implications for bipolar disorder. *Bipolar Disorders*, *7*(1), 42–48. doi:10.1111/j.1399-5618.2004.00162.x

Shaner, N. C., Campbell, R. E., Steinbach, P. A., Giepmans, B. N. G., Palmer, A. E., & Tsien, R. Y. (2004). Improved monomeric red, orange and yellow fluorescent proteins derived from Discosoma sp. red fluorescent protein. *Nature Biotechnology*, *22*(12), 1567–1572.

Sharma, A. K., & Rohrer, B. (2004). Calcium-induced calpain mediates apoptosis via caspase-3 in a mouse photoreceptor cell line. *Journal of Biological Chemistry*, *279*(34), 35564–35572. doi:10.1074/jbc.M401037200

Sheehan, J. P., Swerdlow, R. H., Parker, W. D., Miller, S. W., Davis, R. E., & Tuttle, J. B. (1997). Altered calcium homeostasis in cells transformed by mitochondria from individuals with Parkinson's disease. *Journal of Neurochemistry*, *68*(3), 1221–1233.

Song, Z., McCall, K., & Steller, H. (1997). DCP-1, a Drosophila cell death protease essential for development. *Science*, *275*(5299), 536–540. doi:10.1126/science.275.5299.536

Sun, Y., Wallrabe, H., Seo, S.-A., & Periasamy, A. (2010). FRET Microscopy in 2010: The Legacy of Theodor Förster on the 100th Anniversary of his Birth. *ChemPhysChem*, *12*(3), 462–474. doi:10.1002/cphc.201000664

Tait, S. W. G., & Green, D. R. (2008). Caspase-independent cell death: Leaving the set without the final cut. *Oncogene*, *27*(50), 6452–6461. doi:10.1038/onc.2008.311

Towbin, H., Staehelin, T., & Gordon, J. (1979). Electrophoretic transfer of proteins from polyacrylamide gels to nitrocellulose sheets: Procedure and some applications. *Proceedings of the National Academy of Sciences of the United States of America*, *76*(9), 4350–4354.

Valentin, G., Verheggen, C., Piolot, T., Neel, H., Coppey-Moisan, M., & Bertrand, E. (2005). Photoconversion of YFP into a CFP-like species during acceptor photobleaching FRET experiments. *Nature Methods*, *2*(11), 801. doi:10.1038/nmeth1105-801

Varghese, S., Lee, S., Huang, Y. C., & Christakos, S. (1988). Analysis of rat vitamin D-dependent calbindin-D28k gene expression. *Journal of Biological Chemistry*, *263*(20), 9776–9784.

Verrier, S. E., & Söling, H. D. (2006). Photobleaching of YFP does not produce a CFP-like species that affects FRET measurements. *Nature Methods*, *3*(7), 491–492. doi:10.1038/nmeth0706-491b

Volbracht, C., Leist, M., Kolb, S. A., & Nicotera, P. (2001). Apoptosis in Caspase-inhibited Neurons. *Molecular Medicine*, *7*(1), 36–48.

Wang, H.-J., Cao, J.-P., Yu, J.-K., Zhang, L.-C., Jiang, Z.-J., & Gao, D.-S. (2008). Calbindin-D28K expression induced by glial cell line-derived neurotrophic factor in substantia nigra neurons dependent on PI3K/Akt/NF-κB signaling pathway. *European Journal of Pharmacology*, *595*(1), 7–12. doi:10.1016/j.ejphar.2008.07.044

Wasserman, R. H., & Fullmer, C. S. (1989). On the molecular mechanism of intestinal calcium transport. *Advances in Experimental Medicine and Biology*, *249*, 45–65. doi:10.1007/978-1-4684-9111-1_5

Wasserman, R. H., & Taylor, A. N. (1966). Vitamin D3-induced calcium-binding protein in chick intestinal mucosa. *Science*, *152*(3723), 791–793. doi:10.1126/science.152.3723.791

Watanabe, H., Imaizumi, M., Ojika, T., Abe, T., Hida, T., & Kato, K. (1994). Evaluation of biological characteristics of lung cancer by the human 28 kDa vitamin D-dependent calcium binding protein, calbindin-D28k. *Japanese Journal of Clinical Oncology*, *24*(3), 121–127.

Winsky, L., & Kuźnicki, J. (1995). Distribution of calretinin, calbindin D28k, and parvalbumin in subcellular fractions of rat cerebellum: effects of calcium. *Journal of Neurochemistry*, *65*(1), 381–388. doi:10.1046/j.1471-4159.1995.65010381.x

Xia, Z., & Liu, Y. (2001). Reliable and global measurement of fluorescence resonance energy transfer using fluorescence microscopes. *Biophysical Journal*, *81*(4), 2395–2402. doi:10.1016/S0006-3495(01)75886-9

Yan, R., Xu, D., Yang, J., Walker, S., & Zhang, Y. (2013). A comparative assessment and analysis of 20 representative sequence alignment methods for protein structure prediction. *Scientific Reports*, *3*(2619). doi:10.1038/srep02619

Zhang, J. H., Morita, Y., & Hironaka, T. (1990). Ontological study of calbindin-D28k-like and parvalbumin-like immunoreactivities in rat spinal cord and dorsal root ganglia. *The Journal of Comparative Neurology*, *302*(4), 715–728. doi:10.1002/cne.903020404

Zhou, Q., Yen, A., Rymarczyk, G., Asai, H., Trengrove, C., Aziz, N., et al. (2016). Impairment of PARK14-dependent Ca2+ signalling is a novel determinant of Parkinson's disease. *Nature Communications*, *7*(10332). doi:10.1038/ncomms10332

Appendix

Suppl.: pCMV5 vector plasmid

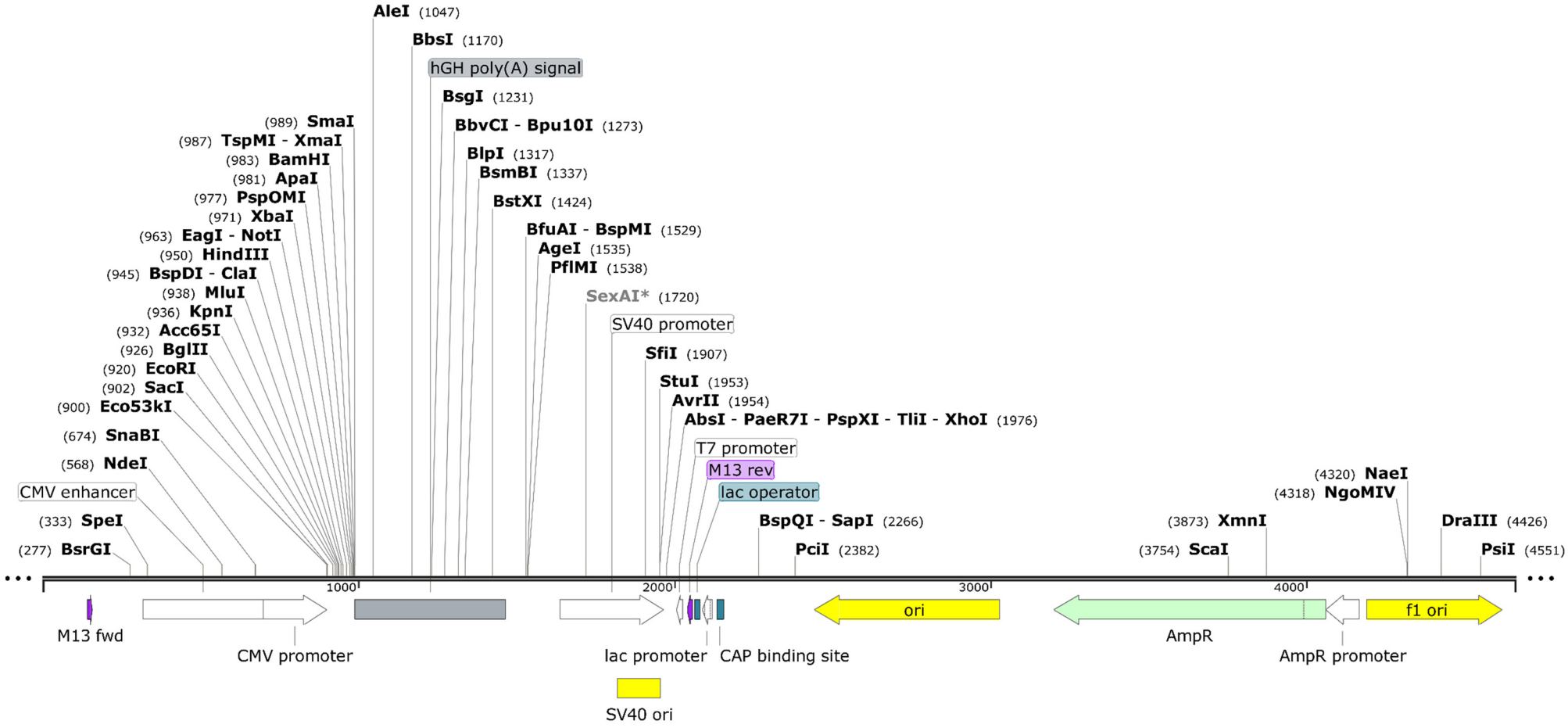

SnapGene Viewer, Version 2.8.3

Suppl.: mAmetrine forward and reverse primer

Forward primer:

1. `5'-N6-gaattc-ATG-GTG-AGC-AAG-GGC-GAG-3'`

   -EcoR1: 5'-g/aattc-3'-
   Gene specific part of mAmetrine from the *mAmetrine-DEVD-dtTomato* sequence

2. `5'-N6-gaattc-ACC-ATG-GTG-AGC-AAG-GGC-3'`

   In accordance with the Kozak rule, the upstream ACC codon from the original *mAmetrine-DEVD-tdTomato* sequence was included and the downstream GAG from the draft was removed in order to preserve the primer's length.

3. `5'-N6-gaattc-GCC-ACC-ATG-GTG-AGC-AAG-3'`

   Then the 3'-GC clamp (downstream GGC) was removed in order to prevent unwanted stronger 3' binding to the DNA.
   In order to preserve the primer's length, the upstream GCC codon from the original *mAmetrine-DEVD-tdTomato* sequence was included.

4. `5'-GAC-TAT-gaattc-GCC-ACC-ATG-GTG-AGC-AAG-3'`

   In regard of an optimal annealing temperature and prevention of unwanted loop formation this N6 sequence was chosen.

   Gene specific part of the primer:
   61 % GC content
   39 % AT content

   Complete primer:
   50 % GC content
   50 % AT content

Reverse primer:

1. `5'-N6-aagctt-ACC-GGC-AGT-GGC-AGC-GGA-3'`

   -Hind3: 5'-a/agctt-3'-
   mAmetrine-DEVD-dtTomato sequence including the plasmid linker:
   ggt-acc-ggc-agt-ggc-agc-gga
   (protein translation: GTGSGSG)
   Part of the linker was used as the gene specific part (preserving the functional linker):
   5'-acc-ggc-agt-ggc-agc-gga-3'

2. `5'-N6-aagctt-ACC-GGC-AGT-GGC-AGT-GGA-3'`

   The GC content of the gene specific part of the primer was reduced from 72 % to 67 % by exchanging the

Suppl.: mAmetrine forward and reverse primer

AGC codon for an AGT codon (alternate codon for Serine).

3. `5'-N6-aagctt-TCC-ACT-GCC-ACT-GCC-GGT-3'`

   The reverse complement of the gene specific part was created.

4. `5'-TAG-ATC-aagctt-TCC-ACT-GCC-ACT-GCC-GGT-3'`

   In regard of an optimal annealing temperature and prevention of unwanted loop formation this N6 sequence was chosen.

Gene specific part of the primer:
67 % GC content
33 % AT content

Complete primer:
53 % GC content
47 % AT content

NEB TM calculator [Phusion High-Fidelity DNA Polymerase (HF Buffer], 500 nM)

Gene specific part:
Anneal Temp: 66 °C
Forward primer: 66 °C
(**GCCACCATGGTGAGCAAG**)
Reverse primer: 71 °C
(**TCCACTGCCACTGCCGGT**)
[Tm difference is at the recommended limit of 5 °C.]

Complete primer:
Anneal Temp: 72 °C
Forward primer: 76 °C
(**GACTATGAATTCGCCACCATGGTGAGCAAG**)
Reverse primer: 79 °C
(**TAGATCAAGCTTTCCACTGCCACTGCCGGT**)

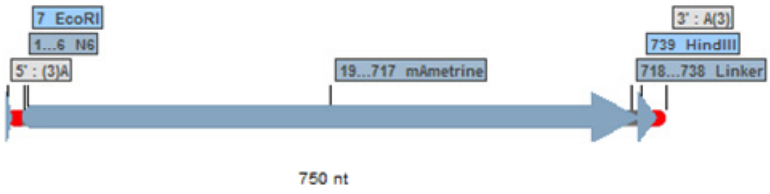

PCR simulation created with Serial Cloner 2.61

Suppl.: CBD28k forward and reverse primer

Forward primer:

1. `5'-N6-aagctt-ATG-GCA-GAA-TCC-CAC-CTG-3'`

   -Hind3: 5'-a/agctt-3'-
   Gene specific part from the *Mus Musculus Calbindin 1* sequence

2. `5'-N6-aagctt-ACG-ATG-GCA-GAA-TCC-CAC-3'`

   In accordance with the Kozak rule, the upstream ACG codon from the original *Mus Musculus Calbindin 1* sequence was included and the downstream CTG from the draft was removed in order to preserve the primer's length.

3. `5'-N6-aagctt-ACC-ACG-ATG-GCA-GAA-TCC-3'`

   56 % GC content of the gene specific part of the primer is in the recommended range of 40 – 60 %.
   The 3'-GC clamp (downstream CAC) was removed in order to prevent unwanted stronger 3' binding to the DNA.
   In order to preserve the primer's length, the upstream ACC codon from the original *Mus Musculus Calbindin 1* sequence was included.

4. `5'-N6-aagctt-ACT-ACG-ATG-GCA-GAA-TCC-3'`

   Due to a calculated Tm difference of 10 °C, the ACC codon of the primer's gene specific part was exchanged for an ACT codon (alternate codon for Threonine).

5. `5'-TAA-GTA-aagctt-ACT-ACG-ATG-GCA-GAA-TCC-3'`

   In regard of an optimal annealing temperature and prevention of unwanted loop formation this N6 sequence was chosen.

   Gene specific part of the primer:
   56 % GC content
   44 % AT content

   Complete primer:
   43 % GC content
   57 % AT content

Reverse primer:

1. `5'-N6-ggatcc-TCT-GCT-GGA-GAC-AAC-TAG-3'`

   -BamH1: 5'-g/gatcc-3'-
   Gene specific part from the *Mus Musculus Calbindin 1* sequence

Suppl.: CBD28k forward and reverse primer

2. `5'-N6-ggatcc-CTA-GTT-GTC-TCC-AGC-AGA-3'`

3. `5'-TAA-GTA-ggatcc-CTA-GTT-GTC-TCC-AGC-AGA-3'`

The reverse complement of the gene specific part was created.

In regard of an optimal annealing temperature and prevention of unwanted loop formation this N6 sequence was chosen.

Gene specific part of the primer:
50 % GC content
50 % AT content

Complete primer:
47 % GC content
53 % AT content

NEB TM calculator [Phusion High-Fidelity DNA Polymerase (HF Buffer], 500 nM)

Gene specific part:
Anneal Temp: 54 °C
Forward primer: 58 °C
(**ACTACGATGGCAGAATCC**)
Reverse primer: 54 °C
(**CTAGTTGTCTCCAGCAGA**)

Complete primer:
Anneal Temp: 70 °C
Forward primer: 67 °C
(**TAAGTAAAGCTTACTACGATGGCAGAATCC**)
Reverse primer: 70 °C
(**TAAGTAGGATCCCTAGTTGTCTCCAGCAGA**)

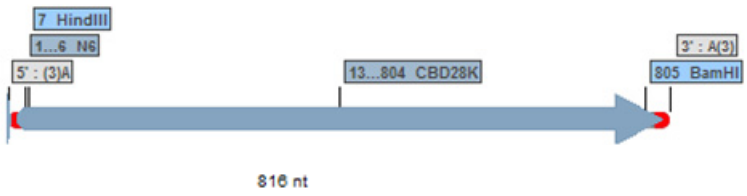

PCR simulation created with Serial Cloner 2.61

Suppl.: tdTomato forward and reverse primer

Forward primer:

1. `5'-N6-gaattc-ATG-GTG-AGC-AAG-GGC-GAG-3'`

   -EcoRI: 5'-G/AATTC-3'-
   Gene specific part of tdTomato from the *mAmetrine-DEVD-dtTomato* sequence

2. `5'-N6-gaattc-GGT-ATG-GTG-AGC-AAG-GGC-3'`

   In accordance with the Kozak rule, the upstream GGT codon from the original *mAmetrine-DEVD-tdTomato* sequence was included and the downstream GAG from the draft was removed in order to preserve the primer's length.

3. `5'-N6-gaattc-GAT-GGT-ATG-GTG-AGC-AAG-3'`

   Then the 3'-GC clamp (downstream GGC) was removed in order to prevent unwanted stronger 3' binding to the DNA.
   In order to preserve the primer's length, the upstream GAT codon from the original *mAmetrine-DEVD-tdTomato* sequence was included.

4. `5'-TAT-GTA-gaattc-GAT-GGT-ATG-GTG-AGC-AAG-3'`

   In regard of an optimal annealing temperature and prevention of unwanted loop formation this N6 sequence was chosen.

   Gene specific part of the primer:
   50 % GC content
   50 % AT content

   Complete primer:
   40 % GC content
   60 % AT content

Reverse primer:

1. `5'-N6-ggtacc-ATG-GAC-GAG-CTG-TAC-AAG-3'`

   -KpnI: 5'-ggtac/c-3'-
   Gene specific part of tdTomato from the *mAmetrine-DEVD-dtTomato* sequence without stop codon TAA

2. `5'-N6-ggtacc-CTT-GTA-CAG-CTC-GTC-CAT-3'`

   The reverse complement of the gene specific part was created.

3. `5'-CAC-CTA-ggtacc-CTT-GTA-CAG-CTC-GTC-CAT-3'`

   In regard of an optimal annealing temperature and prevention of

unwanted loop formation this N6 sequence was chosen.

Gene specific part of the primer:
50 % GC content
50 % AT content

Complete primer:
53 % GC content
47 % AT content

NEB TM calculator [Phusion High-Fidelity DNA Polymerase (HF Buffer], 500 nM)

Gene specific part:
Anneal Temp: 53 °C
Forward primer: 56 °C
(**GATGGTATGGTGAGCAAG**)
Reverse primer:53 °C
(**TACCTTGTACAGCTCGTC**)

Complete primer:
Anneal Temp: 72 °C
Forward primer: 70 °C
(**TATGTAGAATTCGATGGTATGGTGAGCAAG**)
Reverse primer: 73 °C
(**CACCTAGGTACCCTTGTACAGCTCGTCCAT**)

PCR simulation created with Serial Cloner 2.61

Suppl.: CASP3 forward and reverse primer

Forward primer:

1. `5'-N6-ggtacc-`
   `ATG-GAG-AAC-AAC-AAA-ACC-3'`

   -KpnI: 5'-ggtac/c-3'-
   Gene specific part from the Mus Musculus Casp3 sequence

2. `5'-N6-ggtacc-`
   `ACC-ATG-GAG-AAC-AAC-AAA-3'`

   In accordance with the Kozak rule, the upstream ACC codon from the original RIKEN CASP3 sequence was included and the downstream ACC from the draft was removed in order to preserve the primer's length.

   39 % GC content of the gene specific part of the primer is almost in the recommended range of 40 – 60 %.

3. `5'-GGT-CGT-ggtacc-`
   `ACC-ATG-GAG-AAC-AAC-AAA-3'`

   In regard of an optimal annealing temperature and prevention of unwanted loop formation this N6 sequence was chosen.

   Gene specific part of the primer:
   39 % GC content
   61 % AT content

   Complete primer:
   50 % GC content
   50 % AT content

Reverse primer:

1. `5'-N6-atcgat-`
   `CTG-TAC-TTT-TAT-CAC-TAG-3'`

   -ClaI: 5'-at/cgat-3'-
   Gene specific part from the Mus Musculus CASP3 sequence

2. `5'-N6-atcgat-`
   `CTA-GTG-ATA-AAA-GTA-CAG-3'`

   The reverse complement of the gene specific part was created.

3. `5'-GCG-GGC-atcgat-`
   `CTA-GTG-ATA-AAA-GTA-CAG-3'`

   In regard of an optimal annealing temperature and prevention of unwanted loop formation this N6 sequence was chosen.

   Gene specific part of the primer:
   33 % GC content
   67 % AT content

   Complete primer:
   47 % GC content
   53 % AT content

Suppl.: CASP3 forward and reverse primer

NEB TM calculator [Phusion High-Fidelity DNA Polymerase (HF Buffer], 500 nM)

Gene specific part:

Anneal Temp: 40 °C

Forward primer: 56 °C

(**ACCATGGAGAACAACAAA**)

Reverse primer: 40 °C

(**CTAGTGATAAAAGTACAG**)

Complete primer:

Anneal Temp: 72 °C

Forward primer: 77 °C

(**GGTCGTGGTACCACCATGGAGAACAACAAA**)

Reverse primer: 72 °C

(**GCGGGCATCGATCTAGTGATAAAAGTACAG**)

PCR simulation created with Serial Cloner 2.61

Suppl.: IMPase secondary structure

PSIPRED secondary structure prediction

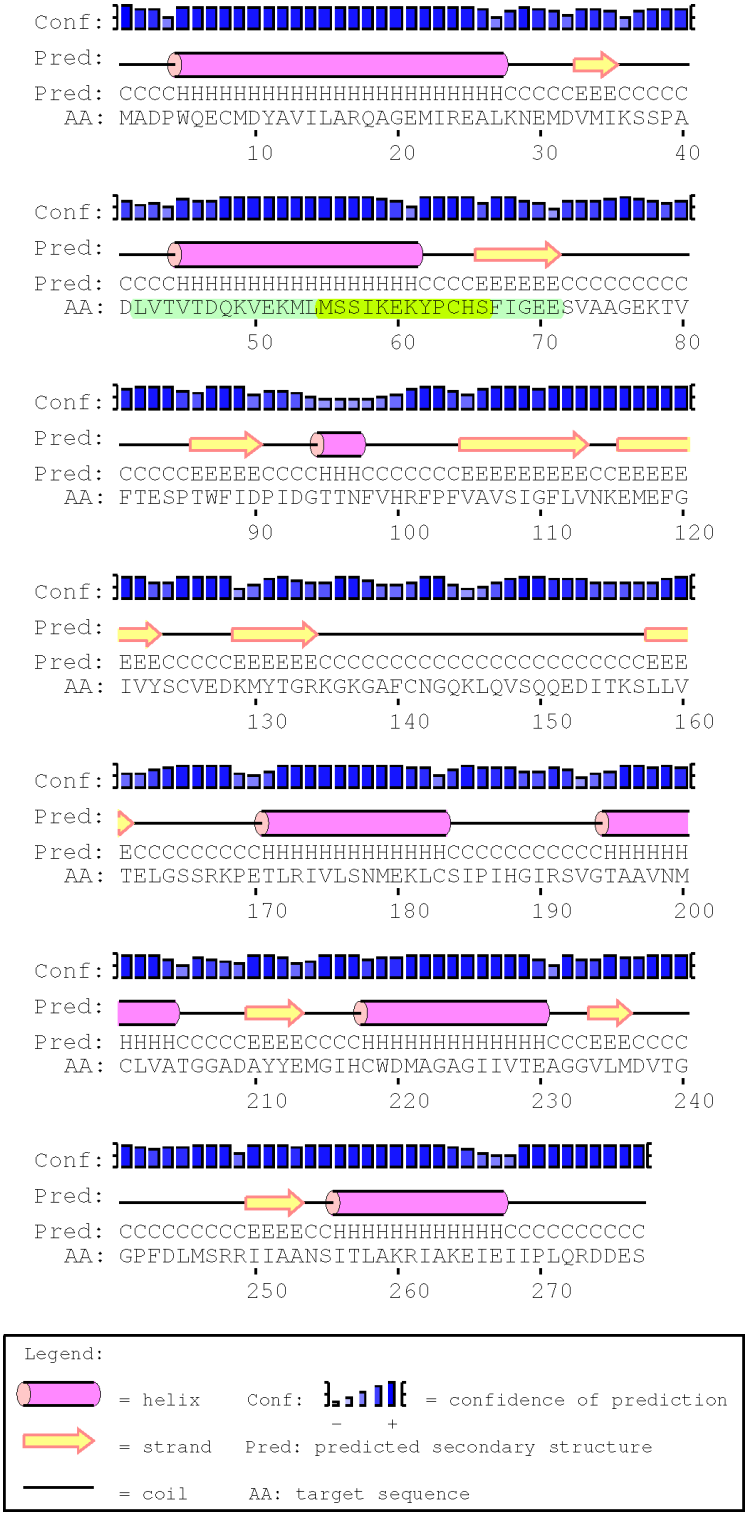

*green: helix building sequence w/ interaction site

*yellow: 12 amino acid interaction site

PSSpred

The following is the secondary structure prediction (C - Coil,
H - helix, E - strand).

```
seq:   1 MADPWQECMDYAVILARQAGEMIREALKNEMDVMIKSSPADLVTVTDQKVEKMLMSSIKE  60
SS:        CCCHHHHHHHHHHHHHHHHHHHHHHHHHHCCCCEEEEECCCCCCHHHHHHHHHHHHHHHHHH
conf:    9863999999999999999999999699851899658998501899999999999999

seq:  61 KYPCHSFIGEESVAAGEKTVFTESPTWFIDPIDGTTNFVHRFPFVAVSIGFLVNKEMEFG 120
SS:        HCCCCCEEEEECCCCCCCCCCCCCEEEEECCCCCHHHHCCCCCEEEEEEEECCEEEEE
conf:    7999936863258887655578982699815998302221898438999999999899999

seq: 121 IVYSCVEDKMYTGRKGKGAFCNGQKLQVSQQEDITKSLLVTELGSSRKPETLRIVLSNME 180
SS:        EEECCCCCCEEEEECCCCEEECCEECCCCCCCCCHHHCEEEECCCCCCCCHHHHHHHHHHH
conf:    9962236914899669853547743246899974316699658888872478999999999

seq: 181 KLCSIPIHGIRSVGTAAVNMCLVATGGADAYYEMGIHCWDMAGAGIIVTEAGGVLMDVTG 240
SS:        HHHHHHCCCCCCCCHHHHHHHHHHHHCCCCEEEECCCCHHHHHHHHHHHHHHHCCEEECCCC
conf:    997222143256438999999998488619995699978999999999984948985999

seq: 241 GPFDLMSRRIIAANSITLAKRIAKEIEIIPLQRDDES 277
SS:        CCCCCCCCCEEEECCHHHHHHHHHHHHHHCCCCCCCCC
conf:    9754578857995688999999999974489888889
```

Suppl.: pIMPase design and construction

IMPase interaction site (with helix):

LVTVTDQKVEKML-MSSIKEKYPCHS-FIGEE (residues 42 - 71)

The following linker was chosen due to its favorable secondary structure:

GTGSGSGSGSTG (considered alternatives: **EAAA**, **GSGSGSG**, **EAAAK**, **EEEKKKK**)

An oligopeptide was designed and constructed with additional KpnI (**5'-GGTAC/C-3'**) and ClaI (**5'-AT/CGAT-3'**) restriction sites and N6 sequence:

GTGSGSGSGSTGLVTVTDQKVEKMLMSSIKEKYPCHSFIGEE

→ Reverse Translation:

GGCACCGGCAGCGGCAGCGGCAGCGGCAGCACCGGCCTGGTGACCGTGACCGACCAGAAGGTGGAGAA
GATGCTGATGAGCAGCATCAAGGAGAAGTACCCCTGCCACAGCTTCATCGGCGAGGAGTGA

→ Addition of restriction sites and N6 sequence:

GTA-GGC-GGT-ACC-GGC-ACC-GGC-AGC-GGC-AGC-GGC-AGC-GGC-AGC-ACC-GGC-CTG-GTG-ACC-GTG-ACC-GAC-CAG-AAG-GTG-GAG-AAG-ATG-CTG-ATG-AGC-AGC-ATC-AAG-GAG-AAG-TAC-CCC-TGC-CAC-AGC-TTC-ATC-GGC-GAG-GAG-TGA-TAA-ATC-GAT-TAG-CGC

Oligopeptide primer pair (Annealing temperature: 68 °C | 5 cycles):

5'-GTA-TTA-GGT-ACC-GGA-AGT-GGA-AGC-GGC-AGC-GGC-AGC-GGC-AGC-ACC-GGC-CTG-GTG-ACC-GTG-ACC-GAC-CAG-AAG-GTG-GAG-AAG-ATG-CTG-3'

5'-GCG-CTA-ATC-GAT-TTA-TCA-CTC-CTC-GCC-GAT-GAA-GCT-GTG-GCA-GGG-GTA-CTT-CTC-CTT-GAT-GCT-GCT-CAT-CAG-CAT-CTT-CTC-CAC-CTT-CTG-GTC-3'

Amplification forward primer (Kpn1):

5'-GTA-TTA-ggt-acc-GGA-AGT-GGA-3'

Amplification reverse primer (Cla1):

5'-GCG-CTA-atc-gat-TTA-TCA-CTC-3'

Annealing temperature: 61 °C | 30 cycles

Suppl.: mAmetrine (w/ linker and w/o TAA stop codon) + EcoR1 + CBDK28k (w/ stop codon) inserted in pCMV5 MCS

green = mAmetrine
red = linker region
blue = CBD28k

5’-ATAGAGAGCTCGTTTAGTGAACCGTCA
G/AATTC
GCCACCATGGTGAGCAAGGGCGAGGAGCTGTTCACCGGGGTGGTGCCCATCCTGGTCGAGCTGGACGGCGACGTA
AACGGCCACAAGTTCAGCGTGCGCGGCGAGGGCGAGGGCGATGCCACCAACGGCAAGCTGACCCTGAAGTTCATC
TGCACCTCCGGCAAGCTGCCCGTGCCCTGGCCCACCCTCGTGACCACCCTGTCTTACGGCGTGCAGTGCTTCGCC
CGCTACCCCGACCACATGAAGCAGCACGACTTCTTCAAGTCCGCCATGCCCGAAGGCTACGTCCAGGAGCGCACC
ATCTCCTTCAAGGACGACGGCAGCTACAGGACCCGCGCCGAGGTGAAGTTCGAGGGCGACACCCTGGTGAACCGC
ATCGAGCTGAAGGGCATCGACTTCAAGGAGGACGGCAACATCCTGGGGCACAAGCTGGAGTACAACATGAACGTG
TGGGACGCGTATATCACGGCCGACAAGCAGAAGAACGGCATCAAAGCGAACTTCAAGATCGAGCACAACGTCGAG
GACGGCGGCGTGCAGCTCGCCGACGCGTACCAGCAGAACACCCCCATCGGCGACGGCTCCGTGCTGCTGCCTGAC
AACCACTACCTGAGCTTCCAGAGCAAGCTGTTCAAAGACCCCAACGAGCAGCGCGATCACATGGTCCTGCTGGAG
TTCGTTACCGCCGCCGGGATCACTCTCGGC
GGTACCGGCAGTGGCAGTGGA
A/AGCTT
ACCACGATGGCAGAATCCCACCTGCAGTCATCTCTGATCACAGCCTCACAGTTTTTTGAGATCTGGCTTCATTTC
GACGCTGACGGAAGTGGTTACCTGGAAGGAAAGGAGCTGCAGAACTTGATCCAGGAGCTTCTGCAGGCGCGAAAG
AAGGCTGGATTGGAGCTATCACCGGAAATGAAATCCTTTGTGGATCAATATGGACAGAGAGATGATGGAAAAATA
GGAATTGTAGAGTTGGCTCACGTCTTACCCACAGAAGAGAATTTCTTGCTGCTCTTTCGATGCCAGCAACTGAAG
TCCTGCGAGGAATTCATGAAGACTTGGAGAAAGTATGATACTGACCACAGCGGCTTCATCGAAACCGAGGAACTT
AAGAACTTTCTAAAGGACCTACTAGAGAAAGCAAACAAGACTGTGGATGATACAAAACTAGCAGAGTACACAGAC
CTCATGCTGAAACTATTTGATTCAAATAATGACGGAAAGCTGGAACTGACAGAGATGGCCAGGTTACTACCAGTG
CAGGAAAATTTCCTTCTTAAATTCCAGGGAATCAAAATGTGTGGGAAAGAGTTCAATAAGGCTTTTGAGTTATAT
GATCAGGATGGCAACGGATACATAGATGAAAATGAGCTGGATGCTTTGCTGAAAGATCTGTGTGAGAAGAACAAA
CAGGAATTGGATATTAACAATATTACTACATACAAGAAGAACATAATGGCCTTGTCGGATGGAGGGAAGCTGTAC
CGAACAGACCTTGCTCTTATTCTTTCTGCTGGAGACAACTAG
G/GATCC
CGGGTGGCATCCCTGTGACCCCTCCCCAGTGCCTCTCCTGGCCCTGGAAGTTGCCACTCCAGTGCCCACCAGCCT
TGTCCTAATAAAATTAAGTTGCATCATTTTGTCTGACTAGGTGTCCTTCTATAATATTATGGGGTGGAGGGGGGT
GGTATGGAGCAAGGGGCAAGTTGGGAAGACAACCTGTAGGGCCTGCGGGGTCTATTGGGAACCAAGCTGGAGTGC
AGTGGCACAATCTTGGCTCACTGCAATCTCCGCCTCCTGGGTTCAAGCGATTCTCCTGCCTCAGCCTCCCGAGTT
GTTGGGATTCCAGGCATGCATGACCAGGCTCAGCTAATTTTTGTTTTTTTGGTAGAGACGGGGTTTCACCATATT
GGCCAGGCTGGTCTCCAACTCCTAATCTCAGGTGATCTACCCACCTTGGCCTCCCAAATTGCTGGGATTACAGGC
GTGAACCACTGCTCCCTTCCCTGTCCTTCTGATTTTAAAATAACTATACCAGCAGGAGGACGTCCAGACACAGCA
TAGGCTACCTGGCCATGCCCAACCGGTGGGACATTTGAGTTGCTTGCTTGGCACTGTCCTCTCATGCGTTGGGTC
CACTCAGTAGATGCCTGTTGAATTGGGTACGCGGCCAGCTTGGCTGTGGAATGTGTGTCAGTTAGGGTGTGGAAA
GTCCCCAGGCTCCCCAGCAGGCAGAAGTATGCAAAGCATGCATCTCAATTAGTCAGCAACCAGGTGTGGAAAGTC
CCCAGGCTCCCCAGCAGGCAGAAGTATGCAAAGCATGCATCTCAATTAGTCAGCAACCATAGTCCCGCCCCTAAC
TCCGCCCATCCCGCCCCTAACTCCGCCCAGTTCCGCCCATTCTCCGCCCCATGGCTGACTAATTTTTTTTATTTA
TGC-3’

Suppl.: mAmetrine (w/ linker and w/o TAA stop codon) + EcoR1 + CBDK28k (w/ stop codon) inserted in pCMV5 MCS

TRANSLATION (57 kDa):

MVSKGEELFTGVVPILVELDGDVNGHKFSVRGEGEGDATNGKLTLKFICTSGKLPVPWPTLVTTLSYGVQCFARY
PDHMKQHDFFKSAMPEGYVQERTISFKDDGSYRTRAEVKFEGDTLVNRIELKGIDFKEDGNILGHKLEYNMNVWD
AYITADKQKNGIKANFKIEHNVEDGGVQLADAYQQNTPIGDGSVLLPDNHYLSFQSKLFKDPNEQRDHMVLLEFV
TAAGITLGGTGSGSGKLTTMAESHLQSSLITASQFFEIWLHFDADGSGYLEGKELQNLIQELLQARKKAGLELSP
EMKSFVDQYGQRDDGKIGIVELAHVLPTEENFLLLFRCQQLKSCEEFMKTWRKYDTDHSGFIETEELKNFLKDLL
EKANKTVDDTKLAEYTDLMLKLFDSNNDGKLELTEMARLLPVQENFLLKFQGIKMCGKEFNKAFELYDQDGNGYI
DENELDALLKDLCEKNKQELDINNITTYKKNIMALSDGGKLYRTDLALILSAGDN*

Suppl.: TdTomato (w/o TAA stop codon) + Kpn1 + GTT-Linker + CASP3 (w/ stop codon) inserted in pCMV5 MCS

green = tdTomato
red = linker region
blue = CASP3

5'-ATAGAGAGCTCGTTTAGTGAACCGTCA
G/AATTC
GATGGTATGGTGAGCAAGGGCGAGGAGGTCATCAAAGAGTTCATGCGCTTCAAGGTGCGCATGGAGGGCTCCATG
AACGGCCACGAGTTCGAGATCGAGGGCGAGGGCGAGGGCCGCCCCTACGAGGGCACCCAGACCGCCAAGCTGAAG
GTGACCAAGGGCGGCCCCCTGCCCTTCGCCTGGGACATCCTGTCCCCCCAGTTCATGTACGGCTCCAAGGCGTAC
GTGAAGCACCCCGCCGACATCCCCGATTACAAGAAGCTGTCCTTCCCCGAGGGCTTCAAGTGGGAGCGCGTGATG
AACTTCGAGGACGGCGGTCTGGTGACCGTGACCCAGGACTCCTCCCTGCAGGACGGCACGCTGATCTACAAGGTG
AAGATGCGCGGCACCAACTTCCCCCCCGACGGCCCCGTAATGCAGAAGAAGACCATGGGCTGGGAGGCCTCCACC
GAGCGCCTGTACCCCCGCGACGGCGTGCTGAAGGGCGAGATCCACCAGGCCCTGAAGCTGAAGGACGGCGGCCAC
TACCTGGTGGAGTTCAAGACCATCTACATGGCCAAGAAGCCCGTGCAACTGCCCGGCTACTACTACGTGGACACC
AAGCTGGACATCACCTCCCACAACGAGGACTACACCATCGTGGAACAGTACGAGCGCTCCGAGGGCCGCCACCAC
CTGTTCCTGGGGCATGGCACCGGCAGCACCGGCAGCGGCAGCTCCGGCACCGCCTCCTCCGAGGACAACAACATG
GCCGTCATCAAAGAGTTCATGCGCTTCAAGGTGCGCATGGAGGGCTCCATGAACGGCCACGAGTTCGAGATCGAG
GGCGAGGGCGAGGGCCGCCCCTACGAGGGCACCCAGACCGCCAAGCTGAAGGTGACCAAGGGCGGCCCCCTGCCC
TTCGCCTGGGACATCCTGTCCCCCCAGTTCATGTACGGCTCCAAGGCGTACGTGAAGCACCCCGCCGACATCCCC
GATTACAAGAAGCTGTCCTTCCCCGAGGGCTTCAAGTGGGAGCGCGTGATGAACTTCGAGGACGGCGGTCTGGTG
ACCGTGACCCAGGACTCCTCCCTGCAGGACGGCACGCTGATCTACAAGGTGAAGATGCGCGGCACCAACTTCCCC
CCCGACGGCCCCGTAATGCAGAAGAAGACCATGGGCTGGGAGGCCTCCACCGAGCGCCTGTACCCCCGCGACGGC
GTGCTGAAGGGCGAGATCCACCAGGCCCTGAAGCTGAAGGACGGCGGCCACTACCTGGTGGAGTTCAAGACCATC
TACATGGCCAAGAAGCCCGTGCAACTGCCCGGCTACTACTACGTGGACACCAAGCTGGACATCACCTCCCACAAC
GAGGACTACACCATCGTGGAACAGTACGAGCGCTCCGAGGGCCGCCACCACCTGTTCCTGTACGGCATGGACGAG
CTGTACAAG
GGTAC/C
ACCATGGAGAACAACAAAACCTCAGTGGATTCAAAATCCATTAATAATTTTGAAGTAAAGACCATACATGGGAGC
AAGTCAGTGGACTCTGGGATCTATCTGGACAGTAGTTACAAAATGGATTATCCTGAAATGGGCATATGCATAATA
ATTAATAATAAGAACTTCCATAAGAGCACTGGAATGTCATCTCGCTCTGGTACGGATGTGGACGCAGCCAACCTC
AGAGAGACATTCATGGGCCTGAAATACCAAGTCAGGAATAAAAATGATCTTACTCGTGAAGACATTTTGGAATTA
ATGGATAGTGTTTCTAAGGAAGATCATAGCAAAAGGAGCAGCTTTGTGTGTGTGATTCTAAGCCATGGTGATGAA
GGGGTCATTTATGGGACAAATGGGCCTGTTGAACTGAAAAAGTTGACTAGCTTCTTCAGAGGCGACTACTGCCGG
AGTCTGACTGGAAAGCCGAAACTCTTCATCATTCAGGCCTGCCGGGGTACGGAGCTGGACTGTGGCATTGAGACA
GACAGTGGGACTGATGAGGAGATGGCTTGCCAGAAGATAGCCGGTGGAGGCTGACTTCCTGTATGCTTACTCTAC
AGCACCTGGTTACTATTCCTGGAGAAATTCAAAGGACGGGTCGTGGTTCATCCAGTCCCTTTGCAGCATGCTGAA
GCTGTACGCGCACAAGCTAGAATTTATGCACATTCTCACTCGCGTTAACAGGAAGGTGGCAACGGAATTCGAGTC
CTTCTCCCTGGACTCCACTTTCCACGCAAAGAAACAGATCCCGTGTATTGTGTCCATGCTCACGAAAGAACTGTA
CTTTTATCACTAG
AT/CGAT
AAGCTTATGCATGCGGCCGCATCTAGAGGGCCCGGATCCCGGGTGGCATCCCTGTGACCCCTCCCCAGTGCCTCT
CCTGGCCCTGGAAGTTGCCACTCCAGTGCCCACCAGCCTTGTCCTAATAAAATTAAGTTGCATCATTTTGTCTGA
CTAGGTGTCCTTCTATAATATTATGGGGTGGAGGGGGGTGGTATGGAGCAAGGGGCAAGTTGGGAAGACAACCTG
TAGGGCCTGCGGGGTCTATTGGGAACCAAGCTGGAGTGCAGTGGCACAATCTTGGCTCACTGCAATCTCCGCCTC
CTGGGTTCAAGCGATTCTCCTGCCTCAGCCTCCCGAGTTGTTGGGATTCCAGGCATGCATGACCAGGCTCAGCTA
ATTTTTGTTTTTTTGGTAGAGACGGGGTTTCACCATATTGGCCAGGCTGGTCTCCAACTCCTAATCTCAGGTGAT
CTACCCACCTTGGCCTCCCAAATTGCTGGGATTACAGGCGTGAACCACTGCTCCCTTCCCTGTCCTTCTGATTTT
AAAATAACTATACCAGCAGGAGGACGTCCAGACACAGCATAGGCTACCTGGCCATGCCCAACCGGTGGGACATTT

Suppl.: TdTomato (w/o TAA stop codon) + Kpn1 + GTT-Linker + CASP3 (w/ stop codon) inserted in pCMV5 MCS

GAGTTGCTTGCTTGGCACTGTCCTCTCATGCGTTGGGTCCACTCAGTAGATGCCTGTTGAATTGGGTACGCGGCC
AGCTTGGCTGTGGAATGTGTGTCAGTTAGGGTGTGGAAAGTCCCCAGGCTCCCCAGCAGGCAGAAGTATGCAAAG
CATGCATCTCAATTAGTCAGCAACCAGGTGTGGAAAGTCCCCAGGCTCCCCAGCAGGCAGAAGTATGCAAAGCAT
GCATCTCAATTAGTCAGCAACCATAGTCCCGCCCCTAACTCCGCCCATCCCGCCCCTAACTCCGCCCAGTTCCGC
CATTCTCCGCCCCATGGCTGACTAATTTTTTTTATTTATGC-3’

TRANSLATION (76 kDa):
MVSKGEEVIKEFMRFKVRMEGSMNGHEFEIEGEGEGRPYEGTQTAKLKVTKGGPLPFAWDILSPQFMYGSKAYVK
HPADIPDYKKLSFPEGFKWERVMNFEDGGLVTVTQDSSLQDGTLIYKVKMRGTNFPPDGPVMQKKTMGWEASTER
LYPRDGVLKGEIHQALKLKDGGHYLVEFKTIYMAKKPVQLPGYYYVDTKLDITSHNEDYTIVEQYERSEGRHHLF
LGHGTGSTGSGSSGTASSEDNNMAVIKEFMRFKVRMEGSMNGHEFEIEGEGEGRPYEGTQTAKLKVTKGGPLPFA
WDILSPQFMYGSKAYVKHPADIPDYKKLSFPEGFKWERVMNFEDGGLVTVTQDSSLQDGTLIYKVKMRGTNFPPD
GPVMQKKTMGWEASTERLYPRDGVLKGEIHQALKLKDGGHYLVEFKTIYMAKKPVQLPGYYYVDTKLDITSHNED
YTIVEQYERSEGRHHLFLYGMDELYKGTTMENNKTSVDSKSINNFEVKTIHGSKSVDSGIYLDSSYKMDYPEMGI
CIIINNKNFHKSTGMSSRSGTDVDAANLRETFMGLKYQVRNKNDLTREDILELMDSVSKEDHSKRSSFVCVILSH
GDEGVIYGTNGPVELKKLTSFFRGDYCRSLTGKPKLFIIQACRGTELDCGIETDSGTDEEMACQKIAGGG*

Suppl.: tdTomato (w/o TAA stop codon) + Kpn1 + Linker + partial IMPase sequence (w/ stop codon) inserted in pCMV5 MCS

green = tdTomato
red = linker region
blue = pIMPase

5'-ATAGAGAGCTCGTTTAGTGAACCGTCA
G/AATTC
GATGGTATGGTGAGCAAGGGCGAGGAGGTCATCAAAGAGTTCATGCGCTTCAAGGTGCGCATGGAGGGCTCCATG
AACGGCCACGAGTTCGAGATCGAGGGCGAGGGCGAGGGCCGCCCCTACGAGGGCACCCAGACCGCCAAGCTGAAG
GTGACCAAGGGCGGCCCCCTGCCCTTCGCCTGGGACATCCTGTCCCCCCAGTTCATGTACGGCTCCAAGGCGTAC
GTGAAGCACCCCGCCGACATCCCCGATTACAAGAAGCTGTCCTTCCCCGAGGGCTTCAAGTGGGAGCGCGTGATG
AACTTCGAGGACGGCGGTCTGGTGACCGTGACCCAGGACTCCTCCCTGCAGGACGGCACGCTGATCTACAAGGTG
AAGATGCGCGGCACCAACTTCCCCCCCGACGGCCCCGTAATGCAGAAGAAGACCATGGGCTGGGAGGCCTCCACC
GAGCGCCTGTACCCCCGCGACGGCGTGCTGAAGGGCGAGATCCACCAGGCCCTGAAGCTGAAGGACGGCGGCCAC
TACCTGGTGGAGTTCAAGACCATCTACATGGCCAAGAAGCCCGTGCAACTGCCCGGCTACTACTACGTGGACACC
AAGCTGGACATCACCTCCCACAACGAGGACTACACCATCGTGGAACAGTACGAGCGCTCCGAGGGCCGCCACCAC
CTGTTCCTGGGGCATGGCACCGGCAGCACCGGCAGCGGCAGCTCCGGCACCGCCTCCTCCGAGGACAACAACATG
GCCGTCATCAAAGAGTTCATGCGCTTCAAGGTGCGCATGGAGGGCTCCATGAACGGCCACGAGTTCGAGATCGAG
GGCGAGGGCGAGGGCCGCCCCTACGAGGGCACCCAGACCGCCAAGCTGAAGGTGACCAAGGGCGGCCCCCTGCCC
TTCGCCTGGGACATCCTGTCCCCCCAGTTCATGTACGGCTCCAAGGCGTACGTGAAGCACCCCGCCGACATCCCC
GATTACAAGAAGCTGTCCTTCCCCGAGGGCTTCAAGTGGGAGCGCGTGATGAACTTCGAGGACGGCGGTCTGGTG
ACCGTGACCCAGGACTCCTCCCTGCAGGACGGCACGCTGATCTACAAGGTGAAGATGCGCGGCACCAACTTCCCC
CCCGACGGCCCCGTAATGCAGAAGAAGACCATGGGCTGGGAGGCCTCCACCGAGCGCCTGTACCCCCGCGACGGC
GTGCTGAAGGGCGAGATCCACCAGGCCCTGAAGCTGAAGGACGGCGGCCACTACCTGGTGGAGTTCAAGACCATC
TACATGGCCAAGAAGCCCGTGCAACTGCCCGGCTACTACTACGTGGACACCAAGCTGGACATCACCTCCCACAAC
GAGGACTACACCATCGTGGAACAGTACGAGCGCTCCGAGGGCCGCCACCACCTGTTCCTGTACGGCATGGACGAG
CTGTACAAG
GGTAC/C
GGCACCGGCAGCGGCAGCGGCAGCGGCAGCACCGGC
CTGGTGACCGTGACCGACCAGAAGGTGGAGAAGATGCTGATGAGCAGCATCAAGGAGAAGTACCCCTGCCACAGC
TTCATCGGCGAGGAGTGATAA
AT/CGAT
AAGCTTATGCATGCGGCCGCATCTAGAGGGCCCGGATCCCGGGTGGCATCCCTGTGACCCCTCCCCAGTGCCTCT
CCTGGCCCTGGAAGTTGCCACTCCAGTGCCCACCAGCCTTGTCCTAATAAAATTAAGTTGCATCATTTTGTCTGA
CTAGGTGTCCTTCTATAATATTATGGGGTGGAGGGGGGTGGTATGGAGCAAGGGGCAAGTTGGGAAGACAACCTG
TAGGGCCTGCGGGGTCTATTGGGAACCAAGCTGGAGTGCAGTGGCACAATCTTGGCTCACTGCAATCTCCGCCTC
CTGGGTTCAAGCGATTCTCCTGCCTCAGCCTCCCGAGTTGTTGGGATTCCAGGCATGCATGACCAGGCTCAGCTA
ATTTTTGTTTTTTTGGTAGAGACGGGGTTTCACCATATTGGCCAGGCTGGTCTCCAACTCCTAATCTCAGGTGAT
CTACCCACCTTGGCCTCCCAAATTGCTGGGATTACAGGCGTGAACCACTGCTCCCTTCCCTGTCCTTCTGATTTT
AAAATAACTATACCAGCAGGAGGACGTCCAGACACAGCATAGGCTACCTGGCCATGCCCAACCGGTGGGACATTT
GAGTTGCTTGCTTGGCACTGTCCTCTCATGCGTTGGGTCCACTCAGTAGATGCCTGTTGAATTGGGTACGCGGCC
AGCTTGGCTGTGGAATGTGTGTCAGTTAGGGTGTGGAAAGTCCCCAGGCTCCCCAGCAGGCAGAAGTATGCAAAG
CATGCATCTCAATTAGTCAGCAACCAGGTGTGGAAAGTCCCCAGGCTCCCCAGCAGGCAGAAGTATGCAAAGCAT
GCATCTCAATTAGTCAGCAACCATAGTCCCGCCCCTAACTCCGCCCATCCCGCCCCTAACTCCGCCCAGTTCCGC
CCATTCTCCGCCCCATGGCTGACTAATTTTTTTTATTTATGC-3'

Suppl.: tdTomato (w/o TAA stop codon) + Kpn1 + Linker + partial IMPase sequence (w/ stop codon) inserted in pCMV5 MCS

TRANSLATION (59 kDa):

MVSKGEEVIKEFMRFKVRMEGSMNGHEFEIEGEGEGRPYEGTQTAKLKVTKGGPLPFAWDILSPQFMYGSKAYVK
HPADIPDYKKLSFPEGFKWERVMNFEDGGLVTVTQDSSLQDGTLIYKVKMRGTNFPPDGPVMQKKTMGWEASTER
LYPRDGVLKGEIHQALKLKDGGHYLVEFKTIYMAKKPVQLPGYYYVDTKLDITSHNEDYTIVEQYERSEGRHHLF
LGHGTGSTGSGSSGTASSEDNNMAVIKEFMRFKVRMEGSMNGHEFEIEGEGEGRPYEGTQTAKLKVTKGGPLPFA
WDILSPQFMYGSKAYVKHPADIPDYKKLSFPEGFKWERVMNFEDGGLVTVTQDSSLQDGTLIYKVKMRGTNFPPD
GPVMQKKTMGWEASTERLYPRDGVLKGEIHQALKLKDGGHYLVEFKTIYMAKKPVQLPGYYYVDTKLDITSHNED
YTIVEQYERSEGRHHLFLYGMDELYKGTGTGSGSGSGSTGLVTVTDQKVEKMLMSSIKEKYPCHSFIGEE*